Investigation of the Dependence of Isomeric Cross-Section Ratio on Various Reaction Parameters

Thesis submitted to University of Calicut

in partial fulfilment of the requirements

for the award of degree of

DOCTOR OF PHILOSOPHY

IN

PHYSICS

By

MUHAMMED SHAN P T

Reg. No : PHYPHD54

under the guidance of

Prof. (Dr). M. M. Musthafa

DEPARTMENT OF PHYSICS

UNIVERSITY OF CALICUT

SEPTEMBER 2020

Department of Physics
UNIVERSITY OF CALICUT

Dr. M.M. Musthafa

Professor & Former Head

Department of Physics,

Calicut University P.O
Kerala, India-673 635
Tel: +91 9745509190
E-mail: mmm@uoc.ac.in,
mm_musthafa@rediffmail.com

16th April, 2021

CERTIFICATION OF SUPERVISOR

*This is to certify that all the corrections/suggestions recommended by the adjudicators have been incorporated in the thesis entitled '**Investigation of the dependence of isomeric cross-section ratio on various reaction parameters'**, submitted to the University of Calicut in partial fulfillment of the requirements for the award of the degree of Doctor of Philosophy in Physics by **Mr. Muhammed Shan P.T.**, Department of Physics, University of Calicut.*

Dr. M.M. Musthafa

Department of Physics
UNIVERSITY OF CALICUT

Dr. M.M. Musthafa

Professor & Former Head

Department of Physics,

Calicut University P.O
Kerala, India-673 635
Tel: +91 9745509190
E-mail: mmm@uoc.ac.in,
mm_musthafa@rediffmail.com

19th April, 2021

CERTIFICATION OF SUPERVISOR

This is to certify that all the corrections/suggestions recommended by the adjudicators have been incorporated in the thesis entitled ***'Investigation of the dependence of isomeric cross-section ratio on various reaction parameters'****, submitted to the University of Calicut in partial fulfillment of the requirements for the award of the degree of Doctor of Philosophy in Physics by* ***Mr. Muhammed Shan P. T.****, Department of Physics, University of Calicut and the contents in the thesis and the soft copy are one and the same.*

Dr. M.M. Musthafa

Dr. M.M. MUSTHAFA
Professor
Department of Physics
University of Calicut
Kerala 673 635 India

CERTIFICATE

This is to certify that the thesis entitled **"Investigation of the Dependence of Isomeric Cross-Section Ratio on Various Reaction Parameters"** submitted to the Department of Physics, University of Calicut by **Mr. Muhammed Shan P.T.** in partial fulfilment of the requirements for the award of the degree of Doctor of Philosophy is a bonafide record of research work carried out by him under my supervision and guidance. This thesis has not been submitted by him for the award of any degree, diploma, associateship, fellowship etc. of any university or institute.

University of Calicut — **Prof. (Dr.) M.M. Musthafa**

28-09-2020 — **Research Supervisor**

DECLARATION

I hereby declare that the work presented in this thesis entitled **"Investigation of the Dependence of Isomeric Cross-Section Ratio on Various Reaction Parameters"** is a bonafide record of research work done by me at the Department of Physics, University of Calicut, Kerala, India under the supervision of Prof. (Dr.) M.M. Musthafa. This thesis has not been submitted by me for the award of any other degree, diploma, associateship, fellowship etc. of any university or institute.

Date: 27-09-2020 **Muhammed Shan P.T.**

Dedicated to My Beloved

Parents and Family

Acknowledgements

Your pain is the breaking of shell that encloses your understanding (Khalil Gibran)

I would like to take this opportunity to express my heartfelt gratitude to all those who helped me to fulfill my dream, this thesis.

I express my sincere and whole hearted thanks to my esteemed research supervisor **Prof. (Dr). M. M. Musthafa**, Professor, Department of Physics, University of Calicut, Kerala, for giving me an opportunity to work under his guidance. His understanding, guidance, encouragement, patience and personal involvement have helped me a lot to overcome all the uncertainty arised during this period. I am highly indebted to his untiring perseverance, which helped me to present this work in the right perspective.

I express my sincere gratitude to **Prof. A. M. Vinodkumar**, Head of the Department of Physics and **Prof. P. P. Pradyumnan** and **Prof. Antony Joseph**, former Heads of the Department of Physics, University of Calicut for providing me all the support and essential facilities to carry out the research. I also thank all the faculty members, librarian and office staff of the department for the help they rendered during the entire course of my research study.

I would like to express my special thanks to the **UGC-DAE-CSR Kolkata centre-INDIA**, for the financial support through **Project Fellowship**. I am deeply indebted to **Dr. S. S Ghugre,** who is my co-ordinator, UGC-DAE-CSR

Kolkata centre project, for his kindness and encouragements.

I am really thankful to my research group: Dr. Mohamed Aslam P, K.K Rajesh, T. Najmunnisa, Abdurahiman, K. Hajara, Salma, Midhun, Shaima and I express my gratitude for their encouragement and the fruitful discussions. I lovingly remember the occasion spent with all other research scholars especially Shabeer, Muzammil, Abdul Irshad, Sebastian, Ahammed Raseen, Sulaiman, Jamshihas, Sravan, Sanila, Nithu, Anju K, Nikhil, Prashanth, Ramsiya, Deepthy Maria, Vishnu, Nice, Anjana, Ummukulsu, Jisha, Arjun, Soumya, Jumana, Anju, Nabeela, Sahra, Shabeeba, Safna, Thasneema, Bineesh, Vidya, Bintu, Aswathi, Sitha, Vinod, Sruthi, Habeeb, Baheeja, Amina, Shijina, Megha. Especially, I really enjoyed the non-academic moment spent with our evening tea group members Irshad, Shabeer, Muzammil, Sebastian and Jamshihas.

There are no words to express my gratitude and thanks to My Beloved **Father**, **Mother**, **Wife**, **Son**, **Sisters**, **All family members**, **Teachers**, and **Friends**. Their love has been the major spiritual support in my life.

Above all, I thank **Almighty** who made me what I am and for providing all suitable circumstances for this achievement. As a final word, I would like to thank each and every individual who have been a source of support and encouragement and helped me to achieve my goal and complete my Thesis work successfully.

P. T. Muhammed Shan

List of Figures

List of Tables

Contents

Preface

Study of nuclear reaction mechanism is a fundamental tool to study the properties of nucleus as well as the behavior of nuclear force between the nucleons inside the nucleus and hence to understand the nuclear structure. The nuclear physics study is considered to be started with the discovery of radioactivity by Henry Becquerel in 1896. The history of nuclear reaction was started when Rutherford observed the first nuclear reaction in 1919. A nuclear reaction is a process in which a projectile nucleus is bombarded with a target nucleus, leading to the emission of particles and/or radiation leaving behind the residual nucleus. The outcome from a nuclear reaction is reported and recorded as nuclear data which includes observed reaction yield, energy and angular distribution of particle, half-lives, decay modes, etc. by studying the characteristics of the emitted particle and residual nucleus. An important component of the research and development for nuclear physics is the improvement of the fundamental nuclear data. Nuclear data is the information describing the properties of atomic nuclei and the fundamental physical relationships governing their interactions. These data characterize fundamental physical processes that underlie all nuclear technologies. The applications of nuclear data today include all areas of nuclear science and technology. Apart from energy applications for fission power reactors and fusion reactor technology, there are significant non-energy applications including radiation therapy, nuclear medicine, radiation safety, waste management and environmental research, materials analysis, etc.

In order to understand the interaction mechanism in a nuclear reaction different nuclear reaction models have been proposed. It was Niels Bohr first to

propose a satisfactory model to explain the reaction mechanism. According to him the incident particle fuses with the target forming a compound system and its energy and angular momentum are shared among all the nucleons in the compound system. Then it decays by an emitting particle(s) or gamma rays and de-excite to ground state. This decay of the compound nucleus is independent of its mode of formation. This is termed as a compound nuclear mechanism or independent hypothesis and is found to be validated at lower excitation energy. It was proved experimentally by S.N Ghosal in 1950. On the other hand, at very high excitation energies the direct reaction mechanism will prevail. which is expected to take place within a time of $\approx 10^{-22}$ sec, i.e., the time required for the incident particle to pass through the nucleus. It is expected that emission of particles may also takes place during the equilibration of compound system. The emission of a particle from the nucleus before attaining the equilibrium state is referred to as the Pre-equilibrium Emission. In PE mechanism the projectile may share its energy among a small number of nucleons which may further, interact with other nucleons and during this cascade of nucleon-nucleon interaction through which the projectile energy is progressively shared among the target nucleons a particle may be emitted long before the attainment of statistical equilibrium. And the Pre-equilibrium (PE) emission process has been identified as the prominent reaction mechanism at moderate excitation energies.

The isomeric cross-section ratio(ICR), defined as the ratio of the cross-section for the formation of the isomeric state to the total production cross-section $\frac{\sigma_m}{\sigma_m+\sigma_g}$, is known to depend on the spin of the states, incident energy, and the reaction channels. The actual probability for the isomeric state is total cross-section times the isomeric cross-section ratio and we are looking to produce sufficient yield of the isomeric state for the practical applications. Hence, this data is important. From the nuclear physics point of view, the experimental and theoretical studies on the ICR, as a function of incident particle energy, should, therefore, lead to useful information on the spin-cutoff parameter, angular momentum transfer, the level structure of the product nucleus as well as the progress of nuclear

reaction mechanism. Hence it is important to have information about the various parameters that may affect the relative isomeric population. The knowledge of excitation functions and isomeric cross-section ratio has served as a powerful tool for the study of the nuclear reaction mechanisms. The nuclear reaction data will help to update the existing nuclear data files, re-measurement of cross-sections, new cross-section measurement, development of new computer programs, etc.

The isotopes of indium and indium containing compounds have large varieties of applications in the field of medical, industrial, and astrophysics. Indium radioisotopes namely ^{110} In, ^{111}In, ^{113m} In, and ^{114m} In are widely used for therapeutic and diagnostic purposes, due to their convenient half-life, gamma-ray energy and abundance etc. They are also used for labeling of cellular blood components and a monoclonal antibody, myocardial damage detection, localization of abscess in polyeystic kidney, radiolabeled immunoglobulin therapy, imaging for cancer etc. ^{115}In is an important material in making alloys and is widely used to make gold and platinum much harder. It is also used in multiple junction solar cells. Besides, compounds of indium are used in making optical devices. These important isotopes of indium can be produced from different natural elements like Indium and cadmium etc. Natural Indium is having the isotopes (natural abundance in percentage) ^{113}In(4.29%) ^{115}In(95.71%) and natural Cadmium is having the isotopes (natural abundance in percentage) ^{106}Cd(1.25%), ^{108}Cd(0.89%), ^{110}Cd(12.49%), ^{111}Cd(12.80%), ^{112}Cd(24.13%), ^{113}Cd(12.22%) ^{114}Cd(28.73%) and ^{116}Cd(7.49%). These can produce the desired isotopes of indium through charged-particle induced reactions.

Keeping the above fact in mind, in the present work, a systematic study of proton-induced reaction on natural indium and cadmium resulting in a production of various indium isomers and some cadmium isomers have been analyzed. The excitation function for different residues populated via $^{nat}In(p,x)$ and $^{nat}Cd(p,x)$ reactions have been measured from the threshold up to 21.96 MeV. Isomeric cross-section ratio of above-identified isomers were also determined. The experiment was carried out at Tata Institute of Fundamental Research (TIFR),

Mumbai, INDIA, using a 14UD pelletron accelerator. Theoretical analysis of the data were performed within the framework of two statistical model codes EMPIRE-3.2 and TALYS-1.8.

The experimental cross-section data produced from proton-induced on natural indium via different reaction channels $^{115}In(p,p)^{115m}$In, $^{115}In(p,pn)^{114m}$In, $^{115}In(p,p2n)^{113m}$In, $^{113}In(p,p)^{113m}$In, $^{115}In(p,3n)^{113}$Sn, $^{113}In(p,n)^{113}$SIn, $^{115}In(p,n\alpha)^{111m}$Cd and the excitation function produced from proton-induced on natural cadmium through the reaction channels ^{nat}Cd (p,x) ^{109g}In ^{nat}Cd (p,x) ^{110g,m}In, ^{nat}Cd (p,x) ^{111g,m}In, ^{nat}Cd (p,x) ^{112g,m}In, ^{nat}Cd (p,x) ^{113m}In, ^{116}Cd (p,2n) ^{115m}In, ^{116}Cd (p,n) ^{116m}In, ^{106}Cd (p,pn) ^{105}Cd and ^{nat}Cd (p,x) ^{111m}Cd, have been measured, at incident proton energies from 8 to 22 MeV. The data are analyzed using the statistical model code EMPIRE and TALYS. The data available in the literature are also compared with the present data.

Many of the evaporation residues formed in these reaction channels have isomeric states with a half-life of a few minutes and hours. Isomeric cross-section ratios are also calculated in such cases. A detailed discussion of the individual cases have been done in chapter 4 & 5 of the thesis. The measured excitation function of these isotopes will help efficiently to optimize the production condition. To the best of our knowledge, the excitation function for the ^{105}Cd isotope and the isomeric cross-section ratio of ^{110}In, ^{111}In, ^{112}In isotopes measured and reported for the first time. The general observation of the ICR indicates that reaction favored population of the higher spin state except near the reaction threshold where reactions start populating lower energy state irrespective of the spin state. This trend also found to be increasing with incident energy. Further variation with incident energy is more prominent. Further, the ICR is found to depend on the exit channel also. On analysis of the trend of ICR, there is a strong correlation of relative population with the energy difference between isomeric state and ground state are observed. No correlation between the relative population with the lifetime of state and parity between isomeric state and ground state are observed.

List of Publications

1. **Measurement of excitation functions and analysis of isomeric population in some reactions induced by proton on natural indium at low energy.** Muhammed Shan P.T, M.M Musthafa, Najmunnisa T, Mohammed Aslam P, K K Rajesh, Hajara K, Surendran P, J.P Nair, A.Shanbagh, S.S Ghugre.

   Nuclear Physics A 974 (2018) 9-21 (I. F: 1.695, Elsevier, ISSN:0375-9474)

2. **Systematic study on some isotopes of medical and industrial applications, produced in proton induced reaction on natural cadmium.** P.T.M Shan, M.M Musthafa, Najmunnisa T, Mohammed Aslam P, K K Rajesh, Hajara K, Surendran P, J.P Nair, A.Shanbagh, S.S Ghugre.

   Eur. Phys. J. Plus (2020) 135:385 (I. F: 3.228, Springer, ISSN:2190-5444)

List of International / National conference presentations:

1. Experimental study of isomeric cross-section ration of ^{115}In (p,p')^{115m}In reaction at low energy: Proceedings of the DAE-BRNS Symp. on Nucl. Phys. 61 (2016)

2. Excitation function for ^{106}Cd (p,pn)^{105}Cd Reaction upto 23 MeV: Proceedings of the DAE-BRNS Symp. on Nucl. Phys. 62 (2017)

3. Excitation function for the ^{nat}Cd (p,x)^{111m}Cd reaction and it's isomeric cross section ratio: Proceedings of the DAE-BRNS on Nucl. Phys.63 (2018)

List of Seminars/ Workshops/ Schools attended:

1. Theme meeting cum workshop on EMPIRE-3.2 Held at University of calicut, Kerala during 10-13 November 2014.

2. EXFOR compilation workshop held at Bangalore university, Bangalore during january 2015.

3. National seminar on ibnul-haytham and his world of science. November 2015, University of Calicut, Kerala.

4. NDPCI-BRNS School on Nuclear Reactions and Applications held at BARC Mumbai, during 2-12 November 2016.

5. National workshop on foundations of Fourier Transform and Digital Signal Processing. Jan 2017, S. A. R. B. T. M GOVT. College, Koyilandi, Kerala.

6. EXFOR compilation workshop held at NEHU university, Shillong during March 2017.

7. Error Propagation in Nuclear Data MEASUREMENT-2017 held at Mizoram university, Aizwal during 13-14 March 2017

8. DAE-BRNS-Theme meeting on covariance analysis held at Manipal university, Manippal during 9-13 December 2017.

9. UGC-DAE-CSR Kolkata , CRS Annual science day celebration, Oral presentation, 01-february 2018.

10. EXFOR compilation workshop held at MSU university, Baroda during November 2019.

Chapter 1

Basic Concepts and Thesis Structure

1.1 Introduction

The nucleus and it's characteristics were a mysterious thing to humankind for a long time. The sustained effort of the human mind to explain the conclusive structure of the nucleus has led to many inventions. The theory of the atomic structure of the matter by Dalton, the discovery of the electron by J.J Thomsson, radioactivity by Henry Becquerel, the discovery of atomic nucleus and the nuclear constituent particles by Rutherford discovery of the neutron by Chadwick have laid the foundation of "Nuclear Physics". The study of the nucleus is considered to be started with the discovery of radioactivity by Henry Becquerel in 1896 [1]. A nuclear reaction is considered as the tool to study the properties of the nucleus and the nature of the force between the nucleons. A nuclear reaction is a process in which a projectile nucleus is bombarded with a target nucleus, leading to the emission of particles and/or radiation leaving behind the residual nucleus. The residual nucleus will generally be at an excited energy level. One has the information of the system before the reaction and the system after the reaction but does not have the information of what exactly

happening inside a nucleus during the reaction process. This information is inferred from the reaction outcomes. Thus to explain the reaction mechanism, Niels Bohr [2] proposes a satisfactory model for the nuclear reaction. According to this model, the incident particle fuses with the target forming a compound nucleus system by sharing its energy and angular momentum with all the nucleons in the target. The compound nucleus then decays by emitting particles and/or gamma rays. This decay is independent of the mode of formation. This is known as Bohr's compound nuclear mechanism or independent hypothesis[2]. S.N Ghoshal in 1950 [3] has shown that the ^{64}Zn nuclei formed by the bombardment of a proton on copper-63 and alpha on Nickel-60 decay in a similar pattern. This validated the Bhor's independent hypothesis. Weisskopf and Ewing [4] have developed a detailed nuclear reaction theory on the basis of compound nuclear reaction theory. Hauser-Feshbach [5] developed a theory by accounting the angular momentum and parity of each state in nuclear decay correction for width fluctuation (WFC) is also applied in the model. Analysing nuclear reaction in relatively larger energy, it is observed that the compound nuclear reaction theory is valid at relatively lower excitation energies. On the other hand, at very high excitation energies, the direct reaction mechanism will prevail[6, 7]. However, the emission of a particle from the nucleus before attaining the equilibrium state can be observed in many nuclear reactions induced by fast projectiles, and the process is referred to as the Pre-equilibrium Emission[8–10]. At moderate excitation energies, Pre-equilibrium (PE) emission process has been identified as the prominent reaction mechanism. In PE mechanism, the projectile may share its energy among a small number of nucleons which may further, interact with other nucleons and during this cascade of nucleon-nucleon interaction through which the projectile energy is progressively shared among the target nucleons and there is a reasonable chance that the particles are emitted long before the attainment of statistical equilibrium. Various models like exciton model(EM)[11], Feshbach Kerman Koonin model (FKK)[12], Hydelberg model (NVWY)[13] are proposed for treating the pre-equilibrium emission. A typical energy spectrum of parti-

cle emitted in a nuclear reaction is shown in figure. 1. 1. The gaussian type structure in the lower energy side corresponds to the compound nuclear reaction process, the diffraction type band at the high energy side corresponds to the direct reaction mechanism and the smooth part in between may corresponds to pre-equilibrium emission. In order to test the validity of nuclear reaction models and predict the behaviour of unknown system, it is essential to have a large number of data on nuclear reactions covering a large number of nuclei in the periodic table over a wide range of excitation energy.

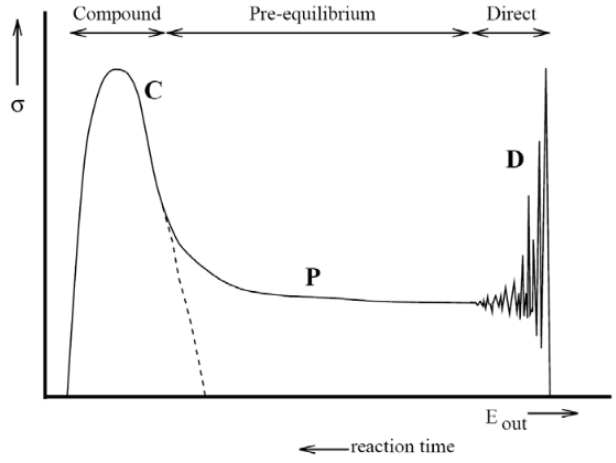

Figure 1.1: Typical spectra of particles emitted in a nuclear reaction at moderate excitation energy.

A nuclear reactor is perhaps the most important field utilizing the knowledge of the nuclear reaction data. Nuclear reaction data is also important in the fields like space science, astrophysics, industrial and Medical Science, etc. In space science, the interaction of radiation with electronic devices in space and the effect on device performance is of significant interest. This is important as India is one of the super powers in nuclear technology and space exploration. Further, the nuclear reaction data at extremely low energy-around Fermi energy-is important in understanding the nucleosynthesis and the formation and structure of the universe. As for industrial purpose, the radioisotope is used as tracer to monitor fluid flow and filtration, detect leaks, measure the wear and tear and corrosion

of component used in machine. It is also used in transportation, weapons and in agricultural field.

In the field of medical science, radioactive isotopes are widely used for therapy and imaging. Particularly, India is emerging as an economic hub for medical industry with the treatment using radioisotopes. Apart from that, a large number of linear accelerators with energies from 5-25 MeV are being commissioned in Medical institutions. There is a fine chance of secondary emission of gamma-ray and neutrons from the different parts of radiotherapy facilities and also from patients leading to the radio-active transmutation of atoms and thereby molecules in the tissues of the human body. This is a matter of serious concern. In order to make a realistic prediction of the behaviour of the nucleus as well as the outcome of nuclear interactions, wheather it is in reactor physics, astrophysics, medical therapy, isotopic production or space applications, exact data on nuclear reaction with high accuracy should be generated.

In several cases, the product nucleus may be formed as the nuclide in the metastable state, which can decay to the unstable or stable ground state with decay constant λ_m. The study of the formation of nuclear isomers in a nuclear reaction will provide important information on the angular momentum transfer, gamma de-excitation processes and coupling of the channel during the reaction processes [14, 15]. The relative population of the isomeric state is generally expressed in terms of isomeric cross-section ratio (ICR). From the measured values of σ_m , the cross-section for the formation of the metastable state of the nuclide and σ_g, the cross section for the formation of the ground state, the isomeric cross-section ratio $\frac{\sigma_m}{\sigma_m+\sigma_g}$, can be estimated. ICR gives important information about the nuclear reaction mechanism, particularly that of the energy. This is particularly important in the case of a highly deformed nucleus, where a state with a larger value of projection quantum number K are produced [16]. Data on population of isomeric state and their decay is important in the field of nuclear medicine and radiodiagnosis. Quim et al. have shown [17] that the isomeric cross section ratio is primarily governed by the spin of the two level involved, rather

than their separation and excitation energies[18, 19]. It depends on spins of the ground state and excited isomeric state as well as incident energy.

Keeping the above facts in mind, as a part of the systematic study of nuclear reactions induced by light ion, the excitation functions for reaction residues populated via $^{115}In(p,p)^{115m}$In, $^{115}In(p,pn)^{114m}$In, $^{115}In(p,p2n)^{113m}$In, $^{113}In(p,p)^{113m}$In, $^{115}In(p,n\alpha)^{111m}$Cd, $^{115}In(p,3n)^{113}$Sn, $^{113}In(p,n)^{113}$Sn, ^{nat}Cd (p,x) ^{109g}In ^{nat}Cd (p,x) ^{110g,m}In, ^{nat}Cd (p,x) ^{111g,m}In, ^{nat}Cd (p,x) ^{112g,m}In, ^{nat}Cd (p,x) ^{113m}In, ^{nat}Cd (p,x) ^{115m}In, ^{nat}Cd (p,x) ^{116m}In, ^{nat}Cd (p,x) ^{105}Cd and ^{nat}Cd (p,x) ^{111m}Cd channels were measured over the proton energy range of 8 - 22 MeV using stacked foil activation technique. One of the isotopes, ^{115}In is an important material in making alloys and is widely used to make gold and platinum much harder. It is also used in multiple junction solar cell[20]. In addition, compounds of indium are used in making optical[21] devices. Two of the radioactive isotopes, namely ^{113m}In and ^{114m}In, included in the present analysis, are widely used in therapeutics and diagnostic purposes[22]. The proton induced on natural cadmium nuclear reaction is also related to different practical applications. Such as, cadmium is an important sample for nuclear technologies: it is used for the production of alloys and in electroplating. Production of medical isotopes: the reaction product like ^{114m,111,110,109}In are used in therapeutic and diagnostic purposes[23]. Also, it is used in the dose estimation and waste handling by the production of long-lived products. Theoretical analysis of the data was performed within the framework of two statistical model codes EMPIRE-3.2[24] and TALYS-1.8[25] and it is also compared with the literature[26–38]. Isomeric cross section ratio for isomeric pairs $^{115}In^{m,g}$, $^{114}In^{m,g}$, $^{113}In^{m,g}$, $^{113}Sn^{m,g}$, $^{112}In^{m,g}$, $^{111}In^{m,g}$, $^{110}In^{m,g}$ and $^{111}Cd^{m,g}$ were also calculated. The excitation function of ^{105}Cd and the isomeric cross-section ratio of ^{110}In, ^{111}In and ^{112}In isotopes measured and it is reported for the first time. The isomeric cross-section ratio of the different isomers have been analyzed and various dependence of isomeric cross-section ratio on different factors such as the spin of states, life time of the isomeric states, energy of different levels, decay mode as well as the dependence

of the exit channel has been well explained for a large number of a nucleus with wide range of energy .

1.2 Structure of the thesis

This thesis furnishes a comprehensive experimental and theoretical study on some proton induced reactions on indium and cadmium. The production cross-section and isomeric cross section ratio have been analysed. The excitation function for the isotopes, thus, produced are measured up to 23 MeV employing stacked foil activation technique. The theoretical analysis have been done using the statistical model codes EMPIRE-3.2[19] and TALYS 1.8[20]

A general outline of the study is presented in the first chapter of the thesis. Detailed introduction to the current scenario in nuclear physics, the importance of nuclear data, the relevance of the present work and detailed literature survey are presented here.

In Chapter 2, a brief outline of the nuclear reaction theory and reaction kinematics are discussed. Various nuclear reaction model and the details of the statistical nuclear reaction computer codes based on the above models and relevant parameters are also discussed.

Chapter 3 goes through a detailed experimental analysis of the work. A detailed note on the TIFR pelletron accelerator, activation method, target preparation, gamma-ray spectroscopic system, formulation to calculate cross-section and a detailed error analysis has been done in this chapter.

Chapter 4 is devoted to describing the overall result and discussion of the present work. In the first part of this chapter, we have investigated the excitation functions for reaction residues populated via $^{115}In(p,p)^{115m}$In, $^{115}In(p,pn)^{114m}$In, $^{115}In(p,p2n)^{113m}$In, $^{113}In(p,p)^{113m}$In, $^{115}In(p,n\alpha)^{111m}$Cd, $^{115}In(p,3n)^{113}$Sn and $^{113}In(p,n)^{113}$Sn channels. These were measured over the proton energy range of 8 - 22 MeV. Isomeric cross section ratio for isomeric pairs $^{115}In^{m,g}$, $^{114}In^{m,g}$, $^{113}In^{m,g}$, $^{113}Sn^{m,g}$ and $^{111}Cd^{m,g}$ were also determined. The detailed analysis of each reaction mechanism.

In the second part, the study is extend to the calculation of the cross-section of ^{nat}Cd (p,x) ^{109g}In ^{nat}Cd (p,x) ^{110g,m}In, ^{nat}Cd (p,x) ^{111g,m}In, ^{nat}Cd (p,x) ^{112g,m}In, ^{nat}Cd (p,x) ^{113m}In, ^{nat}Cd (p,x) ^{115m}In, ^{nat}Cd (p,x) ^{116m}In, ^{nat}Cd (p,x) ^{105}Cd and ^{nat}Cd (p,x) ^{111m}Cd reaction channels. And the isomeric cross-section ratio of ^{110}In, ^{111}In and ^{112}In isotopes have been measured.

Chapter 5 summarizes the findings of the thesis and expresses future recommendation of this work.

Bibliography

[1] H.Bequerel, compt.Rend.,122(1896)450.

[2] N.Bohr, Nature,137(1936)344

[3] S.N Ghosal, phy.rev.80(1950)939

[4] V. F. Weisskopf and D. H. Ewing, Phys. Rev., 57(1940)472.

[5] W. Hauser, H. Feshbach, The inelastic scattering of neutrons, Phys. Rev. 87 (1952) 366.

[6] A. M. Lane, Nucl. Phys. 11(1959)625.

[7] 18. A. M. Lane and J. E. Lynn, Nucl. Phys. A11(1959)646.

[8] P. E. Hodgson, Heavy ion collision proceedings of International Summer School,La Rabia, Spain, (1992)220.

[9] E. Gadioli and E. Gadioli - Ebra, Nuclear theory for applications - 1980, IAEA -SMR 68/1, Vienna, (1981)3.

[10] H. Jahn, Nuclear theory for applications - 1982, Vienna, IAEA - SMR 93, (1984)39.

[11] J. J. Griffin, Phys. Rev. Lett., 17(1966)478.

[12] H. Feshbach, A. K. Kerman and S. Koonin, Ann. Phys (NY).,125(1980)429.

[13] H. Nishioka, J. M. Verbaarschot, H. A. Weidenmuller, and S. Yoshida,Ann. Phys.,172(1986)67.

[14] C.L.Raoand L.Yaffe,Can.J.Chen 45(1967)2711.

[15] A.H Khan,G.B. Saha and L.Yaffe,Can.J.Chen.47(1969)3817

[16] H. Ejiri et al.,phys. Lett. B, 78(2) (1978) 3.

[17] S.M.Quim, S.Sudar and A.Fessler,J. Radiochin. Acta 93(2005) 503.

[18] B. Satheesh and M.M. Musthafa, Int. J. Mod. Phys. E, 20, 2119-2131 (2011).

[19] B. Satheesh and M.M. Musthafa, Int. J. Mod. Phys. E, 21(2012)1250059

[20] R. Dahal ,J.Li , K.Aryal , J.Y.Lin and H. X. Jiang, Applied Physics Letters 97, 073115(2010).

[21] M. G. Mason, L.S.Hung, and C.W.Tang, Journal of applied physics, Volume 86, Number 3 (1999).

[22] Wagner, Henry N. Principles of Nuclear Medicine. Saunders, 1995.

[23] S.M. Qaim, F. Ta rka nyi, S. Taka cs, A. Hermanne, M. Nortier, P.Oblozinsky, B. Scholten, Yu.N. Shubin, Z. Youxiang, Production cross-sections for diagnostic radioisotopes (Chapter 5), 5.2. Positron emitters, in: Charged Particle Cross-Section Database for Medical Radioisotope Production: Diagnostic Radioisotopes and Monitor Reactions, IAEA-TECDOC-1211, Vienna, 2001, p. 234. Available from: http://www-nds.indcentre.org.in/reports-new/tecdocs/iaea-tecdoc-1211.pdf.

[24] M. Herman et al.,EMPIRE-II, Nuclear Reaction Model Code 3.2, Nuclear Data Section (IAEA, Vienna, 2005).

[25] A.J. Koning, S. Hilaire and S Goriely.,TALYS-1.8, Nuclear reaction program, Nuclear Data Section (IAEA, Vienna, December 26 2015) December 26, 2015.

[26] F.Tarkanyi, F. Ditroi, A.Hermanne, S.Takacs, M.Baba , Applied radiation and isotopes, Vol 107 10 (2016) 391.

[27] M Al-Abyad , H.M.EL-Showaimy , M.B.Challan, A.M.Khalaf and M.N.H.Comsan, in Arab J. of Nucl. Sci. and Application 44 (2011) 111-121.

[28] M.U. Khandaker, K. Kim, M.W. Lee, K.S. Kim, G.N. Kim, Y.S. Cho, Y.O. Lee, Nucl.Instrum.Meth.B 266 (2008) 48774887.

[29] F.M. Nortier, S.J. Mills, G.F. Steyn, Appl. Radiat. Isot. 41 (1990) 1201.

[30] S.M. Kormali, D.L. Swindle, E.A. Schweikert, J. Radioanal. Chem. 31(1976) 437.

[31] F.S. Al-Saleh, Exfor data base:(¡http://www-nds.iaea.org/exfor/¿ Exfor D0467005) 2008.

[32] N.G. Zaitseva, O. Knotek, A. Kowalew, P. Mikecz, E. Rurarz, V.A. Khalkin, V.A.Ageev, A.A. Klyuchnikov, L.A. Kuzina, A.F. Linev, Appl. Radiat. Isot. 41 (1990) 177.

[33] E.A. Skakun, A.P. Kljucharev, N. Rakivnenko, I.A. Romanij, Russ. Acad. Sci. Phys. 39 (1) (1975) 18.

[34] K. Otozai, S. Kume, A. Mito, H. Okamura, R. Tsujino, Y. Kanchiku, H. Gotoh, Nucl. Phys. 80 (1966) 335.

[35] A.V.Muminov, S.Mukhamdev, A.Vasidov, Atomnya Energiya 49(1980)101.

[36] S.A. Said, E.K. Elmaghraby, F.I. Asfour, Appl. Radiat. Isot.64 (2006) 1655.

[37] E.A. Skakun, V.G. Batiy, Y.N. Rakivnenko, O.A. Rastrepin, Yadernaya Fizika 45 (1987) 614.

[38] A.Hermanne, F.Tarkanyi, S.Takacs, P.Van den Winkel, R.Adam Rebeles, A.Ignatyuk and S.F. Kovalev, Applied Radiation and Isotopes 68 (2010) 14 -17

Chapter 2

Basic Nuclear Reaction Theory & The computer codes used for theoretical prediction

2.1 Nuclear Reaction

A nuclear reaction is found to occur when two nuclei interact with each other. Generally, the collisions may be elastic or inelastic. Experimentally it is achieved by bombarding projectile a like proton, neutron, α-particle, γ ray photon, or a heavy nucleus on a target nucleus[1]. In order to overcome the Coulomb repulsive force between the two nuclei, the projectile should have enough kinetic energy to approach the target nucleus. If the incident energy is below Coulomb barrier, a nuclear reaction will not take place. The interaction occurs within an inter nuclear distance of 10^{-14}m. The energy and angular momentum exchange may take place between the nuclei during the interaction stage and a compound nucleus is formed. This nucleus de-excite by the emission of one or more nucleons leaving behind the residual nucleus or emit radiation.

2.1.1 Kinematics of Nuclear Reaction

A nuclear reaction is explained by recognizing the incident particle, target nucleus, and the ejectile particle. A nuclear reaction can be represented as

$$a + X \rightarrow Y + b \tag{2.1}$$

or

$$X(a, b)Y \tag{2.2}$$

where a is the incident particle, X is the target nucleus, Y is the product nucleus and b is the ejectile particle. Depending on the projectile used, the particle detected and residual nucleus, the nuclear reaction is classified as scattering, pick up and stripping, capture, photo disintegration reaction etc[2, 3].

A nuclear reaction is said to be scattering, if the projectile and ejectile are the same (a=b and X=Y). The scattering is called elastic if the residual nucleus is left in its ground state it is inelastic when the residual nucleus is left in its excited state. When the projectile and the target nucleus exchange nucleons and the projectile gains nucleons from the target the reaction is said to be pick up.If the projectile losses nucleons (the target gains nucleons) it is called stripping reaction. If the emission of particles do not take place and the compound system emits gamma-radiation(X(a,γ)Y), it represents capture reaction. When gamma ray photon as the projectile then the reaction is said to be photo-disintegration.

To account the reaction energy, which includes the kinetic energies or the rest mass energies of the reactant and product are formulated. The difference between kinetic energies of the product and reactant so called Q-value of the reaction, and it can be represented as:

$$Q = E_b \left(1 + \frac{m_b}{M_Y}\right) - E_a \left(1 - \frac{m_a}{M_X}\right) \tag{2.3}$$

Where, E_b is the kinetic energy of the ejectile, E_a is the kinetic energy of the

projectile particle, m_b, m_a, M_Y, M_X are the masses of ejectile particle, projectile particle, residual nucleus and target nucleus respectively.

The Q value can also be calculated from the mass difference formula and is:

$$Q = (M_X + m_a - M_Y - m_b)c^2 \tag{2.4}$$

where, c is the speed of light.

Depending upon the Q-value, the reactions are broadly classified into exoenergetic (Q -value is positive) and endoenergetic reactions (Q value is negative). Further, the system needs minimum energy to occur a nuclear reaction and is called threshold energy. The threshold energy is given by:

$$E_{th} = -Q\frac{M_X + m_a}{M_X} \tag{2.5}$$

2.1.2 Nuclear reaction cross section

One of the very important quantities in the measurement of nuclear reaction is the cross-section. The cross-section is defined as the probability of occurence of the nuclear reaction. The probability is defined as the ratio of the number of nuclear reaction per unit time to the number of incident particle per unit time. Let the area of the target is A, the intensity of the incident beam is I and the number of reaction per unit time is N_r then the probability can be represented as:

$$P_r = \frac{N_r}{IA} \tag{2.6}$$

It can also express in terms of effective cross section σ_r and the number of particle in the target N_t as:

$$P_r = \frac{N_t\sigma_r}{A} \tag{2.7}$$

From equation 2.6 and 2.7 we can write

$$\frac{N_t \sigma_r}{A} = \frac{N_r}{IA} \quad or \sigma_r = \frac{N_r}{IN_t} \tag{2.8}$$

The above discussions are for general cases like elastic scattering, inelastic scattering or nuclear reaction with different emitted particle from the incident channel. The discussions below are some of the specific reaction cross-section for different channels:

1. Total Cross-Section : It is the cross section for all the channels, in all the direction. It is measured by considering the number of particles in the incident beam and the target as the absorber. Let n be the number of incident particle passing through the thickness of the material dx and δn is the number absorbed by the target. Thereby considering that the $\Delta n/n$ as the probability, then by using the equations 2.7 and 2.8 we can express the total cross section as:

$$\frac{\Delta n}{n} = \frac{dn}{n} = -\sigma_t \frac{N_t}{A} = -\sigma_t \ \rho \ dx \tag{2.9}$$

where σ_t = the total cross section
ρ = the density of the nuclei in the target
A = Area of the target in which the projectiles are incident

2.Partial Cross-Section : The total cross section may be the benefaction of the various partial cross sections like elastic scattering, inelastic scattering and different reaction cross section from different channel. Hence we can write:

$$\sigma = \sigma_1 + \sigma_2 + \sigma_3 + ... = \sum_i \sigma_i \tag{2.10}$$

3. Differential cross section: There should be different angular distribution for each channel. Then it can be deffined the differential cross section for the given channel and is the sum of the differential cross section for the zenith (θ)

and azimuthal angle (ϕ).

Let the incident beam of intensity (I) interact with the target for the t time. The number of target particle is N_t and a detector is placed in some angle. Then the number of particle collected in the detector (dN) for a particular solid angle $d\Omega$ is :

$$\begin{aligned} dN &\propto t\ d\Omega\ I\ N_t \\ dN &= \sigma(\theta,\phi)\ t\ d\Omega\ I\ N_t \end{aligned} \tag{2.11}$$

where $d\Omega = Sin\theta\ d\theta\ d\phi$

When the number of particle in the target can be represented as:

$$N_t = n_a\ A \tag{2.12}$$

Where n_a is the areal density and A is the area of cross-section. Then it can define the number of projectile particle N_p as :

$$N_p = I\ A\ t \tag{2.13}$$

Then the equation 2.11 become,

$$dN = \sigma(\theta,\phi)\ d\Omega\ n_a\ N_p \tag{2.14}$$

Hence,

$$\sigma(\theta,\phi) = \frac{dN}{d\Omega\ n_a\ N_p} \tag{2.15}$$

Where $\sigma(\theta,\phi)$ is the differential cross section. Some time it is required to measure the cross section with energy as well as the angular dependence. Then it is written as:

$$\sigma(\theta,\phi,E) = \frac{d^2N(\theta,\phi,E)}{d\Omega\ dE\ n_a\ N_p} \tag{2.16}$$

It may be understood that the reaction cross-section from different measurement as a function of angle and energy will give the idea about the reaction mechanism in different reaction.

2.1.3 Reaction mechanism

Nuclear reaction mechanism can be categorized into direct reaction, compound nuclear reaction, and pre-equilibrium reaction. The direct reaction takes place within the time interval of about 10^{-22} s, which is the time taken by the projectile to traverse through a nucleus. Here the projectile interacts with a nucleon or a nucleus as a whole and emission take place immediately. When the incident energy is higher, the projectile enters into the target nucleus, as it interact with only surface nucleon and emit particles with slightly less energy than the incident energy. The important features of direct reactions are it usually takes place at higher energies, The availability of more number of high energy emitted particles and its angular distribution is forward peaking, uniform change of cross section with energy for the given channel without resonance. The angular distribution of the direct reaction is described by the modified plane wave Born approximation[4].

In compound nuclear reaction meachanism the projectile interacts with the target nucleus and it shares all its energy and momentum among all the nucleons untile it reaches a statistical equilibrium. After some time, due to the statistical fluctuation the nucleon or a group of nucleons near the surface may get enough energy to escape as a molecule. It is the smallest possible energy as well as it is the height of coulomb potential for charged particle and it is known as coulomb barrier. The compound nucleus formation have the life of the order of 10^{-16}sec. There is no memory of formation of a compound nucleus. And it does not have the information, on what exactly happens during the reaction. Which have information about the outcomes only. Since, all it's nucleons are mixed together, irrespective of the energy and origin. Then it decay by emitting radiation or particles. It is expected that the decay of the compound nucleus

depends only on the quantum mechanical parameter of the compound nucleus such as excitation energy, angular momentum and parity of the states, and is totally independent of it's the mode of formation. This is known as Bohr's independent hypothesis[5]. In this method, the emitted particle spectrum will be in isotropic distribution. And it is functioning in the lower excitation energies. The compound nuclear reaction mechanism was proved by S.N.Ghoshal[6].

At intermediate energies, it can happen that the particle is neither ejected immediately after the collision as in the case of direct reaction nor after the formation of a compound nucleus. The projectile may interact with some of the nucleons and share its energy and momentum which may further interact and share with the other nucleons and during this cascade, some of the nucleons may get emitted long before the attainment of equilibrium. It is referred to as pre-equilibrium reaction. At intermediate energies the pre-equilibrium is the major reaction mechanism[7, 8]. A brief description of the compound nuclear reaction theory and some of the compound nuclear mechanism and pre-equilibrium mechanisms which were actually used in the statistical theoretical model codes are explained in the following sections.

2.1.4 General Theory

To derive the compound nuclear reaction cross section, it followed a similar manner that is used for the scattering and reaction cross-section measurement by considering the basic quantum mechanical procedure of the scattering of nucleons. So, the plane wave is given by

$$e^{ikz} \approx \sum_{l} \frac{i^{l+1}}{2kr}(2l+1)[e^{-i(kr-l\pi/2)} - e^{i(kr-l\pi/2)}]P_l(cos\theta) \tag{2.17}$$

By introducing a new factor $\eta_l = |\eta_l|e^{2i\delta_l}$, where η_l the complex amplitude for the l^{th} partial wave and is related to the phase shift δ_l So the total outgoing

wave function $\psi(r)$ after an interaction is:

$$\psi(r) \approx \sum_l \frac{i^{l+1}}{2kr}(2l+1)[exp - i(kr - \frac{l\pi}{2}) - \eta_l \; exp \; i(kr - \frac{l\pi}{2})]P_l(cos\theta) \quad (2.18)$$

From above equation it is evident that the η_l indicate the changes in phase shift and amplitude of the outgoing part of the wave. Then ψ_{sc} can be represented as

$$\psi_{sc} = \psi(r) - e^{ikr} \quad (2.19)$$

$$= \sum_l \frac{i^{l+1}}{2kr}(2l+1)(1-\eta_l)exp[i(kr - \frac{l\pi}{2})]P_l(cos\theta) \quad (2.20)$$

Then the scattering cross section σ_{sc} can be represented as:

$$\sigma_{sc}(\theta) = \frac{N_{sc}(\theta) \; d\Omega}{v d\Omega} \quad (2.21)$$

Where, v dΩ is the incident flux, N_{sc} is the number of particle scattered per second from the target in all direction and is given by.

$$N_{sc}(\theta)d\Omega = \frac{\hbar}{2iM}|(\frac{\partial\psi_{sc}}{\partial r}\psi^*_{sc} - \frac{\partial\psi^*_{sc}}{\partial r}\psi_{sc})|_{r=r_0} \; r^2 d\Omega \quad (2.22)$$

$$= \frac{\hbar k}{M}|\psi_{sc}(r,\theta)|^2 r_0^2 d\Omega \quad (2.23)$$

and $v = \hbar k/M$

Finally the scattering cross section is given by:

$$\sigma^l_{sc} = \int \sigma_{sc}(\theta)d\Omega = \frac{\pi}{k^2}(2l+1)|1-\eta_l|^2 \quad (2.24)$$

Similarly, for the reaction cross-section, it is by considering the net flux absorbed by the nucleus within the radius r. The total wave function with the effect of target is given in equation 2.18 favour for this condition. Hence the equation for

N_r is:

$$N_r = -\frac{\hbar}{2iM}\int(\frac{\partial\psi}{\partial r}\psi^* - \frac{\partial\psi^*}{\partial r}\psi)r_0^2\ sin\theta\ d\theta\ d\phi \tag{2.25}$$

It is seen that the N_r doesn't have any angular dependence, as it is the case of absorption not any emission. Hence we obtained the reaction cross section as:

$$\sigma_r = \frac{N_r}{V} = \pi\lambda^2(2l+1)[1-|\eta|^2] \tag{2.26}$$

By different value of η_l, the reaction cross section will vary as:
From the above equation it can be see that, for $\eta_l = -1$

$$\begin{aligned} \sigma_{sc,l} &= 4(2l+1)\pi\lambda\!\!\!^{-2} \\ and\ \sigma_r &= 0 \end{aligned} \tag{2.27}$$

Also for $\eta_l = 0$

$$\sigma^{'}_{rection} = \sigma^{'}_{sc} = \pi\lambda\!\!\!^{-2}(2l+1) \tag{2.28}$$

On the other hand, for $\eta_l = 1$

$$\sigma^{'}_{rection} = \sigma^{'}_{sc} = 0 \tag{2.29}$$

2.1.5 Compound Nucleus Model

The theoretical calculation of reaction cross-section has been done by Ewing and Weisskopf[9] by developing a partial wave analysis method from the Bohr's independent hypothesis[5]. The angular momentum and parity conservation are not considered in this method. Hauser and Feshbach formulated a theoretical model (HF Model) which accounts these conservations and also an advanced H-F method with width fluctuation correction formalism has been developed. Nuclear level density parameter also plays an important role in the prediction of the compound nuclear reaction cross-section.

2.1.6 Hauser Feshbach theory

In the Hauser-Feshbach model the reaction cross section is written as the product of two factors, the cross section $\sigma_a^{CN}(E, J\pi)$ for the formation of the compound nucleus in a state of spin and parity associated to the incident channel and the decay probability $P_b(E, J\pi)$ with the excitation energy E_x into the channel b.

$$\sigma_{a,b}(E) = \sum_{J,\pi} \sigma_a^{CN}(E, J\pi) P_b(E, J\pi) \tag{2.30}$$

At particular orbital angular momentum ℓ, the compound nucleus cross-section is:

$$\sigma_a = \pi \lambda\!\!\!^{-2}_a (2\ell + 1) T_a \tag{2.31}$$

where $\lambda\!\!\!^{-}_a$ is the reduced wavelength in the incident channel, T_a is the transmission coefficient and is given by $T_a = 1 - | < S >_{aa} |^2$, where S_{aa} is average S - matrix. The decay probability can be expressed in terms of transmission coefficient as,

$$P_b(E, J\pi) = \frac{T_b(E_x, J_\pi)}{\sum_c T_c(E_x, J_\pi)} \tag{2.32}$$

with respect to the reaction channels it might be emission of photon, particle or fission. Thus we get,

$$\sigma_{a,b} = \pi \lambda\!\!\!^{-2}_a (2\ell + 1) \frac{T_a T_b}{\sum_c T_c} \tag{2.33}$$

This is the compound nuclear reaction cross-section for the particular projectile a and target b, with specific angular momentum ℓ. Where T_a and T_b are the transmission coefficient of incident and exit channel, and T_c is the collective transmission coefficient for all exit channels. So, when we consider the interacting particle with the spin, then there will be a spin weighting terms in the

cross-section equation. Suppose the spin of the projectile and spin of the target combined to form the spin of channel is 's', which in turn combine with the angular momentum to form total angular momentum J. Similarly in the case of outgoing channel, the probability of getting particular 's' is,

$$P(s) = \frac{(2s+1)}{(2i+1)(2I+1)} \tag{2.34}$$

Similarly for J is,

$$P(J) = \frac{(2J+1)}{(2s+1)(2\ell+1)} \tag{2.35}$$

Now the cross section equation become,

$$\sigma_{a,b} = \pi \lambda\!\!\!^{-2}_{a} \sum_{J\pi} \frac{(2J+1)}{(2s+1)(2\ell+1)} \frac{T_a T_b}{\sum_c T_c} \tag{2.36}$$

Here π represent the parity of the compound nucleus. The angular momenta ℓ, s and J depend on the transmission coefficient. To record the correlation between the channels in elastic scattering we used the width fluctuation correction method by Hofmann-Richert, Tepel and Weidenmueller (HRTW)[10, 11].

2.1.7 Width fluctuation correction

The Hauser-Feshbach model (HF) think that there are no correlation among the formation and decay of the definite compound nucleus. But in elastic case, both the entrance and exit channels are the same. It shows an increase in the cross-section of the elastic channel than the Hauser-Feshbach prediction. If only one elastic channel among a large number of inelastic channels we can neglect the case. But, when there are only a less number of open channels, the elastic channel contribution may have a serious effect. So, to address this issue a new model is developed by Hoffman, Richert, Tepel and Widenmueller (HRTW)[10, 11]. Thus, the nuclear reaction without the contribution of direct reaction, the width

fluctuation correction reads:

$$\sigma_{ab} = \frac{\pi}{k_a^2} \frac{T_a T_b}{\sum_c T_c} \; W_{ab} = \sigma_{ab}^{HF} \; W_{ab} \tag{2.37}$$

where, σ_{ab} is the average energy cross-section from the channel a to b, $\frac{\pi}{k_a^2}$ is the kinetic factor, σ_{ab}^{HF} is the H-F cross-section, k_a is the wave-number of the projectile, W_{ab} is the width fluctuation correction factor and T_c is the transmission co-efficient and is calculated with the optical model S-matrix element $T_c = 1 \; - \left|\langle S_{cc} \rangle\right|^2$.

2.1.8 Nuclear Level Density

Nuclear level density plays a vital role in the prediction of the nuclear reaction cross-section. The nuclear level density $\rho(E)$ defined by Bethe[12] is a characteristic property of every nucleus and it is defined as the number of levels per unit energy at certain excitation energy. In other words, it is the number of different ways in which individual nucleons can be placed in the various single particle orbitals, such that the excitation energy lies in the range E to E+dE. It increases rapidly with excitation energy. Then the average level density is given by

$$\rho(E) = \frac{dN}{dE} \tag{2.38}$$

where N (E) is the cumulative number of levels up to the excitation energy E. It does not have data for every nucleus in a wide range of excitation energy and angular momentum so we have largely dependent on models to predict the nuclear level density. There are six level density models of which three are phenomenological and three are microscopic level densities [13]. Out of many options for level density calculations, Fermi gas with a constant temperature model [14] and Gilbert-Cameron Model [15] are employed in our calculation.

2.1.9 Fermi-Gas Model

The scheme of nuclear energy levels of nuclei differ significantly from one nucleus to another. The spacing between the nuclear levels will be much larger than atomic energy levels by an order of 10^{4-6}. Light nuclei showing wide spacing than heavy A nuclei, also there is a noticeable discontinuity in the case of magic nuclei. There is no satisfactory theory to account for this, even though spin-parity distribution effect and nucleon pairing effect are taken into consideration. The intrinsic level density in terms of the spin J, parity π and excitation energy E_x as

$$\rho(E_x, J, \pi) = \rho(E_x)\rho(J, \pi) \tag{2.39}$$

where the energy dependence is

$$\rho(E_x) = \frac{expS}{\sqrt{Det}} \tag{2.40}$$

where S is the entropy and Det is in Eq.2.43. The spin J, and parity π dependence is given by

$$\rho(J, \pi) = \frac{1}{2}\frac{(2J+1)}{\sqrt{8\pi\sigma^3}} \exp[-\frac{(J+1/2)^2}{2\sigma^2}] \tag{2.41}$$

Where σ^2 so called spin cut-off parameter, and the magnitude is quantum mechanically with suitable substitution given by,

$$\sigma^2 \approx 0.623A^{7/6}(\frac{E}{E_F})^2 \tag{2.42}$$

The Fermi-gas model determining the dependence of the factors such as the excitation energy, entropy and the other thermodynamic functions of a nucleus

on its temperature T are

$$E_x = a(kT)^2; \quad S = 2aT; \quad Det = \frac{144a^3T^5}{\pi} \tag{2.43}$$

where a is the level density parameter and is mainly depend on the energy and mass. To consider the odd-even effect of the nuclei, the excitation energy is replaced with the effective energy U

$$U = E_x - \delta \tag{2.44}$$

Where δ is closely related to the pairing energy. With all the substitution the level density becomes,

$$\rho(E_x, J, \pi) = \frac{2J+1}{48\sqrt{2}\sigma^{3/2}a^{1/4}U^{5/4}} \exp[2\sqrt{aU} - \frac{(J+1/2)^2}{2\sigma^2}] \tag{2.45}$$

This equation shows that the Fermi-Gas level density model depends on the leveldensity parameter (a), cross-section (σ) and pairing energy term (δ).

2.1.10 Gilbert-Cameron Model

The Gilbert-Cameron Model is recommended for the nucleon induced reaction with excited compound nucleus up to 20 MeV. It promises an accurate explanation of the level densities in the energy region up to the neutron binding energy. The collective effects are implicitly included in the level density parameter a, this method leads to the overprediction of the level density. There has been a regular differences in the level density calculation for even-even, and odd-odd nuclei corresponding to the even-odd differences of the nuclear masses. So, to take it into account, a new term the effective excitation energy, U^* is introduced.

$$U^* = U - \delta \tag{2.46}$$

Where, $\delta = n\frac{12}{\sqrt{A}}$
with

$$n = \begin{cases} 0, & \text{for odd-odd} \\ 1, & \text{for odd-even} \\ 2, & \text{for even-even} \end{cases} \tag{2.47}$$

The cumulative number of levels as a function of energy is described with the function,

$$N(U) = exp\big[(U - U_0)/T\big], \tag{2.48}$$

where U_0 and T are the free parameters. The quantity N(U) is defined as the,

$$\rho_{lev}(U) = \frac{dN}{dU} = \frac{1}{T}exp\big[(U - U_0)/T\big], \tag{2.49}$$

and the parameter T correspond to the nuclear temperature.

Thus, in order to explain the level density for the whole energy range, both the models are combined. ie, at low energy dependence predicted by the above equation combine with the high energy Fermi-gas model.

2.1.11 Optical Model

The interaction between the projectile and target can't be studied using the exact models like compound nuclear formation and direct reaction. This can be described by an intermediate method, where all the method is included. To account all these aspects, a model called optical model is evolved. In this model the target is considered as the potential called optical potential and in general it can be given as[16, 17]:

$$U(r) = -V(r) - iW(r) + (\frac{\hbar^2}{\mu c^2})^2(\frac{1}{r}\frac{df(r)}{dr})(V_{S.O} + iW_{S.O})I.S \tag{2.50}$$

The first two term explain the coulumb and combined nuclear effect and which have the shape of Woods-Saxon[18] equation and the last term explain the spin-orbit coupling. While the term $(\frac{1}{r}\frac{df(r)}{dr})$ represent the surface potential, and it expresses that the spin orbit coupling is a surface phenomenon.

The differential elastic scattering cross-section according to equation $\sigma_{sc}(\theta)\ d\Omega = \frac{\pi}{k^2}\left|\sum_{l=0}\sqrt{2l+1}\ (1-\eta_l)\ Y_{l,0}(\theta)\right|$ is given by:

$$\frac{d\sigma_{el}}{d\Omega} = \frac{\pi}{k}^2\left|\sum_l (2l+1)^{1/2}(1-\eta_l)Y_{l,o}(\theta)\right|^2 \tag{2.51}$$

It is then the total cross section that,

$$\sigma_{total} = \sigma_{sc} + \sigma_{re} = \frac{\pi}{k^2}(2l+1)[2R_e(1-\eta_l)] \tag{2.52}$$

For substituting the target nucleus with the optical potential as given in Eq.2.50, the detailed properties of the target nucleus cannot be considered. The η_l in the above equation corresponds to the average properties of the nucleus. This situation can be simulated using mathematical method of averaging certain energy range which corresponds to the overlapping of levels. Under these circumstances the average cross-section can be written as:

$$\begin{aligned}
<\sigma_{sc}> &= \pi\lambda\!\!\!^{-2}\sum_l (2l+1) < |1-\eta_l|^2 > \\
&= \pi\lambda\!\!\!^{-2}\sum (2l+1)[1- <\eta_l> - <\eta_l^*> + <|\eta_l^2|>] \\
&= \pi\lambda\!\!\!^{-2}\sum_l (2l+1)|1- <\eta_l>|^2 + \pi\lambda\!\!\!^{-2}\sum_l (2l+1)[<|\eta_l^2|> - |<\eta_l>|^2] \\
&= \sum_l <\sigma_{se}^l> + \sum_l <\sigma_{ce}^l>
\end{aligned} \tag{2.53}$$

where $1/k^2 = \lambda\!\!\!^{-2}$, $<\sigma_{se}^l>$ and $<\sigma_{ce}^l>$ are called the shape elastic scattering and compound elastic scattering respectively. Similarly the averaged reaction

cross section is:

$$\begin{aligned} < \sigma_r > &= \pi \lambda\!\!\!^{-2} \sum_l (2l+1) < 1 - |\eta_l|^2 > \\ &= \pi \lambda\!\!\!^{-2} \sum_l (2l+1)[1 - | < \eta_l > |^2 - (< |\eta_l|^2 > - | < \eta > |^2)] \\ &= \sum_l < \sigma_c^l > - \sum_l < \sigma_{ce}^l > \end{aligned} \tag{2.54}$$

$$where < \sigma_c^l >= \pi \lambda\!\!\!^{-2}(2l+1)(1 - | < \eta > |^2) \tag{2.55}$$

and is called the compound nucleus formation cross section. The equation 2.53 indicate that the elastic scattering is the sum of the shape elastic scattering cross section (σ_{se}) and compound elastic scattering cross section (σ_{ce}). Also it correspond to difference between $< |\eta_l|^2 > - | < \eta_l > |^2$ which tend to zero indicates that the incident energy increases. Then $< \sigma_{ce}^l >$ tends to zero. So the reaction cross section $< \sigma_{re} >$ correspond to the total cross section for the compound formation. It is easy to see that the total cross section $< \sigma_T >$ is

$$< \sigma_T >=< \sigma_{se} > + < \sigma_c > \tag{2.56}$$

At lower energies the role of shape elastic scattering and compound elastic scattering are significant by using the averaging process. At energy above 10 MeV for heavy and medium nuclei:

$\sigma_{ce} << \sigma_{se} and \sigma_{ce} << \sigma_c. Then < \sigma_{el} > \approx < \sigma_{se} >$. Hence, at higher energies $< \sigma_{ce} > \rightarrow 0$ and at lower energy (below 10 MeV) $< \sigma_{ce} >$ is accountable.

2.1.12 Pre-Equilibrium Model

The detailed explanation to the pre-equilibrium phenomenon is given by the work of J.J Griffin[19] by exciton pre-equilibrium statistical process through exciton model. Simultaneously the Hybrid models is developed in semi classical scenario. The quantum mechanical explanations are given by Feshbach,Kerman

and Koonin by developing the multistep direct reaction (MSD) and Multistep compound (MSC) reaction mechanism.

2.1.13 Exciton Model

The great invention for the understanding of the pre-equilibrium model was done by introducing the exciton model by Griffin[19]. This model expects that the projectile, by interacting with the target, gives rise to a simple arrangement distinguished by a few number of excited particles and holes called excitons (n=p+h). As the transition rate of these excitons and de-excitons are corresponding to the level density required by Fermi's Golden rule. The particle and holes behavior in exciton model as shown in Fig. 2.1. According to Ericson's [20, 21] the level density for exciton number n at excitation energy for p particle and h holes is:

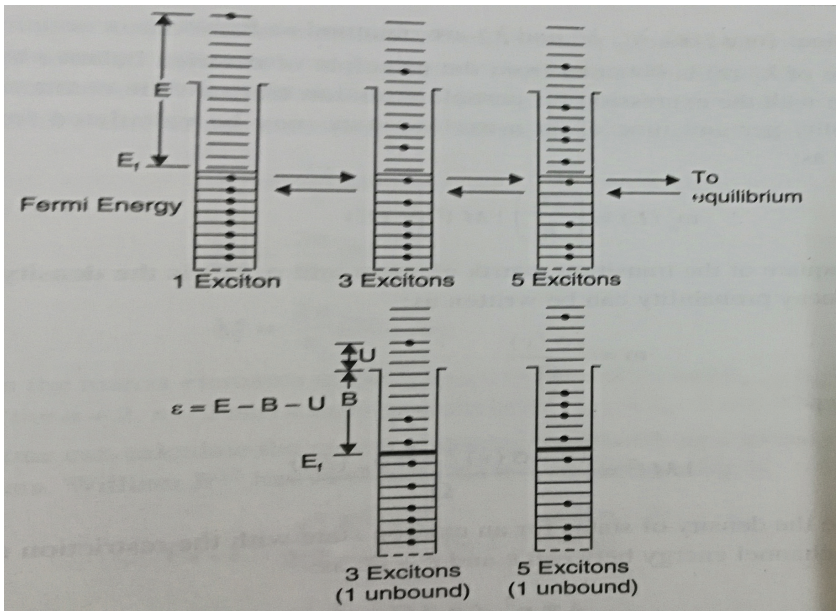

Figure 2.1: Schematic diagram of behaviour of particle and holes in exciton model.

$$\rho_{p,h}(E) = \rho_n(E) = \frac{g^n E^{n-1}}{p!h!(p+h-1)!} \tag{2.57}$$

where p and h are the number of particles and holes and g is the single-particle level density. It is seen that for small value of n, the level density function increases quickly and hence the rate of transition $\delta n = 2$ is larger than the $\delta n = -2$. As n increasing the particle level density moderately levels off, so the transition probability becomes the same ($n = +2$ become same as for $n = -2$) and hence, it is in equilibrium. In this development from $n = 3$ to $\bar{n}$, the particle emission takes place from the given exciton state at any time. Then the energy differential cross section for pre-equilibrium emission may written as:

$$\sigma_{PEQ} = \sigma_{abs} \sum_{\substack{n=n_0 \\ \Delta n=\pm 2,0}} D_n P_n(E) \tag{2.58}$$

where $\sigma_{PEQ} \rightarrow$ Experimentally detected absorption cross-section by the target

$D_n \rightarrow$ Depletion factor (Probability of reaching n exciton state, without prior emission)

$P_n(E) \rightarrow$ Probability of emission of n exciton state of the projectile.

The depletion factor D_n related to the $P_n(E)$ through the equation:

$$D_n = \prod_{n'=n_0} [1 - \int dE P_{n'}(E)] \tag{2.59}$$

The term in the bracket in the above equation giving the net probability of reaching n exciton state after taking into account the depletion of the state due to prior emission. The emission probability can be defined as the ratio of the rate of emission from n exciton state in a particular channel to the sum of the rate of transition to all the states including emission to all channels. If $\lambda_c^n(E)$ is the emission rate from n exciton state to definite channel c with energy E and the emission from n = +2, -2 and 0 transitions are λ_+^n, λ_-^n and λ_0^n respectively.

Then the emission probability can be defined as:

$$P_n(E) = \frac{\lambda_c^n(E)}{\lambda_+^n + \lambda_-^n + \lambda_0^n + \int dE\ \lambda_c^n(E)} \tag{2.60}$$

Then we have to find the expression for $\lambda_c^n(E),\ \lambda_+^n,\ \lambda_-^n\ and\ \lambda_0^n$ as follows.

(i) The $\lambda_c^n(E)$ value can be obtained from the principle of M. Blann et.al[21]. It starts with the emission of particle from the state $n = p + h$. The decay probability can be obtained from the perturbation theory as:

$$w_n(E) = (\frac{2\pi}{\hbar})|M|^2\rho_n(E) \tag{2.61}$$

where M is the transition matrix element and $\rho_n(E)$ is the density of exciton states. With a clear understanding the decay probability can be written as:

$$w = \frac{\nu\ \sigma(\nu)}{\Omega} \tag{2.62}$$

Also we can writte:

$$|M|^2 = \frac{(\hbar\nu\sigma(\nu)/2\pi\rho_n(E))}{\Omega} \tag{2.63}$$

Then the density of exciton state with the limitation that the exciton is in continuum with the energy E and $E + dE$ as:

$$\rho_{n-1}(U) = \frac{4\pi\ p^2\ dp\ d\Omega}{(2\pi\hbar)^3\ dE} \tag{2.64}$$

If the equation 2.64 is substituted for $\rho_n(E)$ in equation 2.61, and also use equation 2.63, then

$$w_n(E)dE = \frac{mE\sigma_{inv}(E)}{\pi^2\hbar^3}\frac{\rho_{n-1}(U)}{\rho_n(E)}dE \tag{2.65}$$

where m is the reduced mass of the ejectile, E is the channel energy and $\sigma_{inv}(E)$ is the inverse cross-section. $\rho_{n-1}(U)$ and $\rho_n(E)$ are the level density of the residual nucleus and composite state (particle and hole) respectively.

Then it can be generalizing the equation 2.61 by considering the number of emitted particle with ν nucleons, hence the $\rho_{n-1}(U)$ can be substituted by $\rho_{n-\nu}(U) = \rho_{n'}(U)$. And also the equation 2.61 multiplied with the spin degeneracy of the emitted particle, i.e. $(2S+1)$. Then it can be recognized that the $\lambda_c^n(E)$ have the same meaning as the $w_n(E)$. Thus the general expression for the emission rate is,

$$\lambda_c^n(E) = \frac{\rho_{n'}(U)}{\rho_n(E)} X \frac{(2S+1)\ m\ \epsilon\ \sigma_{in}\ (\epsilon))}{\pi^2\ \hbar^3} \tag{2.66}$$

where n' is the excitation number after ν nucleon emission, so $n' = n - v$ and U is the residual excitation energy given as $U = E - B - \epsilon$. Then it possible to calculate the pre-equilibrium cross-section using equation 2.58.

ii) Using the Fermi's transition rate rule, the expression for the $\lambda_+^n, \lambda_-^n, \lambda_o^n$ as follows:

$$\begin{aligned}
\lambda_+^n &= \frac{2\pi}{\hbar}\Big|M_+\Big|^2\rho_{n+2} \\
\lambda_-^n &= \frac{2\pi}{\hbar}\Big|M_-\Big|^2\rho_{n-2} \\
\lambda_0^n &= \frac{2\pi}{\hbar}\Big|M_0\Big|^2\rho_0
\end{aligned} \tag{2.67}$$

where $\Big|M_0\Big|, \Big|M_+\Big|, \Big|M_-\Big|$ are the respective transition element in matrix form and ρ_{n+2}, ρ_{n-2} and ρ_0 are the level densities of the state corresponding to the $n+2, n-2$ and n exciton state respectively.

2.1.14 The Hybrid Model

This model is the combination of the Harp-Miller-Berne (HMB) Model and exciton model. The modified form of this model called Geometry Dependent-Hybrid (GDH)[40] model, by considering the surface effect.

So, according to this model the emission cross-section for the nucleons proton and neutron as:

$$\sigma_{P\ E\ Q}(E) = \sigma_{a\ b\ s} \sum_{\substack{n=n_0 \\ \Delta n=\pm 2,0}} D_n P_n^x(E) \tag{2.68}$$

The above equation is in identical with the exciton model, but the only difference is the evaluation of the function p_n^x and it is of the form:

$$p_n^x(E)\ dE\ = f_n^x \left[\frac{g\rho_{n-1}\ (U)\ dE}{\rho_n\ (E_c)}\right] \frac{\lambda_x^n(E)}{\lambda_t^n\ +\ \lambda_x^n(E)} \tag{2.69}$$

where f_n^x denoted the number of x type of exciton in the n exciton state, $\lambda_x^n(E)$ is the emission rate. The ratio $g\rho_{n-1}\ (U)\ dE/\rho_n\ (E_c)$ gives the probability of the number of excitons in a particular state and $g\rho_{n-1}\ (U)\ dE$ is represented as the level density available to the outgoing particle.

Also, the emission rate in the above equation can be described as:

$$\lambda_x^n\ =\ \frac{\sigma_{inv}\ v\ p_c}{g_v\ V} \tag{2.70}$$

Here σ_{inv} is the inverse cross-section, v is the velocity of the particle, g_v is the single-particle density and V is the volume canceled by the same value in ρ_c. In this g_v is made geometry-dependent and is expressed in semi-empirical format as:

$$g_v\ =\ g_v(R)\ =\ \left[\frac{40}{V(r)}\right] \frac{A}{28} \tag{2.71}$$

where V(r) is a nuclear potential and can be expressed as:

$$V(r) = 40\Big[\frac{< d\ (R) >}{\bar{d}}\Big]^{\frac{2}{3}}\ \ MeV \tag{2.72}$$

where 40 MeV is the potential depth in the center of the nucleus and d(R) is the nuclear density factor. Thus introduce the geometry-dependent factor.

2.1.15 Multi-step Direct (M.S.D) and Multi-step Compound (M.S.C) Model

This model was developed by Feshbach,Kerman and Koonin[22] (FKK) and has been extended by Kalbach[23] for the pre-equilibrium reaction mechanism. The counting of levels and particles are done through the quantum mechanical analysis. In this model, the initial stages are developed by considering the excitation process by two-body interactions. The theory behind the Multi-step Direct (M.S.D) model is, that at every excitation there should be at least one particle in the continuum and so there is a finite probability of particle emission per stage. Obviously, the M.S.D model works only in the first few interactions only when the particle just enters the nucleus. The particle momentum is in the direction of the projectile and hence it is peaked in the forward direction.

After a few number of two-body interactions the complete sharing of its energy and momentum has taken place, the excited number of particles will be higher, but the energy per particle is small. Also, at this stage there is no particle in the continuum, but the statistical fluctuation in energy will provide a particle in the continuum. Hence the direction of emission will be either isotropic or symmetric about 90. This corresponds to the Multi-step Compound (M.S.C) nucleus formation, where there is an equilibrium in energy sharing has taken place but the energy per particle in each state is less. In this way this theory of pre-equilibrium explained the energy sharing process through two non interacting chains called P-chain (At least one particle is in the continuum) and Q-chain (All the particles are in the bound state). Hence, after the initial two-body interaction the reaction may proceed through either of the p-chain or Q-chain path.

With all the above consideration, one can get the cross-section as:

$$\sigma_{PEQ} \;=\; \sigma_{MSD}\;(E) \;+\; \sigma_{MSC}\;(E) \tag{2.73}$$

The above equation assumes that there is no interference between the two methods. The values of $\sigma_{MSD}\;(E) and \sigma_{MSC}\;(E)$ are calculated using the quantum mechanical FKK model. The quantum mechanical calculation based on the exciton model gives $\sigma_{PEQ}(E)$ from the following given equation:

$$\begin{aligned} \sigma_{PEQ} \;&=\; \sigma_{abs} \sum_{\substack{n=n_0 \\ \Delta n=\pm 2,0}} D_n\;\lambda_c^n(E)\;T_U(p,h) \\ &=\; \sigma_{abs}\;\sum D_n\;P_n(E) \end{aligned} \tag{2.74}$$

where $p_n(E)$ expressed as in exciton model as:

$$P_n(E) = \lambda_c^n(E)\;T_U(p,h) \tag{2.75}$$

In the above equation both the D_n and λ_c^n have the same functioning as in the exciton model, though the calculations are in different. T_u(p,h) is expressed as:

$$T_u(p,h) = \frac{1}{\lambda_+^n \;+\; \lambda_-^n \;+\; \lambda_0^n \;+\; \int\; dE\;\lambda_c^n(E)} \tag{2.76}$$

Physically the above equation corresponds to the mean life of the n-exciton state with p particle and h holes. While calculating D_n we have to account the P-chain and Q-chain interaction. Therefore to calculate D_n, we replace it by S(p,h), which represent the probability of reaching n-states with a different configuration of p and h. Because P-chain and Q-chain have different S values, it is expressed as:

$$D_n = S_U(p,h) \ + \ S_b(p,h) \tag{2.77}$$

where $S_U(p,h)$ is the probability of having at least one particle in the continuum directly through the P-chain or due to statistical fluctuation from the Q-chain and $S_b(p,h)$ represent the probability of all the particle in the bound state, which doesn't lead to emissions. Similarly, $\lambda_c^n(E)$ is replaced by $\lambda_c^U(E)$. Then in the $\lambda_c^U(E)$ calculation the level density of all the bound and unbound state $\rho_n(E_c)$ is replaced with the level density of all unbound states $\rho^v(p,h,E_c)$ and expressed as:

$$\lambda_c^U(p,h) = \frac{\rho(p-v\ :;h,U)}{\rho^U(p,h,E_c)} \tag{2.78}$$

Then the equation 2.75 is replaced with:

$$\sigma_{PEQ} = \ \sigma_{abs} \sum_{p=p_0}^{\bar{p}} S_U \ (p,h) \ T_U(p,h) \ \lambda_c^U(p,h,E) \tag{2.79}$$

where the summation is now over particle p, with $\bar{p}$ as the number of excited particle in the compound state.

Then one can calculate σ_{MSD} and σ_{MSC} obtained from the equation 2.80 and 2.74. The value of σ_{MSD} can be calculated in a similar manner with the replacement of $S_U(p,h)$ by $S_d(p,h)$, which is the probability for the formation of (p,h) configuration with at least one particle in the continuum. It ensures the system is always in the P-chain prior to the emission and finally contribute to MSD. Then

$$\sigma_{MSD} = \ \sigma_{abs} \sum_{p=p_0}^{\bar{p}} S_d \ (p,h) \ T_U(p,h) \ \lambda_c^U(p,h,E) \tag{2.80}$$

The quantities $S_U(p,h), S_d(p,h), T_U(p,h) and\ \rho^U(p,h,E)$ have been calculated quantum mechanically by Kalbach[23].

2.2 Nuclear Reaction Codes

To validate the data and test the predictive power of the nuclear theories, statistical nuclear reaction models are developed. Computer codes are developed corresponding to specific models. The nuclear reaction computer code with specific nuclear reaction models are used for generating nuclear reaction data and nuclear data analysis. In the present work, theoretical analysis have been done using two independent statistical nuclear reaction computer codes EMPIRE-3.2[24] and TALYS-1.8[25]. It is to be noted that in order to derive unique behaviour of the nucleus and the reactions, analysis has been done using single parameter set for all the reactions over the entire energy range of measurement.

2.3 TALYS 1.8

The TALYS-1.8 nuclear reaction program can provide a complete prediction and simulation of nuclear reactions. It simulates reactions that includes neutron, proton, photon, deuteron, triton, hellium and alpha particles, in the energy region of 1 keV to 200 MeV, by using all the reliable nuclear models. TALYS have two important purposes; First of all, it used as a nuclear physics meachanism to compare nuclear reaction models with experimental result and secondly, nuclear data prediction where no experimental data exists.

The parameter of the nuclear structure and models are executed through an inherent reference library of the Reference Input Parameter Library (RIPL). The predictions are based on the pure theoretical analysis of which the direct reaction, compound nuclear reaction and pre-equilibrium reaction meachanism models. The models utilized are the Hauser-Feshbach model[26] with the width fluctuation correction (WFC) formalism for the compound nuclear reaction mechanism. The level densities performs one of the fundamental factor of nuclear reaction cross-section calculations. One of the major characteristic properties of nucle-

aus/nuclear reaction is dependence of level density with the excitation function. There are different level density models derived from phenomenological analytical function or from microscopic models explained in detail in the above section. The Gilbert-Cameron model is used as default level density model in this work. The optical model is used for the analysis of the direct reaction mechanism. The optical model calculation are performed by the coupled channel code ECIS-97[27] for deformed nuclei and Distorted Wave Born Approximation for spherical nuclei. The optical model potentials (OMP) of Koning and Delaroche[28] for transmission of both neutron and proton. The pre-equilibrium reaction is analyzed using classical exciton model and a powerful phenomenological method by Kalbach[29]. In the exciton model, the default two-component model is considered in the present analysis. Thus the net, pre-equilibrium cross-section for the present reactions are given by the sum of exciton model, nucleon transfer and knock-out reaction contribution. For the different projectile and ejectile particle numbers, the reaction mechanism like, stripping, knock-out and pick-up plays a significant role and it is deal in TALYS with the powerfull model by kalbach[34] which predict in much better for the complex particle cross-section. There are varieties of phenomenological and microscopic level density models[30], of which the Fermi gas model with constant temperature approach[31] is employed in the present case. The TALYS input file have been taken in a right way during the calculations, which includes the following parameters: The essential inputs like the atomic number, mass number, incident energy or energies, different reaction mechanism (direct, compound or pre-equilibrium) and different level density model, various exit channels.

2.4 EMPIRE-3.2

The code EMPIRE3.2 is a nuclear reaction computer code, comprising various nuclear models, designed and developed for calculations in the energy ranges from 1 keV to few hundred of MeV for different projectile particles[21]. The incident particle can be any of the light ions (eg: photon, proton, ... upto alpha) or the

heavy ion. This code accounts for all the major nuclear reaction mechanisms, like direct reaction, compound reaction and pre-equilibrium reaction. Each reaction mechanisms are well deffined by the different nuclear reaction models, such as optical model, Hauser-Feshbach model, Multi-step Direct, NVWY Multi-step Compound and exciton model. Some of the models have been well explained in the above section.

The code EMPIRE makes use of the Hauser-Feshbach model for statistical part of the nuclear reaction. The Hauser-Feshbach performance involves different gamma-ray cascade, multi-particle emission, various gamma-ray strength function including different level density approaches. EMPIRE-specific level densities are described by several models. Presently Fermi gas model with constant temperature[17] is taken for the calculation. At below 5 MeV incident energies the HF model with width fluctuation correction formalism (HRTW formalism[10, 11]) account the correlation of the channels. The Hauser-Feshbach model explicitly takes into account the conservation of spin and parity of each partial wave in each stage of de-excitation. Hence the model helps to evaluate the population of isomeric states and to determine the isomeric cross-section ratio. The pre-equilibrium part of the reaction is carried out with different PE modules, that are used to serve the emission of particle or gamma's before the attainment of equilibrium. The exciton model formalisms (DEGAS or PCROSS) for the classical approach and NVWY model[13] based on MSD, MSC[14] (Multi-Step Direct, Multi-Step Compound) approach for pre-equilibrium mechanism in the quantum mechanical regim. The selection will be done on the order of preference in the input lines. The exciton model can be enabled using mean-free path parameter, can be chosen from 1.02 to 2. However, in the present case, MFP=1.5 is found to better reproduce the experimental data over the measured range[10]. The direct reaction contribution can be accumulated using the optical model. Depending on the nature of target, the calculation can be proceed with the distorted-wave Born approximation for spherical nuclei (Spherical optical model) or the coupled-channels model for the deformed nuclei (deformed

optical model). The particle transmission coefficients were generated via the optical model of Koning and Delaroche[15] for neutrons and protons, and also McFadden and Satchler[16] for alpha particles.

Further, an exhaustive library of input parameters RIPL (Reference input Parameter Library) covers various inputs, such as nuclear masses, gamma ray strength functions, optical model parameters, discrete levels and decay schemes, ground state deformations, level densities, moments of inertia and fission barriers etc. The results produced in the ENDF format is internationally accepted format for nuclear reaction data. The comparative plots with the experimental data from EXFOR can also produce using this code.

2.5 Nuclear Data Libraries

The evaluated proton cross-section data serve as the backbone of data for nuclear applications. The interested incident energy covers an extremely large energy range. There is no simple way to interpret the physics of proton interacting with atomic nuclei throughout this broad range of energies and different nuclei. comparatively, nuclear physics uses different ways and many distict models to discuss underlying physics. The published peer-reviewed experimental data and different theoretical results on proton-nuclear reactions are compiled by several nuclear data agencies worldwide.

The experimental nuclear reaction database, such as EXFOR (Experimental Nuclear Reaction Data)[35] keep experimental nuclear reaction data and their bibliographic information, as well as the information about the authors, institute and the detaile measurements and analysis in a compressed way. The history (e.g., whom the data is compiled and the last update dates), and the status (e.g., the common deatils of the experiment, the source of the data) of the data set is also included in this format. Sometimes a huge amount of data may be inconsistent and is to be evaluated before they can be used - for example - in medical purposes and in reactor physics calculations. Such kind of assessment consists in the judgment and comparison of experimental data, validation, evaluation

of the systematic errors and statistical errors, checking for internal consistency and uniformity with standard proton cross-sections,etc. At the end the process adopted values, obtained by appropriate averaging procedure, are borrowed. The author often compare experimentally measured cross-sections with the nuclear model calculated data (with EMPIRE [24] or TALYS [25]) in favour of a single complete data set. Due to the enormous number of different variables included in the evaluation process, it includes the arbitrary experimental data and of the nuclear model parameters, several different evaluated data files are compiled and managed in worldwide.

The important general purpose libraries are managed by the following libraries (and their countries)

I) Evaluated Nuclear Data File (updated in December 2011) (ENDF/B-VII.1) [36]- USA.

II) Joint Evaluated Fission and Fusion Library. The updated version (JEFF-3.1.2)[37] is released in February 2012. - Europe.

III) Japanese Evaluated Nuclear Data Library (JENDL4.0), updated version is released in May 2010 [38]. - Japan.

IV) China Evaluated Nuclear Data Library (CENDL-3.1), released in 2009 [39].- China.

Bibliography

[1] Friedlander, G., Kennedy, J.W., Macias, E.S., and Miller, J.M.Nuclear Reactions. Nuclear and Radiochemistry, A willey- Interscience Publication,John Willey and Sons, 1981.

[2] Arthur Beiser: Perspective of Modern physics, McGraw-Hill Book, New york-1969.

[3] S.B. Patel An introduction to Nuclear physics (1991), University of Bombay, John Wiely, New Delihi, India.

[4] S.T.Buttler:Phy.Rev.80,1095(1950); Nature 166, 709 (1950); Proceedings of Roy.Society (London) 208A, (1951)559.

[5] N.Bohr, Nature,137(1936)344.

[6] S.N Ghosal, Phys.Rev.80(1950)939

[7] K.Chen, G.Friedlander, G.D Harp, J.M.Miller : Phys.Rev.166(1966)949

[8] H. Ejiri et al., Nucl. Phys. A 305 (1978) 167.

[9] V. F. Weisskopf and D. H. Ewing, Phys. Rev., 57(1940)472.

[10] H.M.Hotmann, J.Richert, J.W.Tepel, and H.A.Weidenmuller, Ann Phys 90(1975)403

[11] H.M.Hotmann, T.Mertelmeier, M. Hermann and J.W.Tepel, Z .Physik A 297(1980)153

[12] H. A. Bethe, Rev. Mod. Phys. 9(1937)69.

[13] A.J. Koning, S. Hilaire, M.C. Duijvestijn, AIP Conf. Proc. 769 (2005) 1154.

[14] A.J. Koning, M.C. Duijvestijn, A global pre-equilibrium analysis from 7 to 200 MeV based on the optical model potential, Nucl. Phys. A 744 (2004) 15.

[15] J. Ernst, W. Friedland and H. Stockhorst, Z. Physik., A328(1987)333.

[16] H.Feshbach, C.Porter and V.F Weisskopf., Phy.Rev.96,448(1954)

[17] H.S.Hans and S.C.Snowdon., Phy.Rev.108,1028(1957)

[18] R.D.Woods and O.S.saxon:Phy. Rev. 95, 577 (1954)

[19] J. J. Griffin, Phys. Rev. Lett., 17(1966)478.

[20] T.Ericson:Advances in physics,25 (1960).

[21] M.Blann: Annual Reviews of Nuclear Sciences V.25,123 (1975).

[22] H.Feshbach, A.kerman and S.Koonin:Annls Physics, (N.Y), 125, 429 (1980)

[23] C.Kalbach: Phy. Rev.C23, 124 (1981); Phy. Rev.C24, 819 (1981); Phy. Rev.C37, 2350 (1988)

[24] M. Herman, R. Capote, M. Sin, A. Trkov, B.V. Carlson, P. Oblozinsk y, C.M. Mattoon, H. Wienke, S. Hoblit, Young-Sik Cho, G.P.A. Nobre, V.A. Plujko and V. Zerkin, EMPIRE-3.2 Malta- modular system for nuclear reaction calculations and nuclear data evaluation, INDC(NDS)-0603 BNL-101378-2013.

[25] A.J. Koning, S. Hilaire, S. Goriely, TALYS-1.8, Nuclear Reaction Program, Nuclear Data Section, IAEA, Vienna, December 26 2015.

[26] Hauser, W., Feshbach, H. The Inelastic Scattering of Neutrons. Phys. Rev. 87 (1952) 366-373.

[27] J. Raynal, Notes on ECIS94, CEA Saclay Report No. CEA-N-2772, (1994).

[28] A.J. Koning and J.P. Delaroche, Nucl. Phys. A713, 231 (2003).

[29] C. Kalbach, Phys. Rev. C 37, 2350 (1988).

[30] A.J.Koning, S.Hilaire and M.C.Duijvestijn, AIP Conf. Proceedings.769(2005) 1154.

[31] A.J. Koning and M.C. Duijvestijn, A global pre-equilibrium analysis from 7 to 200 MeV based on the optical model potential, Nucl. Phys. A 744, 15 (2004)

[32] H. Feshbach, A. K. Kerman and S. Koonin, Ann. Phys (NY).,125(1980)429.

[33] H. Nishioka, J. M. Verbaarschot, H. A. Weidenmuller, and S. Yoshida,Ann. Phys.,172(1986)67.

[34] Kalbach, C. Pre equilibrium reactions with complex particle channels. Phys.Rev. C 71 (2005) 034606-34629.

[35] IAEA-EXFOR. Experimental Nuclear Reaction Data, Available online at: http://www-nds.iaea.org/exfor

[36] Chadwick, M.B., Herman, M. ENDF/B-VII.1 Nuclear Data for Science and Technology: Cross-sections, Covariances, Fission Product Yields and Decay Data. Nuclear Data Sheets, 112 (2011) 2887-2996.

[37] Koning, A.J., et al. The JEFF evaluated data project, in Proc. of the International Conf. on Nuclear Data for Science and Technology, Nice, 2007.

[38] Shibata, K., et al. JENDL-4.0: A New Library for Nuclear Science and Engineering. J. Nucl. Sci. Technol. 48 (2011) 1-30.

[39] Tang, Y., Shi, Z.M., Yu, B.S., Chen, G.C. China Evaluated Nuclear Data Library CENDL-3.1, 2009.

[40] M. Blann, Phys. Rev. Lett., 27(1971)337.

Chapter 3

Experimental Technique

3.1 Introduction

The aim of modeling of nuclear reactions is to get knowledge on the properties of the nucleus. To check the validity of any of the theoretical prediction it is needed to have extensive data of different parameters through different experimental techniques. The nuclear reaction is carried out by an accelerated projectile beam hitting on a target nucleus. The reaction residue can be identified online or offline measurement methods. In online measurement, the emitted particles are detected by a spectroscopic setup placed on a particular angle from the beam path to receive the outgoing particles at that angle exposing a small solid angle subtended by the area of the detector. Similarly, the residual nucleus produced in the nuclear reaction are identified by the detection of recoiled nucleus using suitable detectors for each reaction channel. On the other hand, in the offline analysis the reaction residue is identified by following the activities induced in the sample. This is typically done by measuring the energy and intensities of characteristic gamma rays. Thereby determining the residual nucleus quantitatively and qualitatively. However, in this technique it is limited to isotopes having measurable half-life, typically of the order of a few minutes to a few years. The off-line technique offers good selectivity, sensitivity and simplicity. Hence, the method of activation analysis has been followed in the present measurement.

In the present analysis stacked foil activation method[1] has been employed. In order to get a strong basis, the interested nuclear data are taken from the available literature. In the present case, The experiment has been performed at the Tata Institute of Fundamental Research (TIFR), Mumbai, India, using the 14UD pelletron accelerator. The stacked foil activation technique has been employed. The activities induced in each sample were exposed to a low background 100 cc HPGe detector coupled to the ORTECs PC based multichannel analyzer at the TIFR.

3.2 Pelletron Accelerator

The experiment has been performed at the Tata Institute of Fundamental Research (TIFR), Mumbai, India, using the 14UD pelletron accelerator. In view of its installment, this has been used for the basic research in the nuclear, atomic and material science fields as well as in the accelerator applications. The TIFR has been functioning as a prime facility for light ion as well as heavy ion accelerator-based research work in India. There are various researchers at the application level using this facility at present. Accelerator is the vital part in the nuclear physics research work. A brief description of the accelerator is given:

The charged particle source is placed at the top of the tower. The different beams provided by the ion sources are: (i) direct extraction duo plasmatron (DEDP), (ii) rf source and (iii) SNICS (source of negative ions with Cs sputtering). The cesium sputtering source generates negative ions, which is accelerated in lower energies (150- 250 keV) for a small region. It is then bent through 90^0 vertical accelerating region using an injector magnet. As of the first stage, the negative ion is accelerated due to the electrostatic attraction of the high voltage at the center of the vertical tower. The high voltage is developed at the terminal is due to the chain of steel pellet and hence it named as pelletron accelerator. Secondly, the negative ion acquire a high positive charge by releasing an electron while passing it through the carbon foil or a very small volume of the gas in the terminal. The average charge depends on the ions and the terminal voltage.

Figure 3.1: The pelletron beam hall

Then the high energy positive terminal voltage will act as a repulsive force on the positive ion to accelerate either to the pelletron area or to the LINAC are using two-way analysing magnet. The analysed beam is then directed to one of the beamline in the pelletron experimental hall. The energy (E) of the analysed ion is related to the magnetic field (B) of the analysing magnet given as:

$$B(Gauss) = 720.76\frac{\sqrt{AE(MeV)}}{n} \tag{3.1}$$

Where A is the mass of the analyzed ion and n is the charge state.

Thus the final energy of the ion of charge state n is $(n+1)V_T$, Where V_T is the terminal voltage (the maximum voltage for this accelerator is 14MV)

3.3 Target

To perform a nuclear experiment a thin, isotropic target is a major and demanding requirement. Various techniques such as vacuum evaporation, electrodeposition, rolling, etc. are employed to prepare isotopic targets for experi-

ments. In the present experiment, the rolling method is used and is performed at target laboratory of Bhabha Atomic Research Centre-Tata Institute of Fundamental Research (BARC-TIFR) Pelletron Facility, Mumbai. Generally Stainless steel plates were used in rolling mill to avoid the contamination. The samples used in the present experiment are self-supported natural indium, cadmium and aluminum foil as a degrader. A small square shape thin foil of dimension $10mm\ X\ 10mm$ was cut with a knife. The thickness of the target was calculated, by measuring the weight and area of the square plate target. The thickness of the natural indium metal foil was 13 mg/cm^2 and the thickness of the natural cadmium metal foil was 5 mg/cm^2. The aluminum foils of 2.97 mg/cm^2 mass thickness was used as energy degrader. The samples are mounted on the ladder as a stack.

3.4 Irradiation

The stacked foil activation method is used in the present study of proton-induced reaction cross-section measurement. In this method, a number of the target materials are placed in the form of a stack. Aluminium foil of suitable thickness was inserted between the sample to have the desired energy falling on each samples. Also, the foil is used as backing. In single irradiation, a large number of target nucleus can be irradiated to different incident energies using this method. In the present analysis, for cross-section and isomeric cross-section measurement, stacks were irradiated for 1.28-hour long time, keeping in view the half-lives of medical interested isotopes. The schematic diagram of the stack is as follows and is given in figure 3.2.

The stacks were irradiated using a proton beam, of energy 22 MeV and an average current of 23 nA using the Pelletron accelerator, Mumbai (India). The incident energy reported is the mean energy falling on each sample accounting for the mean energy loss over the sample and the energy degradation in the samples and the other degrading foils in the stack. Energy degradation was calculated using the simulation code SRIM[2, 3]. The beam current was monitored contin-

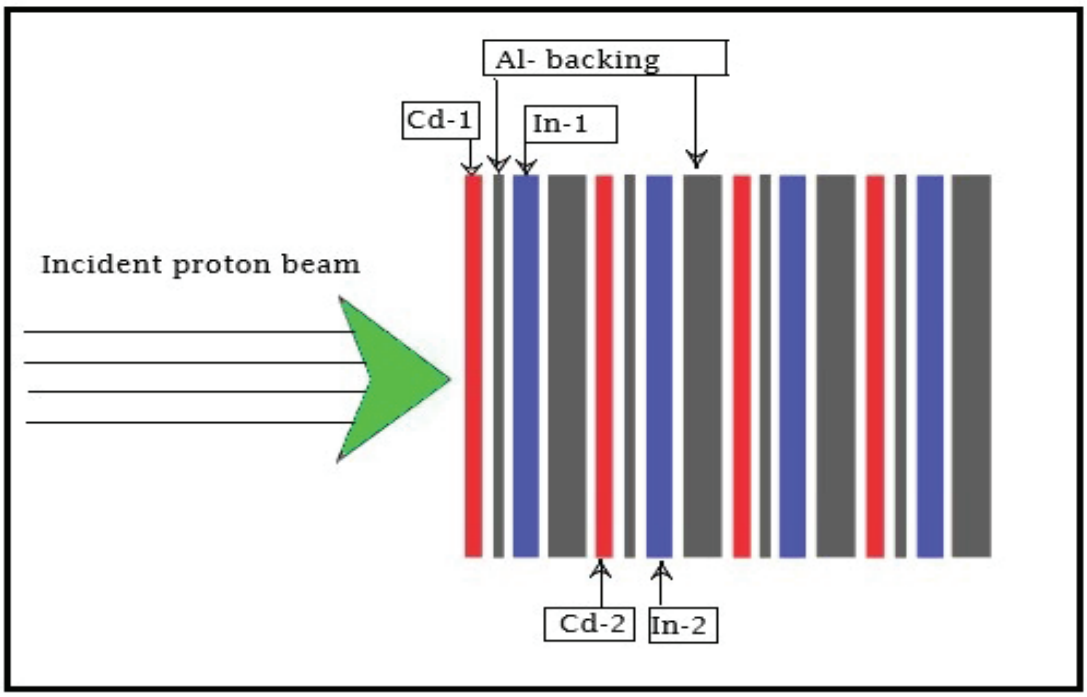

Figure 3.2: Typical sample arrangement in stacked foil activation technique

uously through a current integrator connected to the Faraday cup kept behind the target stack. Thus, the mean energies incident on each sample were 21.96, 21.82, 17.89, 17.68, 12.89, 12.68, 8.89 and 8.61 MeV. The error indicated in the table for energy is the sum of the inherent uncertainty in the beam energy and the energy spread in the thickness of the sample as well as aluminum degraders.

3.5 Detector

The Radiation detectors perform a vital role in any of the experimental nuclear reaction procedures. They are the necessary requirement to detect and characterize the qualities of radiations ejected in nuclear reactions. The fundamental requirement for any of the detectors is its high detection efficiency and a fine energy resolution. The field of radiation detector design, fabrication, the data processing technique, recording technique and the analysing method is ex-

panding and has advanced very quickly. In the stacked foil activation method, two techniques are used to analyse the irradiated targets. One is the 1) Beta counting method and the other is 2) Gamma counting method. In the present study, the activities induced in each sample were followed using a low background 100 cc HPGe detector coupled to the ORTECs PC based multichannel analyzer at the TIFR, which is one of the semiconductor detectors with high energy resolution. A semiconductor detector is simply a highly doped p-n junction diode. As we know, the semiconductor material germanium is selected for gamma-ray spectroscopy, because of the higher atomic number (Z). The fact that the photopeak efficiency varies as Z^5. The depletion region in the p-n junction diode is the active region of the detector.

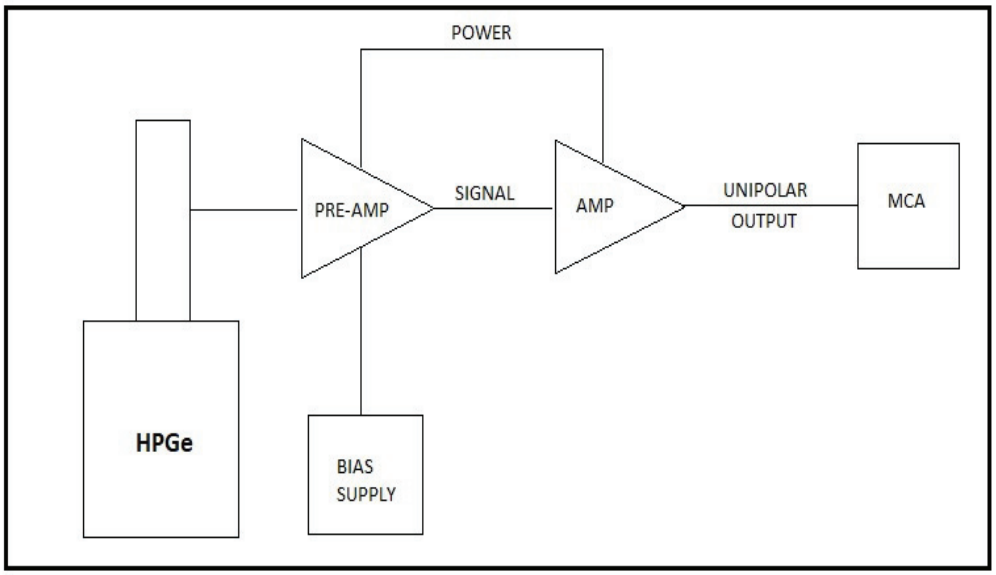

Figure 3.3: The block diagram of gamma ray spectroscopy

A schematic diagram of gamma-ray spectroscopy is shown in Fig 3.3. It consists of a detector, a pre-amplifier connected with the detector, high voltage

power supply, an amplifier and a multichannel analyzer for storing and characterizing the data.The first module in a detection processing block is a pre-amplifier working as an intermediate between the detector and the signal processing electronics. The pre-amplifier helps to converts the ionisation charge produced in the detector during the absorbed event to a step function output pulse and its amplitude is proportional to the total charge developed in that event. The output signal from the pre-amplifier is delivered to the amplifier. The amplifier is not only used for the signal amplification but also used to shape the signal into better spectroscopic performance. There should be an external high voltage for the proper operation of the detector and is called bias supply. The output pulse from the amplifier is fed to the multichannel analyzer (MCA). It is an instrument to examine and determine each pulse to which category it should fit, that is the number of counts in channels. Depending upon the type of MCA, the number of channels is different, but the standard device rage from 1024 to 8192 channels. Finally, it is monitored in a PC. The geometry dependent efficiency of the detector for various gamma energies at fixed geometry was determined using standardized ^{152}Eu point source, which was also used for the calibration of the detector system.

3.6 Data Analysis

With the above detector, a typical gamma-ray spectrum of the activated indium sample irradiated with mean proton energy 21.8 MeV is shown in figure 3.4. The activities of the following isotopes (produced in respective channels) ^{115m}In ((p,p)), ^{114m}In ((p,pn)), ^{113m}In((p,p),(p,3n)), ^{113}Sn ((p,n),(p,3n)) and ^{111m}Cd ((p,nα)) have been identified from their characteristic gamma-rays. Similarly, the typical portion of the gamma-ray spectrum of the activated cadmium sample is also shown in figure 3.5. For the sake of clarity, only the region from 100 keV to 500 keV has been included in the plot. The activities of the isotopes, ^{116m,115m,113m,112g,112m,111g,111m,110m,110g,109g} In and ^{111m,105} Cd have been identified from the characteristic gamma-ray spectrum.

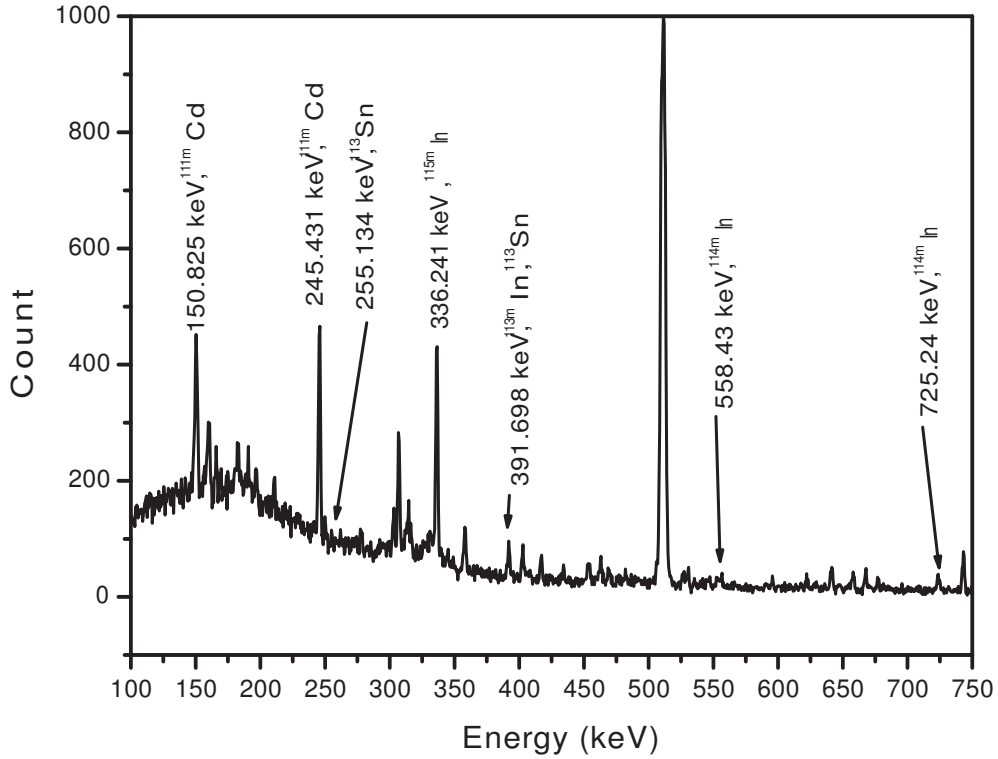

Figure 3.4: Spectrum from Indium irradiated with 21.8 MeV proton.

3.7 Formulation

Let the target contains N_0 number of nuclei irradiated with a beam of flux (ϕ), then the number of activation is given by,

$$N = N_o \phi \sigma_r \tag{3.2}$$

Where $\sigma_r$is the reaction cross-section of the nuclei. The irradiated sample (radioactive) will decay the residual nuclei simultaneously. If suppose t_1, t_2, t_3 are respectively the irradiation time, the cooling time and the counting time of the sample. Then the induced activity during the time t_1 is :

$$\left[\frac{dN}{dt}\right]_t = \frac{\sigma_r \phi N_0 \{1 - exp(-\lambda t_1)\}}{exp(\lambda t_2)} \tag{3.3}$$

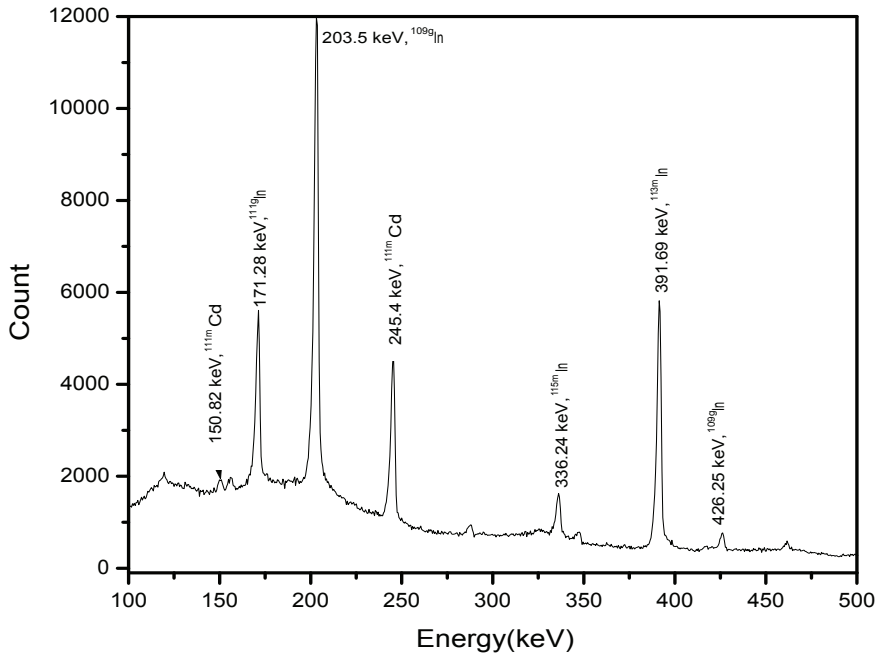

Figure 3.5: Spectrum from Cadmium irradiated with 21.96 MeV proton.

Then, the number of nuclei decayed in t_2 *to* $(t_2 + t_3)$ is given by,

$$\frac{dN}{dt} = \frac{\sigma_r \phi N_0 \{1 - exp(-\lambda t_1)\}\{1 - exp(-\lambda t_3)\}}{exp(\lambda t_2)} \tag{3.4}$$

Where λ is the decay constant and $t_{1/2}$ is the half-life of the residual nucleus. If the activity is detected by a detector of geometry dependent efficiency G_ϵ, then the absolute counting rate C and the observed rate A are related as follows,

$$C = \frac{A}{(G_\epsilon)\theta K} \tag{3.5}$$

where θ is the branching ratio of the gamma-ray and K is self-absorption correction factor of the sample and is given by,

E MeV	^{115m}In (mb)	^{114m}In (mb)	$^{115}In(p,p2n)^{113m}$In (mb)	$^{113}In(p,p)^{113m}$In (mb)
8.61 ± 0.5	$1.18 \pm .1$	-	-	$1.68 \pm .3$
12.68 ± 0.4	6.91 ± 0.7	1.2 ± 0.2	-	$4.28 \pm .43$
17.68 ± 0.37	14.8±1.3	43.8±4.6	-	$5.39 \pm .5$
21.82 ± 0.23	19.3±1.7	85.9±7.7	19.16±1.7	-

Table 3.1: Cross section for proton induced reaction on ^{nat}In forming ^{115m,114m,113m}In, residual nucleus

$$K = \frac{[1 - exp(\mu d)]}{\mu d} \tag{3.6}$$

where μ and d are the gamma-ray absorption coefficient and the thickness of the sample respectively. Thus from the above equations, we get,

$$\sigma_r = \frac{A\lambda exp(\lambda t_2)}{N_0 \phi \theta K G_\epsilon \{1 - exp(-\lambda t_1)\}\{1 - exp(-\lambda t_3)\}} \tag{3.7}$$

Where A represents the total number of activities counted under the corresponding gamma peak, λ is the decay constant of the particular residual nucleus, ϕ is the incident proton flux, N_0 is the number of the target nuclear isotope per unit area of the irradiated sample, G_ϵ geometry dependent efficiency of the detector for the given gamma-ray energy, θ is the branching ratio of the particular gamma-ray, K is the self-absorption correction factor for the gamma-ray in the sample and t_1, t_2, t_3 are respectively the irradiation time, the cooling time and the counting time of the sample.

Thus, the reaction cross-sections measured in the respective cases (proton induced on indium and cadmium) for each incident energy are calculated and are tabulated in tables 3.1, 3.2, 3.3 and 3.4.

E MeV	$^{113}In(p,n)^{113}$Sn (mb)	$^{115}In(p,3n)^{113}$Sn (mb)	^{111m}Cd (mb)
8.61 ± 0.5	381 ± 40.4	-	-
12.68 ± 0.4	415 ± 49.2	-	$0.08 \pm .007$
17.68 ± 0.37	143±12.8	-	1.02±0.1
21.82 ± 0.23	-	171±15.4	3.9±0.4

Table 3.2: Cross section for proton induced reaction on ^{nat}In forming ^{113}Sn and ^{111m}Cd.

E (MeV)	^{116}Cd(p,n)# ^{116m}In (mb)	^{116}Cd(p,2n)# ^{115m}In (mb)	^{nat}Cd(p,x) ^{113m}In (mb)	^{nat}Cd(p,x) ^{112g}In (mb)
8.96 ± 0.5	132 ± 17.4	53.35 ± 4.9	102.73 ± 13.12	252.65 ± 33.7
12.95 ± 0.4	30.2 ± 3.86	149.8 ± 13.18	150.58 ± 16.37	448 ± 59.09
17.89 ± 0.4	24.54 ± 2.3	235.64 ± 18.85	174.46 ± 16.66	91.34 ± 11.9
21.96 ± 0.2	20 ± 2.2	180.5 ± 13.52	145.58 ± 13.03	89.01 ± 9.57

Table 3.3: Cumulative reaction cross-section in (mb) for the ground and isomeric state of the specific residual nucleus ^{116m,115m,113m,112g}In. # Cross-section for the specific reaction channel for the ^{116m,115m}In residual nucleus without mixing channels.

E (MeV)	^{nat}Cd(p,x) ^{112m}In (mb)	^{nat}Cd(p,x) ^{111g}In (mb)	^{nat}Cd(p,x) ^{111m}In (mb)	^{nat}Cd(p,x) ^{110g}In (mb)
8.96 ± 0.5	70.83 ± 8.4	243 ± 26.7	186 ± 26.8	29 ± 3.5
12.95 ± 0.4	526 ± 57.23	308 ± 27.7	241.01 ± 31.3	42 ± 3.8
17.89 ± 0.4	256.29 ± 24.23	408 ± 28.5	220 ± 29	486 ± 43.2
21.96 ± 0.2	311.92 ± 27.67	699 ± 47.46	197 ± 23.68	617 ± 54.3

Table 3.4: Cumulative reaction cross-section in (mb) for the ground and isomeric state of the specific residual nucleus ^{112m,111g,111m,110g}In.

E (MeV)	^{nat}Cd(p,x) ^{110m}In (mb)	^{nat}Cd(p,x) ^{109g}In (mb)	^{106}Cd(p,pn)$^{\#}$ ^{105}Cd (mb)	^{nat}Cd(p,x) ^{111m}Cd (mb)
8.96 ± 0.5	205 ± 24.4	9 ± 1.3	-	4 ± 0.5
12.95 ± 0.4	613 ± 54.5	88 ± 8.7	10 ± 1.3	15 ± 1.9
17.89 ± 0.4	1230 ± 110.7	698 ± 76.8	665 ± 79.8	57.8 ± 7
21.96 ± 0.2	1110 ± 109.9	1052 ± 95	949 ± 116.5	102 ± 10

Table 3.5: Cumulative reaction cross-section in (mb) for the specific residual nucleus ^{110m,109g}In and ^{105,111m}Cd. # Cross-section for the specific reaction channel for the ^{105}In residual nucleus without mixing channels.

3.8 Detailed error analysis

The uncertainty mentioned in the measured cross-section is the sum of both the statistical and systematic errors. The systematic errors may be due to the following factors (a) non-uniform deposition of the target material, (b) beam current fluctuation, (c) statistical uncertainty in the gamma counting, (d) gamma spectrometer efficiency, (e) loss of beam intensity due to the passage through the target stack materials, (f) dead time loss etc. A detailed error analysis of a similar measurement is given in reference[4].

1. The error in the number of target nuclei: The error in the number of target nuclei may occur due to the imperfect measurement of thickness and due to the erratic deposition of the target material. The thickness of the target was calculated by measuring the weight using an electronic balance and the area of the target. The average error measured in the present samples is expected to be $\approx 3\%$

2. The error due to the beam current fluctuation: During the long run of the proton beam, the beam current fluctuates slightly which results in the deviation of incident flux. The necessary arrangements have been done to make the beam current constant. However there is slight change in the beam current noted during the run time, the flux has calculated in individual duration of fluctuation. The changing flux was used in the cross-

section measurement. With the above consideration, the error due to the varying flux is approximately 2%.

3. Statistical uncertainty in the gamma counting: This error may arise due to the uncertainty in the efficiency of the gamma-ray spectroscopy. The uncertainty in gamma counting was minimised by assembling a large number of counts for comparatively large time $\approx$ 3600 sec. This error may be due to the solid angle effect of the sample. Thus the overall uncertainty in gamma counting in the present analysis is to be 0.5%.

4. Dead time loss: The dead time loss arises due to the imperfect placing of the sample and the detector. In the present measurement, it is suitably adjusted and the whole error is found to be $> 1\%$.

5. Loss of beam intensity due to the passage through the target stack materials: During the irradiation of the sample stack, the beam passes through the thickness of the sample material and the beam intensity may decrease. This varying intensity may introduce certain uncertainty, and it is around 0.9%

Apart from the above uncertainty, the error from the decay constant, branching ratio has been taken from the IAEA isotope browser and from the table of isotopes.

Bibliography

[1] E. V. Sayre, Ann. Rev. Nucl. Sci., 13(1963)145.

[2] J. P. Biersack and L. Haggmark, Nucl. Instr. and Meth.,vol. 174, 257, 1980

[3] "The Stopping and Range of Ions in Matter book by J.F. Ziegler , volumes 2 - 6, Pergamon Press, 1977-1985

[4] M.M.Musthafa, B.P.Singh, M.G.V.Sankaracharyulu, H.D.Bhardwaj, and R.Prasad, Phys. Rev. C 52 (1995) 6.

Chapter 4

Result and Discussion

4.1 Proton irradiation on natural indium

In this section, the analysis of the experimental cross-section data of proton induced on natural indium reaction is being discussed. The reaction cross-section produced via different channels $^{115}In(p,p)^{115m}$In, $^{115}In(p,pn)^{114m}$In, $^{115}In(p,p2n)^{113m}$In, $^{113}In(p,p)^{113m}$In, $^{115}In(p,3n)^{113}$Sn, $^{113}In(p,n)^{113}$Sn and $^{115}In(p,n\alpha)^{111m}$Cd have been measured, at incident proton energies from 8.61 to 21.82 MeV. The cross sections calculated for the above isomers are tabulated in Table 3.1 & 3.2. The data are analyzed using the statistical model code EMPIRE[1] and TALYS[2] having an optimized parameter set. The data are compared with the data available in the literature[3][4] and are plotted through figures 4.1-4.9 as a function of proton energy. The nuclear decay data such as energy, spin and parity, half-lives and decay modes for the above nuclei are tabulated in Table 4.1. The calculation of isomeric cross section ratio has been carried out in respective cases. Each case has been analyzed in detail in the following section.

4.1.1 $^{115}In(p,p)^{115m}$In Reaction

Figure 4.1 shows the experimental cross-section data for the formation of metastable state (4.486h) of ^{115m}In along with theoretical calculation and avail-

Nuclide	Half life	Ground state Spin/Parity	Metastable state Spin/Parity	E_γ (keV)	I_γ (%)
^{115m}In	4.486 h	9/2+	1/2-	336.24	45.8
^{114m}In	49.51 d	1+	5+	190.27	15.56
				558.43	3.2
				725.24	3.2
^{113m}In	99.476 min	9/2+	1/2-	391.698	64.94
^{111m}Cd	48.50 min	1/2+	11/2-	150.825	29.1
				245.395	94
^{113}Sn	115.09 d	1/2+	7/2+	225.134	2.11
				391.698	64.97

Table 4.1: Decay characteristic of the investigated reaction product.[5]

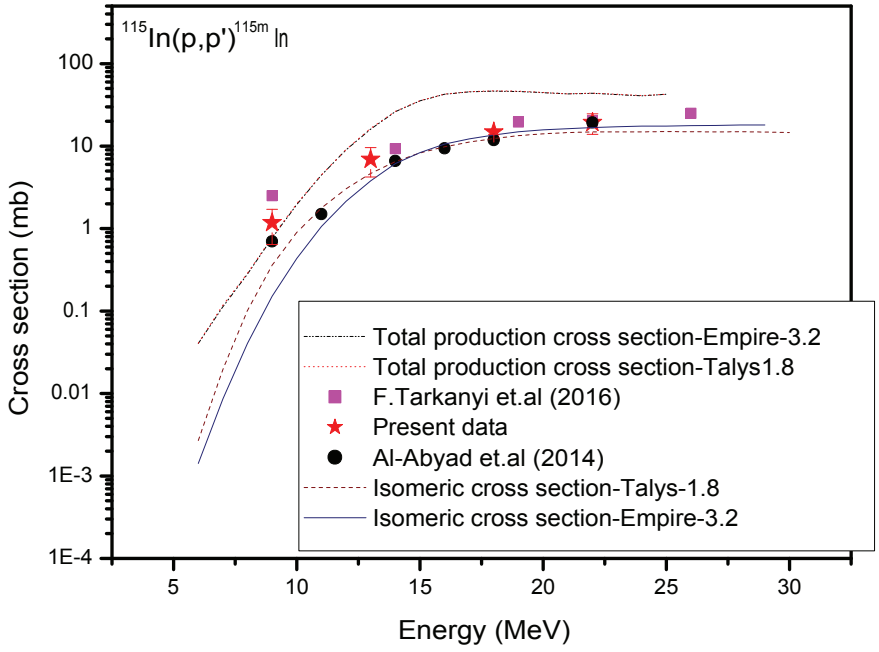

Figure 4.1: Experimentally measured and theoretically calculated excitation functions for the reaction $^{115}In(p,p)^{115m}$In.

able literature data at various incident energies. The ICR calculated for this reaction is plotted in fig 4.2. In this case both the theoretical value and measurement of F.Tarkanyi and Al Abyed[3][4] matches with present data. Lower energy point shows a slight discrepancy in all the cases, where the theoretical

calculations slightly underestimate the measured data. The ground state of this isotope is a stable state and hence the cross section for the ground state population could not be measured. Hence, for the sake of completeness, the total production cross section is also plotted for the case of ^{115}In (Ground + Isomeric) using TALYS and EMPIRE. Both the codes give an identical representation of cross-section.

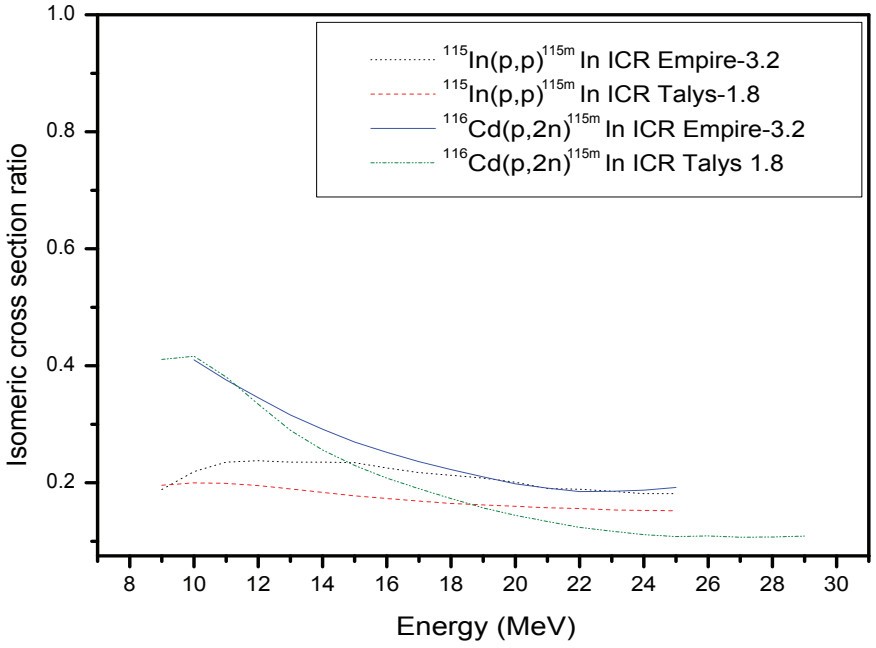

Figure 4.2: Theoretical isomeric cross section ratios for the isomeric pair ^{115m}In produced through different reactions $^{115}In(p,p)^{115m}$In and $^{116}Cd(p,2n)^{115m}$In are plotted as a function of the incident proton energy.

In the case of isomeric cross-section measurement, the ICR shows more or less constant relative population of about $\approx$ 20% to isomeric state (I=1/2+) and $\approx$ 80% ground state(I=9/2+) favouring population of the high spin state for energy above 10 MeV. Higher spin state population increases very slightly with energy. In order to see the effect of multiparticle emission, the ICR for the same nucleus is calculated, as a typical case, for (p,2n) channel. It is found to be decreasing steadily from 0.42 at $\approx$ 10 MeV to around 15% for energy above 22 MeV. This

indicates that multiparticle emission has a critical command on spin distribution as well as the population states. Considering the nature of prediction of models, there is a slight discrepancy in the predictions of TALYS and EMPIRE models. The code EMPIRE predicts a slight enhancement of isomeric state with energy in the beginning and gradual favouring of high spin state with incident energy.

4.1.2 $^{115}In(p,pn)^{114m}$In Reaction

The excitation function measured and calculated, using TALYS and EMPIRE, for the reaction $^{115}In(p,pn)^{114m}$In are shown in figure 4.3 along with literature data[3][4]. ^{114m}In nucleus may be produced through two different reaction channels viz (p,d) and (p,pn) with threshold energies 6.8 MeV and 9.11 MeV. The cross-section is comparable in the lower energy region for both the channels, whereas in the higher energy region,(p,pn) channel contribution is 10 times larger than the (p,d) cross-section. The code TALYS1.8 provides distinct data for both the channels. Whereas code EMPIRE does not separate out them. Since the present case employs activation technique, it is not possible to separate out the two-channel experimentally. Hence (p,d) cross-section and (p,np) cross-section could not be analysed separately. However the entire production for this isotope is considered to be (p,pn) and (p,d) channels and the analysis has been done accordingly.

Also the radioisotope ^{114}In has two metastable states with an energy of 190.3 keV(49.5d) and 502 keV (43.1ms). Isomeric state of 502 keV decays, with a half-life of 43.1ms, to the isomeric state of 190.3 keV. In the present measurement, gamma counting is done after 57 minutes, 502 keV meta-stable state has been completely decayed to 190.3 keV meta-stable state. ^{114m}In(49.51d), which decay to ground state with 96.7% IT. The ground state has the lifetime of 71.9 seconds. Hence the measured isomeric population is the sum of the population of these two isomeric states. The data reported by F.Tarkanyi et.al and the theoretical value are in agreement with present data. Lower energy point shows the slight discrepancy for the present measurement as well as literature data, where the

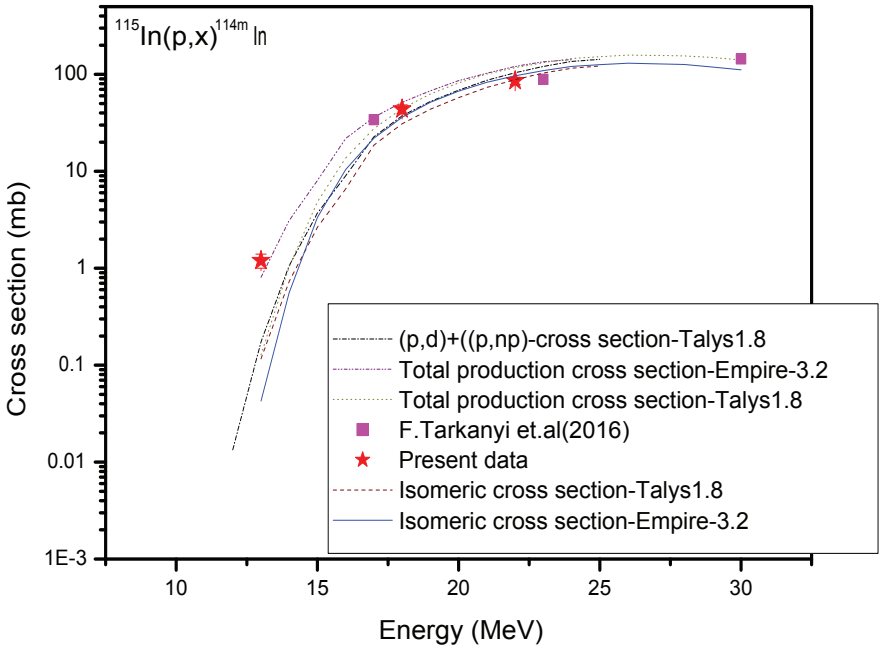

Figure 4.3: Experimentally measured and theoretically calculated excitation functions for the reaction $^{115}In(p,pn)^{114m}$In.

predicted data is slightly lower than the measured data. For the sake of completeness, the total production cross section is also plotted for the case of ^{114}In (Ground + Isomeric) using TALYS and EMPIRE. Both the code shows a similar trend.

The isomeric cross-section ratio for ^{114m}In deduced from theoretical models are plotted in figure 4.4. The ICR shows more or less steady population of $\approx$ 75% isomeric state at 13 MeV (I=5+, $t_{1/2}$ = 49.5d) and $\approx$ 25% for ground state (I=1+) using TALYS and $\approx$ 60% and $\approx$ 40% respectively for EMPIRE calculation favouring the high spin state. The ICR shows a slightly increasing trend with energy for the population of the higher spin state. To see the effect of single particle emission and multiparticle emission ICR are calculated for (p,n) channel and (p,pn) channels. (p,n) channel shows a steady increase of ICR from threshold up to 13 MeV and after that, it reaches more or less steady state (80% high spin state). For (p,pn) emission ICR shows a steady state trend at about

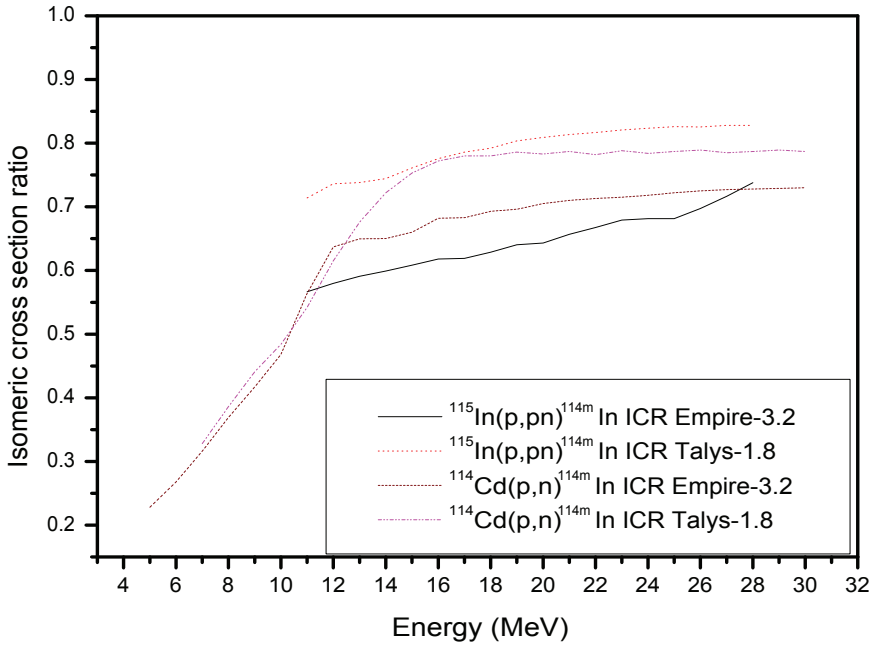

Figure 4.4: Theoretical isomeric cross section ratios for the isomeric pair ^{114m}In produced through different reactions $^{115}In(p,pn)^{114m}$In and $^{116}Cd(p,3n)^{114m}$In are plotted as a function of the incident proton energy.

$\approx$ 80% favouring high spin state, from the threshold itself. In this case, the multiparticle emission is not found to reduce ICR in the case of TALYS whereas it follows the general trend of reducing the higher spin population at higher state for multiparticle emission.

4.1.3 ^{nat}In(p,x)^{113m}In, ^{113}Sn

The isotope ^{113}Sn may be formed through two different reactions $^{113}In(p,n)^{113}$Sn and $^{115}In(p,3n)^{113}$Sn with threshold energies 1.82 MeV and 18.133 MeV respectively. It has one isomeric state with the half life 21.4 minute and the ground state has the half-life of 115.09 days. The isomeric state decay to ^{113}Sn with 91.7% IT-producing gamma ray of 77 keV(I_g=0.5) which could not be identified, separately, due to low energy as well as very low intensity. The ground state will decay to In^{113m} producing a characteristic gamma ray 391.7 keV and

255 keV with branching ratio I_g= 64% and 2.11% respectively. Further ^{113m}In is produced through the reactions $^{113}In(p,p)^{113m}$In in the lower energy region and $^{115}In(p,p2n)^{113m}$In and $^{115}In(p,nd)^{113m}$In with threshold of 16.45 MeV & 14.2 MeV respectively in the higher energy region. As discussed in the previous section (4.2), (p,nd) and (p,2np) cross-section have been calculated separately using code TALYS1.8. In 20 MeV, (p,nd) reaction is significantly larger.

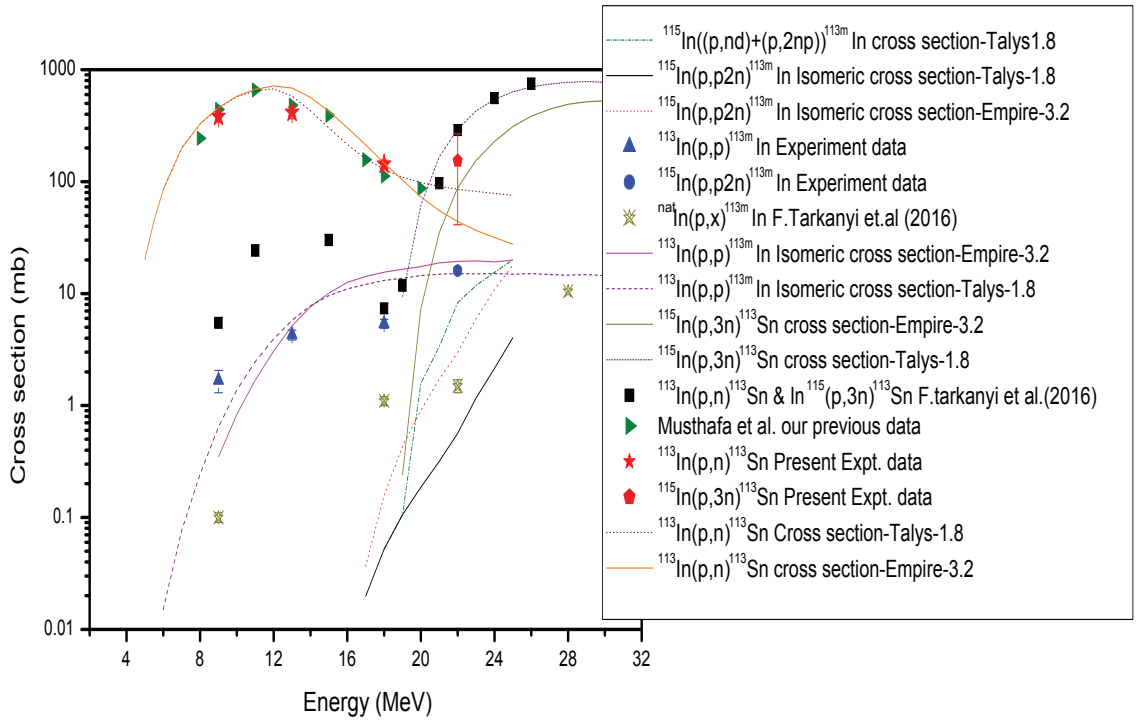

Figure 4.5: Experimentally measured and theoretically calculated excitation functions for the reaction $^{113}In(p,n)^{113}$Sn, $^{115}In(p,3n)^{113}$Sn, $^{115}In(p,p2n)^{113m}$In and $^{113}In(p,p)^{113m}$In.

However after 22 MeV (p,2np) channel supersedes the (p,nd) channel, even up to 10 times, beyond 28 MeV. This indicates that the deuteron formed either by pick up or deuteron as a cluster during the equilibration process withstands disintegration even at higher excitation energies. ^{113m}In has one isomeric state with half life 99.476 minutes and a stable ground state. The isomeric state decays to ^{113}In with 100% IT-producing a gamma ray of 391.7 keV. Hence the observed

activity of 391.7 keV gamma will be the contribution from the production of ^{113m}In and $^{113m+g}$Sn. The contribution from each can be distinguished with reference to the second gamma energy 255 keV (2.8%) of ^{113}Sn. The corresponding contribution of ^{113}Sn in 391.7 keV gamma ray is separated out. The remaining contribution is considered to be from ^{113m}In. Considering all the above factors, excitation functions have been calculated experimentally and theoretically for $^{113m+g}$Sn and ^{113m}In and are shown in figure 4.5 along with the literature data[3]. Calculations using TALYS and EMPIRE reproduce the present measured data for both $^{113m+g}$Sn and ^{113m}In. Using the theoretical analysis the contribution from ^{113}In(p,n) and ^{115}(p,3n) for ^{113}Sn and ^{113}In(p,p) and ^{115}In(p,p2n) for ^{113m}In are separated and are plotted in fig 4.5.

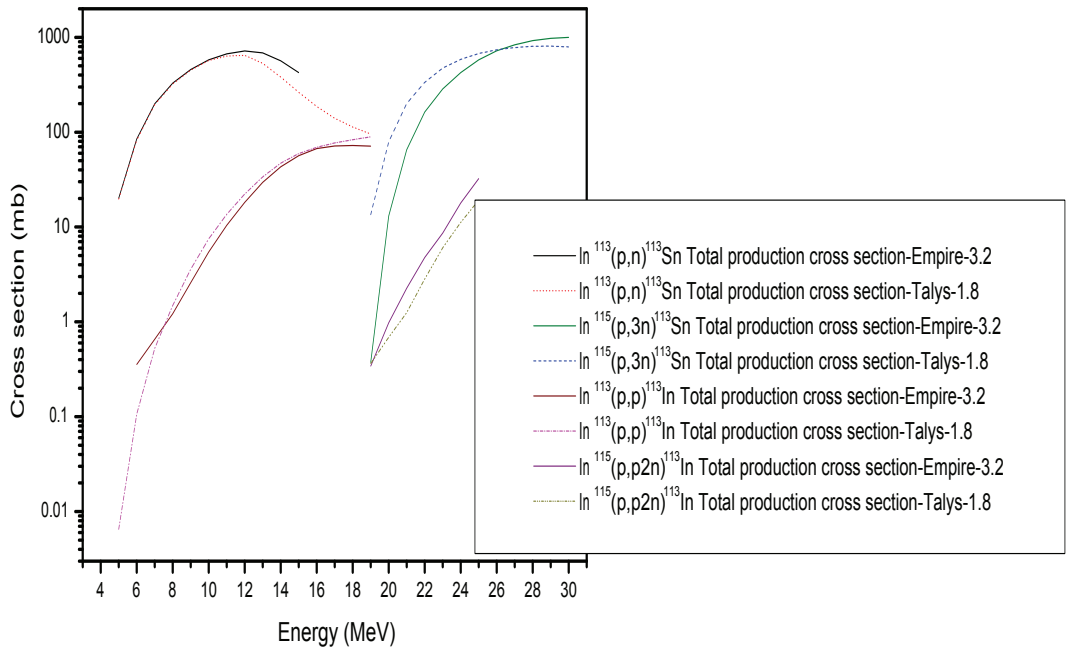

Figure 4.6: Theoretically calculated total excitation functions for the reaction $^{113}In(p,n)^{113}$Sn, $^{115}In(p,3n)^{113}$Sn, $^{115}In(p,p2n)^{113m}$In and $^{113}In(p,p)^{113m}$In.

The previous measurement of M.M Musthafa et.al[6] has reported a slightly higher cross section and this may be due to the fact that, the measurement has been done from the activity of 391.7 keV alone and counted after two half-life

of the ^{113m}In. Due to this, the contribution of ^{113m}In is not properly accounted for in their measurement. Hence, it shows a small over prediction from the data. By properly deducting the contribution of ^{113m}In the data is also in line with the present measurement. Therefore the present data is better suited for preparing evaluated data library.

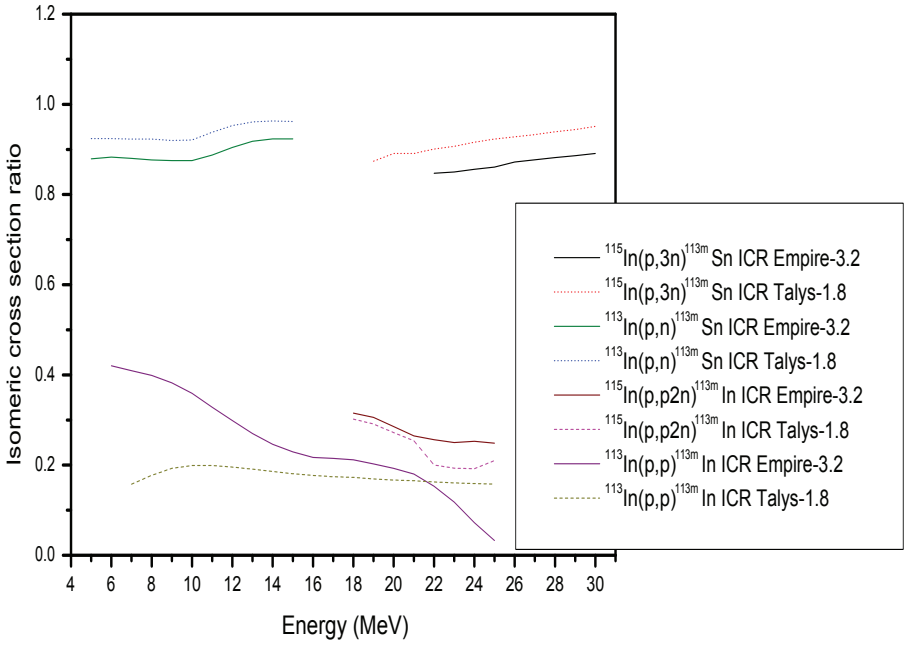

Figure 4.7: Theoretical isomeric cross section ratios for the isomeric pair ^{113m}Sn and ^{113m}In produced through different reactions $^{113}In(p,n)^{113}$Sn, $^{115}In(p,3n)^{113}$Sn, $^{115}In(p,p2n)^{113m}$In and $^{113}In(p,p)^{113m}$In.

The data reported by F.Tarkanyi et.al shows a significantly lower, of more than one order, in both the cases. However, the theoretical representation(TENDL) and experimental data differ significantly in their report[3]. This may be due to the systematic error of the measurement and approximations mentioned. For the sake of completeness total excitation function for these reactions, $^{113}In(p,n)^{113}$Sn, $^{115}In(p,3n)^{113}$Sn, $^{113}In(p,p)^{113m}$In and $^{115}In(p,p2n)^{113m}$In are plotted in fig 4.6 using both the codes TALYS and EMPIRE. The ICR for this two case have been calculated and are shown in fig 4.7.

In the case of isomeric production of ^{113}Sn through different channels, the isomeric cross section ratio shows a steady population of ≈ 85% of isomeric state(I=7/2+) and ≈ 15% ground state(I=1+) favouring the population of the higher spin metastable state. A slightly higher population of the isomeric state is seen in the case of single particle emission than multiparticle emission. This indicates that multiparticle emission carries away larger angular momentum. In the case of ^{113m}In nucleus production through different channels, the population in the higher spin, ground state (I=9/2+) is favoured ≈ 85% than the low spin metastable state(I=1/2+, $T_{1/2}$=99.5 m) at 391.7 keV, here also multiparticle emission slightly reduces the population of higher spin state. However, TALYS calculations show a steady population of ICR with incident energy, whereas EMPIRE calculation indicates that higher spin state is favoured as the incident energy increases.

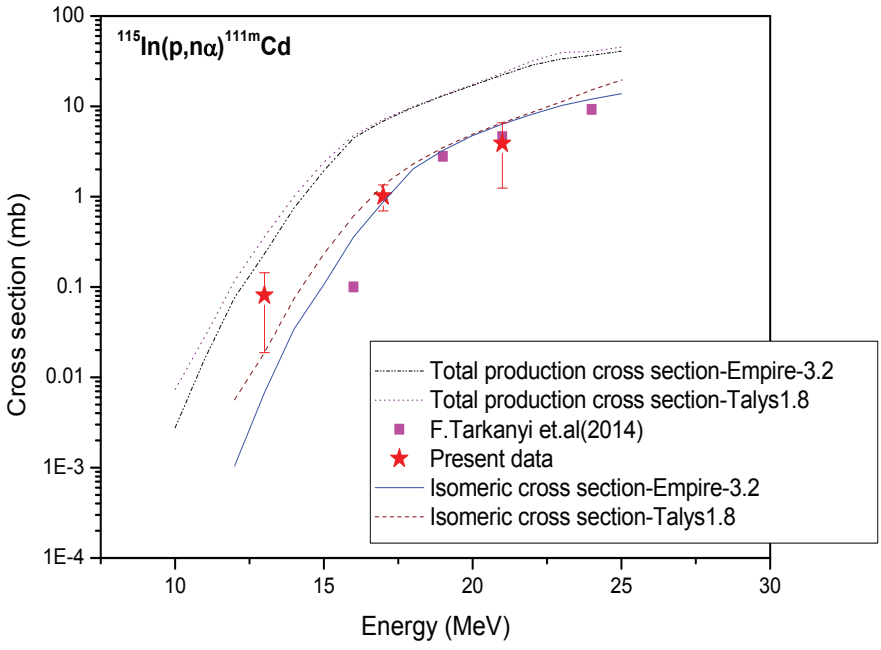

Figure 4.8: Experimentally measured and theoretically calculated excitation functions for the reaction $^{115}In(p,n\alpha)^{111m}$Cd.

4.1.4 $^{115}In(p, n\alpha)^{111m}$Cd Reaction

The nucleus ^{111m}Cd is produced through ^{115}In(p,nα) reaction with a threshold energy of 3.491 MeV. The isotope ^{111}Cd has one isomeric state with a half-life of 48.5 minutes decays directly to its stable ground state by 100% IT. Being stable state the cross section for the population of ground state could not be measured. Hence the observed activity and the measured cross sections represent the population of the isomeric state (^{111m}Cd). Excitation function thus measured for the reaction is plotted in fig.4.8 along with theoretical calculation and literature data[3]. Both the theoretical data and literature data are in satisfactory agreement with the present data. For the sake of completeness excitation function for the total reaction cross section ($^{111m+g}$Cd) is also plotted in the same figure. The isomeric cross section ratio calculated for this case is plotted in fig.4.9.

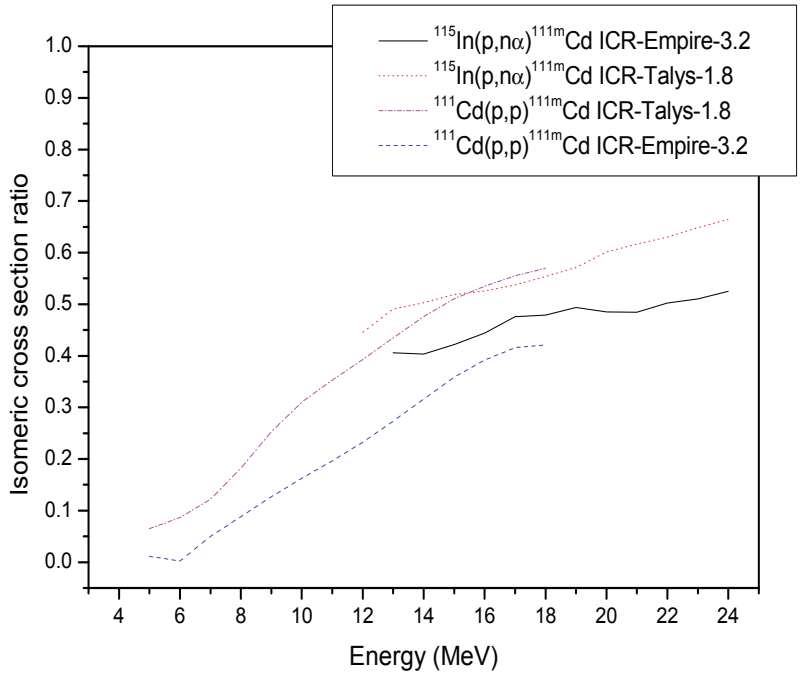

Figure 4.9: Theoretical isomeric cross section ratios for the isomeric pair ^{111m}Cd produced through different reactions $^{111}Cd(p,p)^{111m}$Cd and $^{115}In(p,n\alpha)^{111m}$Cd are plotted as a function of the incident proton energy.

In the case of ^{111m}Cd isotope production, the isomeric cross section ratio shows a population of $\approx 60\%$ of the isomeric state(I=11/2-)at energy 15 MeV and $\approx 40\%$ ground state(I=1/2+) favouring the population of higher spin metastable state with a small increasing trend with energy.

4.2 Proton irradiation on natural Cadmium

In this section, the analysis of the excitation function for the proton induced nuclear reaction on natural cadmium has been done. The isotopes produced via different reaction channels have been measured separatly at the incident energy ranges from 8.96 - 21.96 MeV and are analyzed with the statistical nuclear reaction model codes EMPIRE-3.2[1] and TALYS-1.8[2]. The nuclear decay data such as energy, spin and parity, half-life and decay modes for the above nuclei are tabulated in Table 4.2[5] Many of the evaporation residues formed in these reaction channels have isomeric states with half-life of a few minutes and hours. Isomeric cross-section ratio are also calculated in such cases. The measured excitation functions for the reactions listed in table 3.3 and 3.4 and the relevant isomeric cross-section ratios are plotted through figures 4.10-4.28 along with theoretically calculated data with optimization of parameter sets for code EMPIRE and TALYS. The literature data, wherever available are also plotted in respective figures. In the case of isotopes produced from different channels, due to the varying natural abundance of target isotopes the contribution for the production of the desired isotopes and hence the observed intensities of gamma rays, will be the sum of the contribution from each channel and is given as follows.The observed intensity of each gamma ray $A = A_1 + A_2 + A_3 + ...$ which is proportional to $\sigma_1 N_1 + \sigma_2 N_2 + \sigma_3 N_3 + ...$, where A is the observed total intensity of the gamma ray, A_1, A_2, A_3, etc are the intensities contributed from channels 1,2,3,etc respectively to the total observed intensity, $\sigma_1, \sigma_2, \sigma_3$, etc are the cross-sections for the respective channel and N_1, N_2, N_3, etc are the number of nuclei per unit area of the target isotope corresponding to the respective channel. Hence, the contribution to the gamma ray intensity from each channel is deduced accordingly from the known natural abundance of individual target isotope and theoretically calculated cross-section for each channel at the respective energies. A detailed discussion of the individual cases has been done in the following sections.

Nuclide	Half-life	Ground state Spin/Parity	Metastable state Spin/Parity	E_γ (keV)	I_γ (%)
^{116m}In	54.29min	1+	5+	416.86	27.7
				1097.33	56.2
				1293.56	84.4
^{115m}In	4.49 h	9/2+	1/2-	336.24	45.83
^{113m}In	99.476 min	9/2+	1/2-	391.698	64.94
^{112g}In	14.88 min	1+	4+	617.52	1.0
^{112m}In	20.67 min	1+	4+	156.61	13.33
^{111g}In	2.80 d	9/2+	1/2-	171.28	90.6
				245.35	94.1
^{111m}In	7.7 min	9/2+	1/2-	537	87
^{110g}In	4.9 h	7+	2+	641.68	25.9
				657.76	98.3
				884.69	92.9
				937.50	68.4
^{110m}In	69.1 min	7+	2+	657.76	98
^{109g}In	4.2 h	9/2+	1/2-	203.3	74.2
				623.8	5.64
				1148.5	4.67
				426.3	4.05
^{111m}Cd	48.50 min	1/2+	11/2-	150.825	29.1
				245.395	94
^{105}Cd	55.5 min	5/2+		346.87	4.2
				1302.46	4

Table 4.2: Decay characteristics of the investigated reaction products.[5]

4.2.1 $^{106}Cd(p,pn)^{105}$Cd reaction cross-section

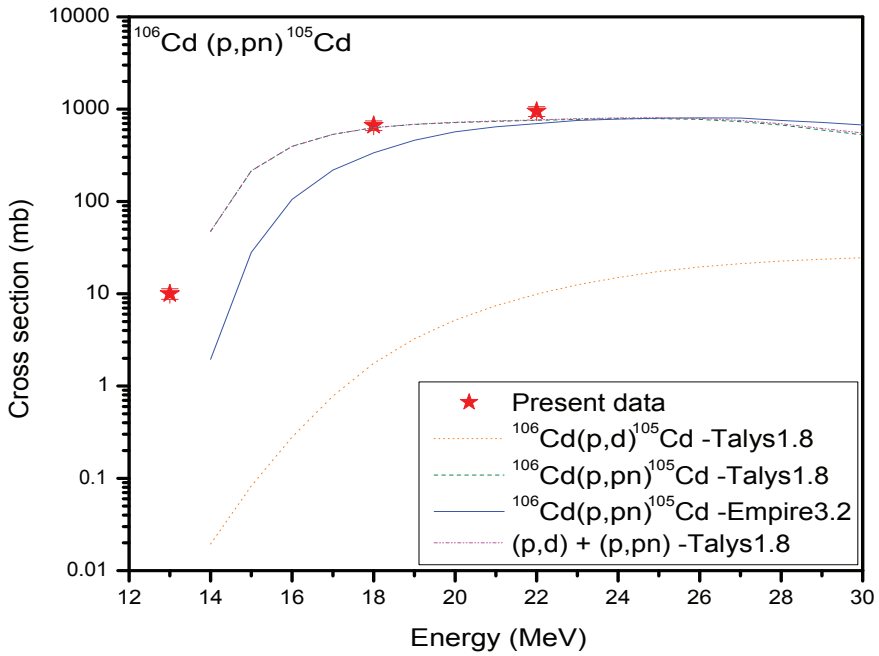

Figure 4.10: Experimentally measured and theoretically predicted excitation function for the ^{105}Cd isotope.

FIG.4.10 shows the measured excitation function for the production of ^{105}Cd in the present experiment along with the theoretically calculated excitation functions. This cross-section produced for the first time. The isotope ^{105}Cd is populated directly via two different reaction channels ^{106}Cd(p,d), ^{106}Cd(p,pn) with threshold energies 8.727 MeV and 10.973 MeV respectively, and which cannot be separated experimentally using activation method. The cross-sections for (p,d) and (p,pn) channels, over the energies, have been calculated separatly using the code TALYS and are also shown in the figure 4.10. It is to be noted that the contribution from the (p,d) reaction channel is $\approx$ 100 times lower than the (p,pn) reaction channel which is much below the experimental uncertainty. Hence, for the sake of data tabulation, the measured cross-section is considered to be a contribution from (p,pn) channel alone. The theoretical prediction of EMPIRE

is lower estimating the data at lower energy. However, the code EMPIRE does not calculate the production of (p,d) and (p,pn) channel separatly. Hence, for the sake of completness, the total production cross-section is also plotted.

4.2.2 $^{nat}Cd(p,x)^{109g}$In reaction cross-section

The isotope ^{109g}In has ground state half-life of ($t_{1/2}$= 4.159 h) and two short-lived isomeric states, ^{109m_1}In ($t_{1/2}$= 1.34 m) and ^{109m_2} ($t_{1/2}$= 210 ms). These two isomeric states decay to the ground state by 100% isomeric transition (IT). Thus the measured cross-section, theoretically predicted data and literature data [7–10] are shown in FIG.4.11. As the gamma-ray counting process has started after 57 minutes, the measured cross-section is considered as the total cross-section of both the states have almost completely decayed to the ground state. Hence, the ground state activity represents the total production of the ^{109}In isotopes.

This isotopes can be formed through the competing different reaction channels ^{108}Cd(p,γ), ^{110}Cd(p,2n) and ^{111}Cd(p,3n) with threshold energies 0 MeV, 12.82 MeV and 19.86 MeV respectively. Hence, the activity at 8.96 MeV is purely contributed by (p,γ) channel. The measured cross-section at 12.95 MeV and 17.89 MeV may have the contribution from both the (p,γ) and (p,2n) channels. In comparison with the TALYS calculation it is seen that the contribution from (p,γ) channel is $\approx$ 0.2% in both the energies and still lesser at higher energies. This is, however, much less than the experimental uncertainty. Hence, the observed yields at these points are considered to be from (p,2n) channel alone. Hence the cross-section reported is the cross-section for ^{110}Cd(p,2n)^{109g}In reaction. At 21.96 MeV it has the contribution from (p,2n) and (p,3n) channels. Calculation using TALYS shows that the observed yield has $\approx$ 80% contribution from (p,2n) channel and $\approx$ 20% from (p,3n) channel. Hence, the contribution of these two channels is deduced accordingly. The EMPIRE calculation in the case of (p,γ) and (p,3n) are significantly lower estimating the data. And in the case of (p,2n) it is significantly lesser at low energy, even by the best optimisation of the parameters.

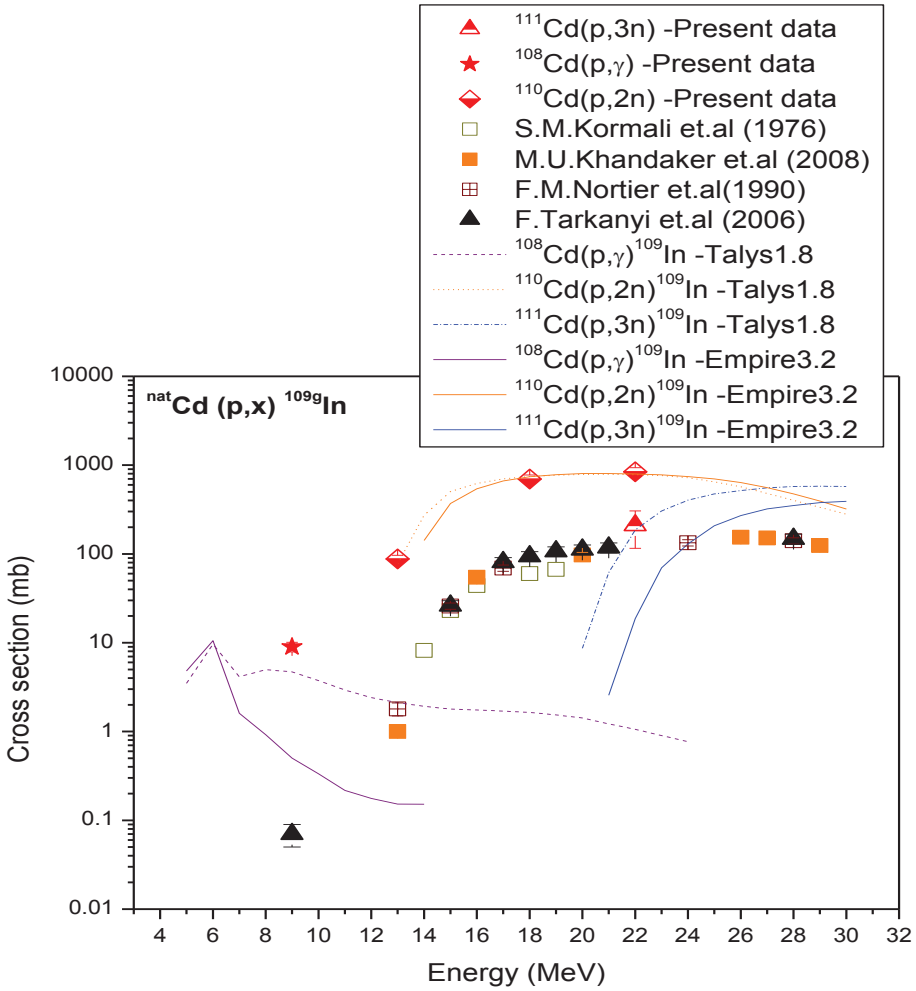

Figure 4.11: Experimentally measured and theoretically predicted excitation function for the ^{109}In isotope.

The data reported by F.Tarkanyi et.al[7], M.U.Khandaker et.al[8] F.M.Nortaire et.al[9] and S.M Kormali et.al[10] are found to be the total yield (cumulative cross section) of particular residue since their data renormalized by the abundance of natural cadmium for each reaction channels, agree with the present measurement. The shape of the theoretical excitation function follows well with the measured data.

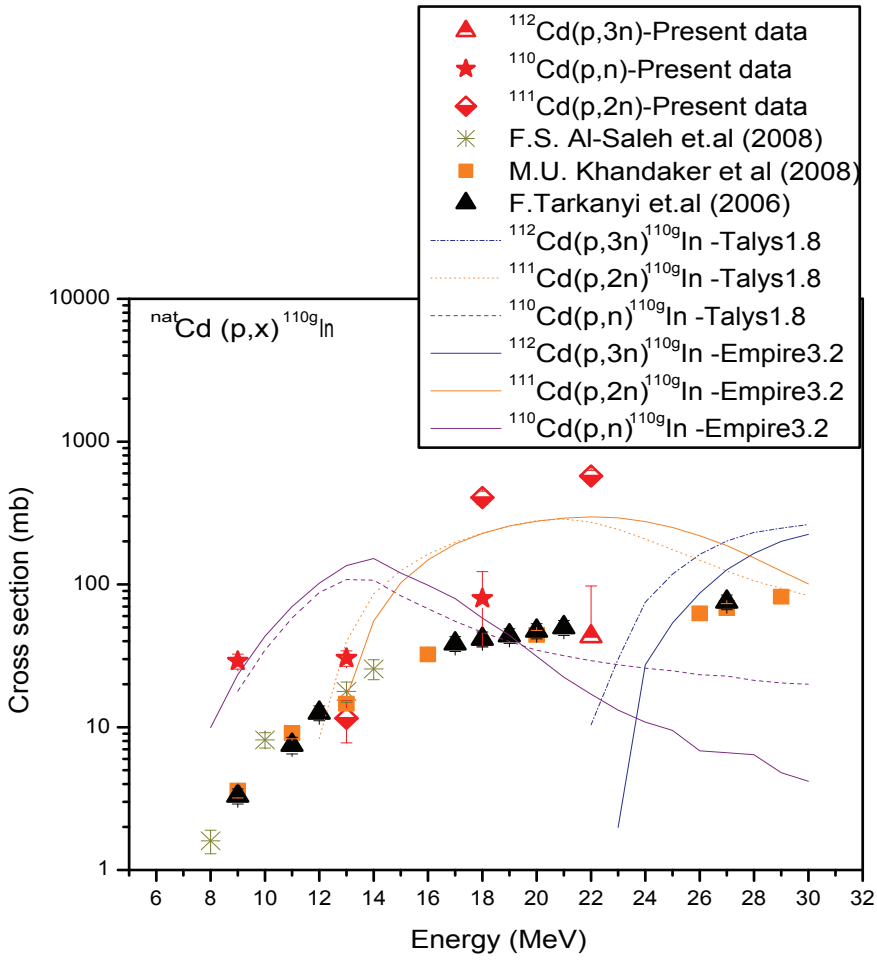

Figure 4.12: Experimentally measured and theoretically predicted excitation function for the ^{110g}In isotope.

4.2.3 $^{nat}Cd(p,x)^{110g,110m}$In reaction cross-section

The production cross-section for this reaction channel $^{nat}Cd(p,x)^{110g,110m}$In is very much interesting and at the same time very much complicated due to the mixing of channels and decay gammas. The ^{110g}In and ^{110m}In can be produced through the competing channels ^{110}Cd(p,n), ^{111}Cd(p,2n) and ^{112}Cd(p,3n) with threshold energies 4.703 MeV, 11.741 MeV, 21.219 MeV respectively. In both the case of ^{110g}In and ^{110m}In , the yield at 8.96 MeV is purely from the ^{110}Cd(p,n) channel alone. The production cross-section at 12.95 MeV and 17.89 MeV may

be the contribution from both the ^{110}Cd(p,n), ^{111}Cd(p,2n) reaction channels. In the case of ^{110g}In, on comparison with the TALYS calculation, the observed contribution has ≈ 72.5% contribution from (p,n) channel and ≈ 27.5% from (p,2n) channel at 12.95 MeV. At 17.89 MeV, the observed yield has ≈ 83.6% contribution from (p,2n) channel and ≈ 16.4% from (p,n) channel. Similarly, at 21.96 MeV it has the contribution from (p,2n) and (p,3n) channels. Calculation using TALYS shows that the observed yield has ≈ 93% contribution from (p,2n) channel and ≈ 7% from (p,3n) channel. For the ^{110m}In case, the observed contribution has ≈ 86% from (p,n) channel and ≈ 14% from (p,2n) channel at 12.95 MeV. At 17.89 MeV, the observed yield has ≈ 91.3% contribution from (p,2n) channel and ≈ 8.7% from (p,n) channel. Similarly, at 21.96 MeV the observed yield has ≈ 96% contribution from (p,2n) channel and ≈ 4% from (p,3n) channel. Hence, the contribution from each channel separated accordingly in all the cases.

The ^{110}In isotope has two isomeric states with the ground state of half-life 4.9 hour and short-lived metastable state with a half-life 69.15 minute both of which decay to stable ^{110}Cd isotope by electron capture(EC)/ β+ emission. Observed high intense gamma-ray of 657.76 keV (I_γ=98%) is the characteristic gamma-ray of both the states. Further, the same is also a characteristic gamma-ray of ^{110m}Ag which may be produced through ^{114}Cd(p,αn) reaction channel. Hence, the activity of 657.76 MeV is complicated and could not be used explicitly for any of the channel. Thus, the production of ^{110g}In is calculated from the other characteristic gamma-rays of energies 884.69 keV (I_γ=93%), 937.5 keV (I_γ=68.4%) and 641.68 keV (I_γ=26%). Similarly, the production of ^{110m}In is calculated from the characteristic gamma-rays of energies 2129 keV (I_γ=2.15%), 2211 keV (I_γ=1.74%) and 2317 keV (I_γ=1.28%) and the cross-section for ^{110m}Ag is calculated using 677.62 keV (I_γ=10.7%) and 687 keV (I_γ=6.53%) gammas.

The experimental excitation function for the reaction $^{nat}Cd(p,x)^{110g,110m}$In thus calculated are plotted in FIG.4.12 and FIG.4.13 respectively along with theoretical predictions and the available literature data[9, 11, 12]. From these figures it is clear that both the theoretical predictions and the measured experi-

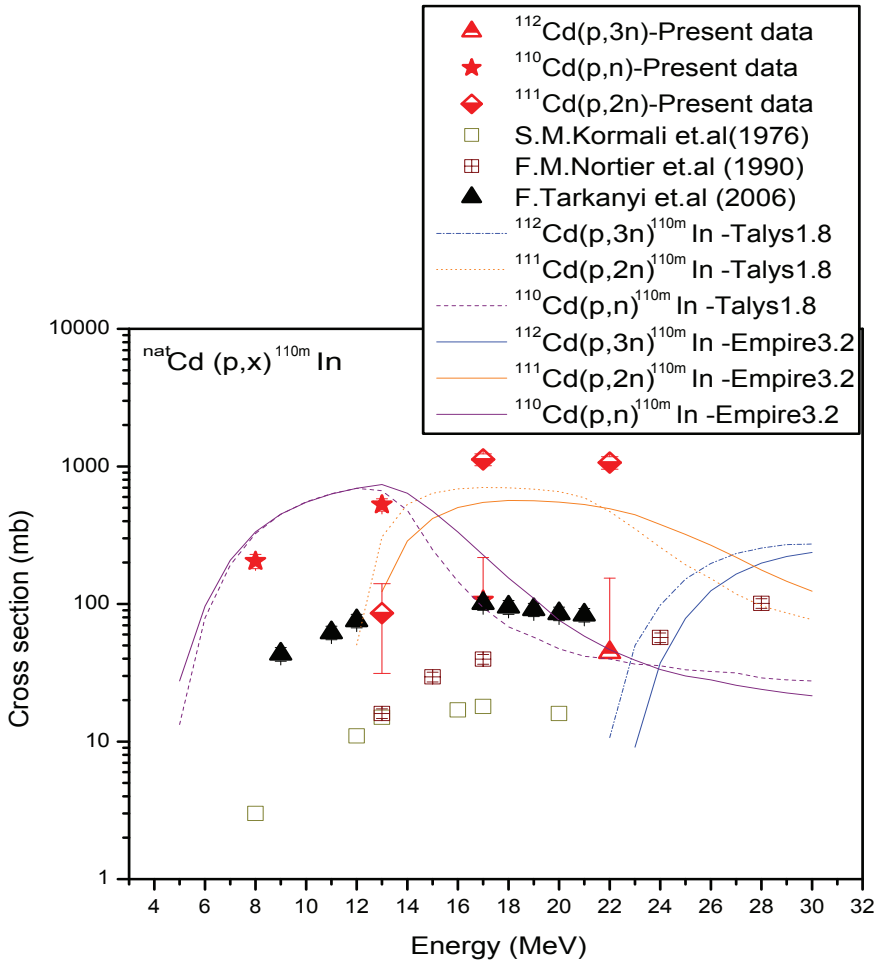

Figure 4.13: Experimentally measured and theoretically predicted excitation function for the ^{110m}In isotope.

mental data show a similar trend. In both the cases, the literature data[7–10, 13] produces the cumulative cross section of the residue not the individual reaction channel cross section. However, these literature data should be normalized to compare with the present data.

Since the cross-section for both isomeric and ground state could be measured, the isomeric cross-section ratio for the production of ^{110}In is also calculated over the energy range and is plotted in FIG 4.14. ICR is also calculated using TALYS and EMPIRE, corresponding to the respective contributing channels, and are

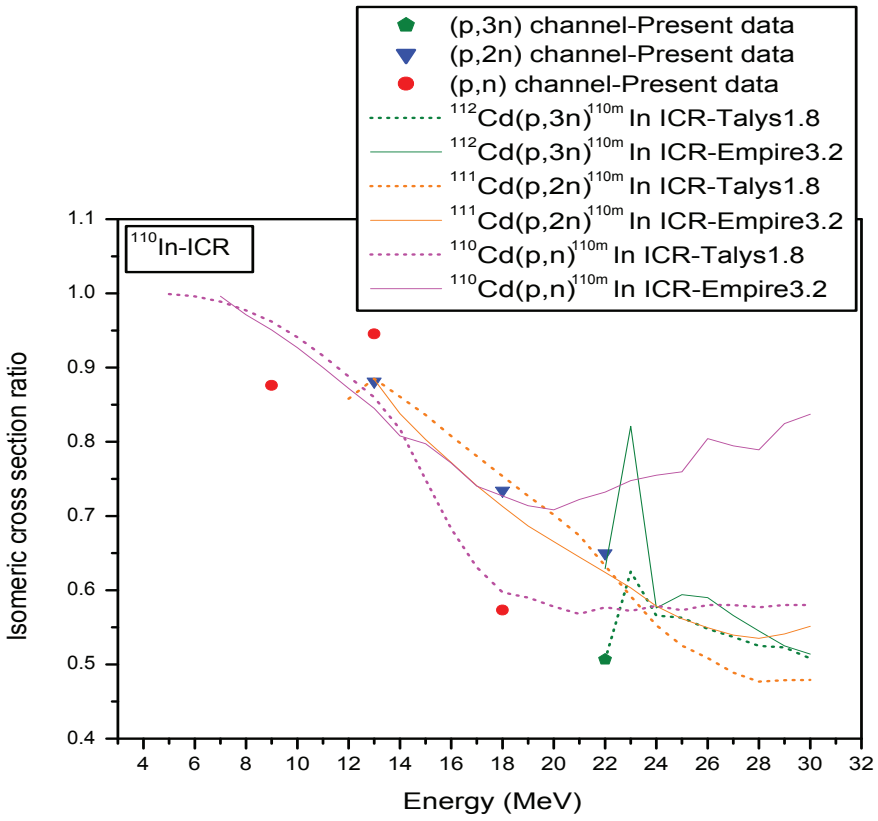

Figure 4.14: Experimentally measured and theoretically predicted isomeric cross-section ratio for the ^{110}In isotope.

plotted in the figure. The ICR shows the general decreasing trend with energy up to 20 MeV and a steady nature beyond that for (p,n) channel. For (p,2n) channel it shows a decreasing trend up to around 28 MeV and steady state after that. This may be interpreted in terms of the relative spin and parity. In the present case, the ground state has the spin of 7+ and the metastable state has the spin of 2+. Hence, as the energy increases the trend of populating higher state increases with increasing energy. The initial hike, in ICR, seen in the data for (p,3n) channel, may be interpreted as follows. At the onset of the reaction channel, the nucleus prefer to populate the ground state. The population to the excited state increase with energy. On further increase of excitation energy, larger angular momentum is transferred and the nucleus tends to occupy the

higher spin state, till it reaches the steady state. This is in tune with our previous observations[14, 15].

4.2.4 $^{nat}Cd(p,x)^{111g,111m}$In reaction cross-section

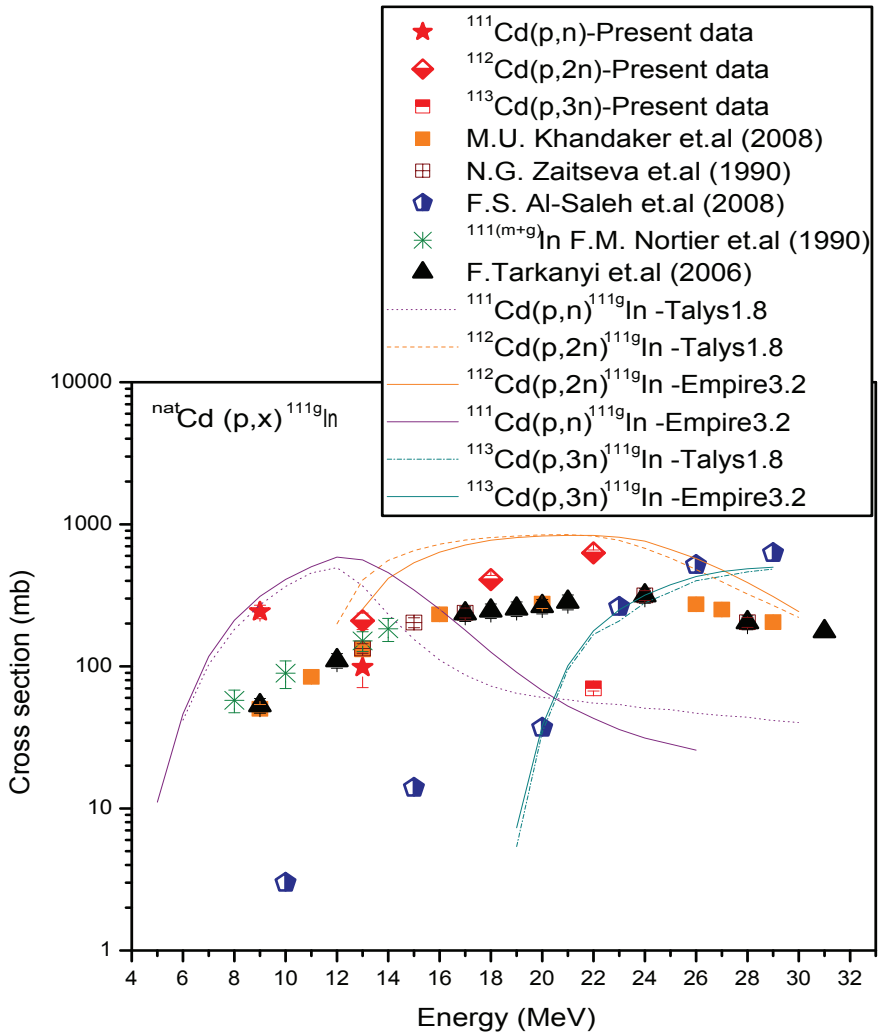

Figure 4.15: Experimentally measured and theoretically predicted excitation function for the ^{111g}In isotope.

The radionuclide ^{111}In has two isomeric states, the ground state ($t_{1/2}$=2.8047 d, J_π=(9/2)+) and the metastable state ($t_{1/2}$=7.7 minute J_π=(1/2)-), and is an important isotope of medical interest. The ground state ^{111}In has two decay

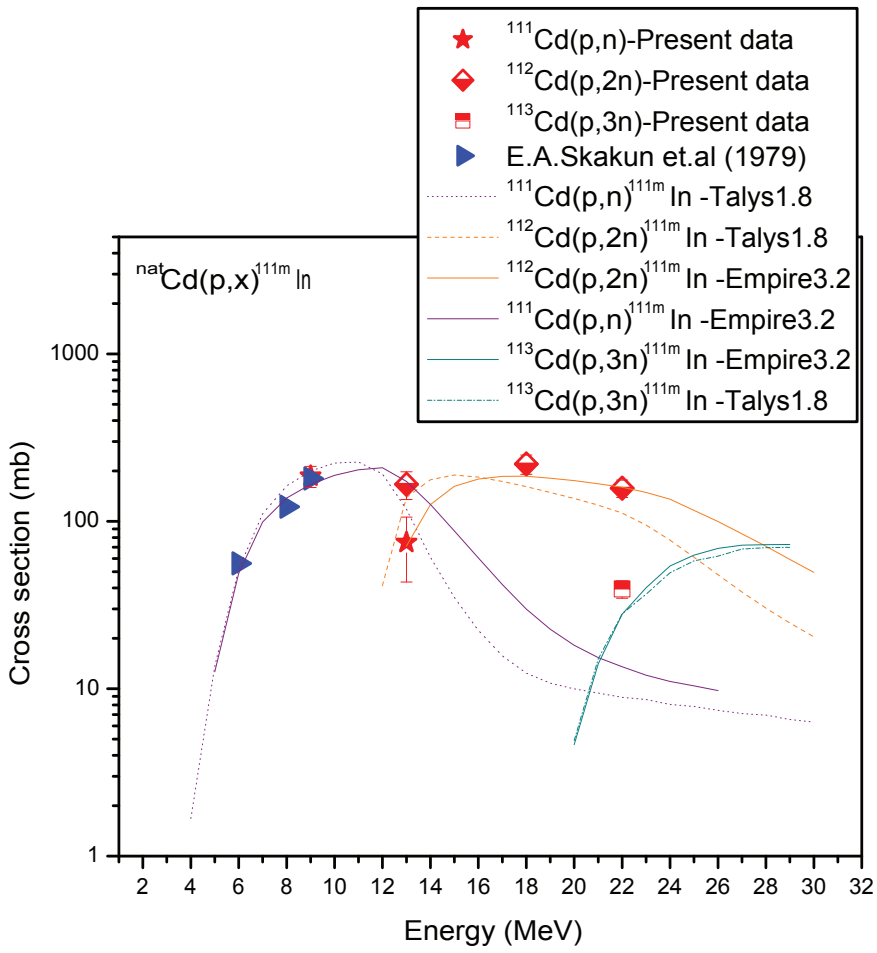

Figure 4.16: Experimentally measured and theoretically predicted excitation function for the ^{111m}In isotope.

gamma-rays of 171.29 keV (I_g=90.6%) and 245.35 keV (I_g=94.1%), of which 245.35 keV shows the mixing of ^{111m}Cd isotope. The contribution of ^{111g}In of 245.35 keV can be separated by considering the activity of 171.29 keV of ^{111g}In nuclei. The radio isotope ^{111m}In ($t_{1/2}$=7.7 minute) decay to the ground state with 100% IT, by emitting a single gamma-ray line of 537 keV. The major competing channels to produce ^{111}In are, ^{111}Cd(p,n), ^{112}Cd(p,2n) and ^{113}Cd(p,3n) with threshold energies 1.657 MeV, 11.135 MeV and 17.73 MeV respectively.

In both the ^{111g}In and ^{111m}In residual nucleus, the cross-section at the in-

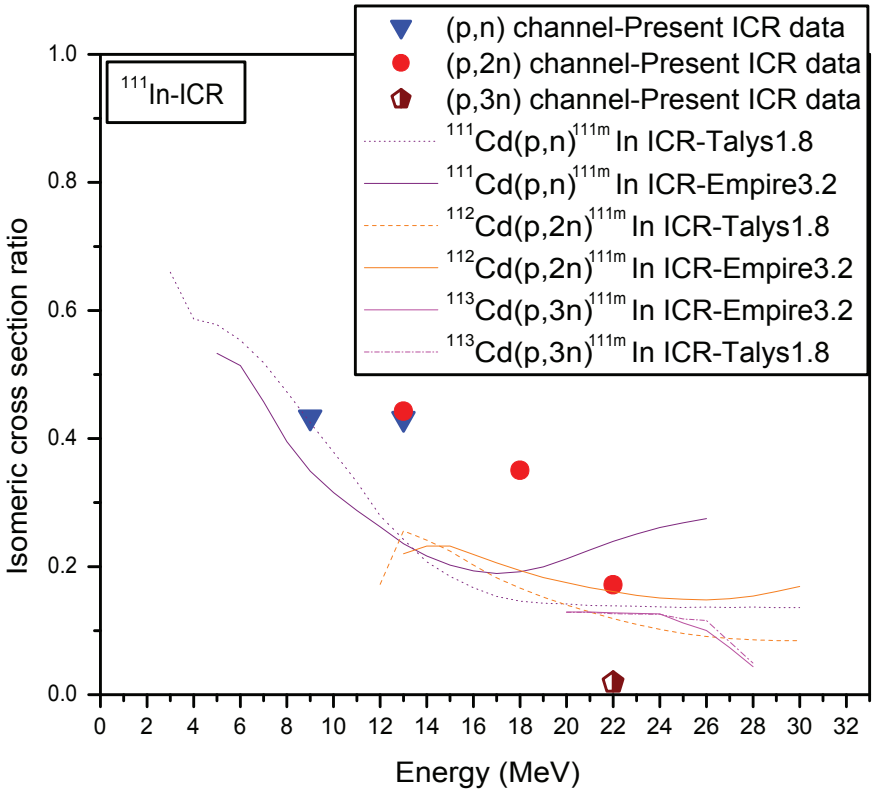

Figure 4.17: Experimentally measured and theoretically predicted isomeric cross-section ratio for the ^{111}In isotope.

cident energy 8.96 MeV is purely from the contribution of ^{111}Cd(p,n) reaction channel. At 12.95 MeV and 17.89 MeV the reaction cross-section may be the contribution from both the (p,n) and (p,2n) reaction channels. Whereas, at 21.96 MeV may have the contribution from both the (p,2n) and (p,3n) channels. Theoretical calculations with TALYS indicate that at 12.95 MeV both (p,n) and (p,2n) channels have almost equal cross-section. Hence the observed intensity of characteristic gamma-ray will have contributions in the ratio ≈13:24 from (p,n) and (p,2n) channels corresponding to the abundances of ^{111}Cd (12.8%) and ^{112}Cd (24.13%) respectively. In the case of ^{111g}In, at 17.89 MeV TALYS calculation shows the gamma-ray intensity has a contribution of ≈5% from (p,n) channel and at 21.96 MeV the (p,n) channel contribution is less than 4%. Whereas in the

case of ^{111m}In residual nucleus at 17.89 MeV and 21.96 MeV, TALYS calculation shows the gamma-ray intensity has a contribution of ≈4% and ≈4% from (p,n) channel respectively. These are well below the limit of experimental uncertainty. Hence the contribution from (p,n) channel at these two points are neglected. Thus the measured cross-section at 17.89 MeV is considered to be purly from the (p,2n) channel in both the ^{111g}In and ^{111m}In cases. In the case of ^{111g}In at 21.96 MeV, calculation using TALYS shows that the observed yield has ≈ 90% contribution from (p,2n) channel and ≈ 10% from (p,3n) channel. Similarly, for the ^{111m}In case, the observed contribution has ≈ 80% from (p,2n) channel and ≈ 20% from (p,3n) channel. Thus the contributions are separated accordingly.

The excitation function thus calculated for the reactions $^{111}Cd(p,n)^{111g}$In, $^{112}Cd(p,2n)^{111g}$In and $^{113}Cd(p,3n)^{111g}$In are plotted in FIG.4.15 and that for the reaction $^{111}Cd(p,n)^{111m}$In, $^{112}Cd(p,2n)^{111m}$In and $^{113}Cd(p,3n)^{111m}$In are plotted in FIG.4.16 along with the theoretical prediction and available literature data[7–9, 13, 16, 17]. The data for the ground state cross-section are significantly lower than the present data, particularly the data of F.S.Al-Saleh[13] is varying by order of 2 at some points. However in the case of population of isomeric state, the reported data by E.A skakun et.al[17] produced using enriched isotope (93.9% enrichment) is in good agreement with the present measurement. There is only one literature data[17] available so far and it is only for the lower incident energy region. Hence, the data produced in the present measurement at higher energy region is a new data and can be used for validation of the IAEA recommended data library.

In this case also, since both the isomeric states($t_{1/2}$=7.7 minute, J_π=(1/2)-) and ground states ($t_{1/2}$=2.805 d, J_π=(9/2)+) have measurable half-life and that the excitation function have been measured for both the populations corresponding to various channels. The ICR has been determined over the measured energy ranges for various channels and are plotted in FIG.4.17, along with the theoretically calculated values. The ICR shows the decreasing trend with energy up to 18 MeV and a steady nature beyond that for (p,n) channel. For (p,2n)

channel it shows a decreasing trend upto around 28 MeV and steady state after that. Whereas in the case of (p,3n) channel there is a steady state upto 26 MeV, and it decreases drastically as energy increases. This may be interpreted in terms of the relative spin distribution. The tendency to populate the state with higher spin state (J_π=(9/2)+) with incident energy irrespective of its ground state (J_π=(9/2)+) or isomeric state (J_π=(1/2)-) in tune with our previous observation[14, 15].

4.2.5 $^{nat}Cd(p,x)^{111m}$Cd reaction cross-section

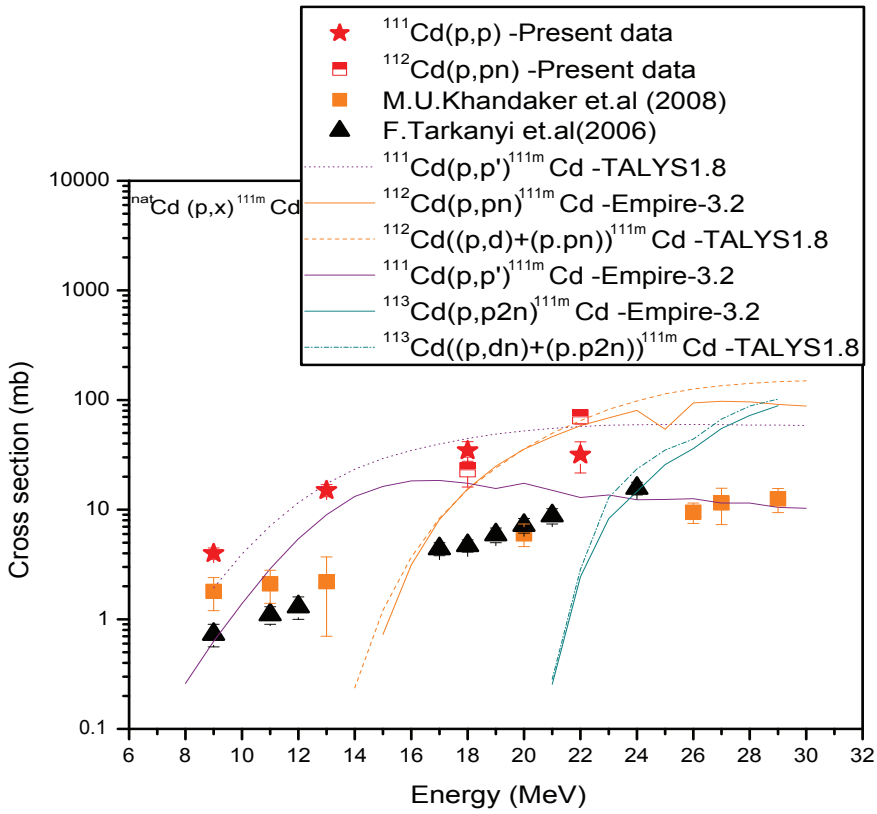

Figure 4.18: Experimentally measured and theoretically predicted excitation function for the ^{111m}Cd isotope.

The ^{111m}Cd nucleus is produced through three different reaction channels viz ^{111}Cd(p,p), ^{112}Cd(p,pn) and ^{113}Cd(p,p2n) with threshold energies 0 MeV, 9.48

MeV and 16.07 MeV respectively. Hence, the measured cross-section at 8.96 MeV is purely the contribution from (p,p) channel. Similarly the contribution from (p,p2n) channel is less than 1.12% in all the desired energy region as compared to the TALYS calculation. The measured activity at 12.95 MeV, 17.89 MeV and 21.96 MeV may have the contribution from both the (p,p) and (p,pn) channels. In comparison with the TALYS calculation, it is seen that the contribution from (p,pn) channel at 12.95 MeV is $\approx$ 0.2%. It is much less than the experimental uncertainty.

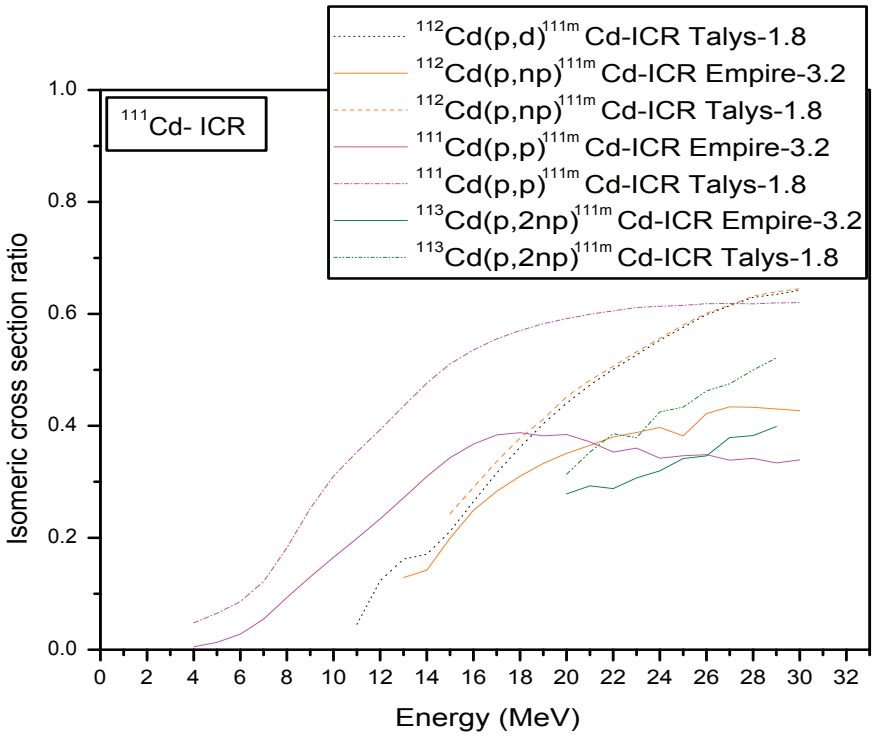

Figure 4.19: Theoretically predicted isomeric cross-section ratio for the ^{111}Cd isotope.

Hence, the measured cross-section at this point is considered to be from (p,p) channel alone. At 17.89 MeV, calculation using TALYS shows that the observed yield has $\approx$ 60% contribution from (p,p) channel and $\approx$ 40% from (p,pn) channel. Hence, the contribution from each channel is separated accordingly. At

21.96 MeV both (p,p) and (p,pn) channels have an almost equal cross-section. Hence the observed intensity of characteristic gamma-ray will have contributions in the ratio ≈13:24 from (p,p) channel and (p,pn) channel corresponding to the abundances of ^{111}Cd (12.8%) and ^{112}Cd (24.13%) respectively. Hence, the contribution from these channel is separated accordingly. The excitation function thus calculated for the reaction $^{nat}Cd(p,x)^{111m}$Cd, the available literature data[7, 8] and the theoretical prediction are plotted in FIG.4.18. In this case, TALYS prediction reproduces the experimental data except at high energy where it is overestimating for (p,p) reaction, whereas the EMPIRE prediction underestimates the data over the entire range. Predictions of both the models for (p,pn) channel are in good agreement with the data. The data reported by F. Tarkanyi et al.[7], M.U.Khandaker et.al[8] shows the cumulative cross section of the residue and it is in agreement with the present measurement, only after re-normalization.

The ^{111}Cd isotope has one stable ground state and a metastable state. The Isomeric state of 396.2 keV, with a half-life of 48.50 minutes, decay to the ground state by 100% IT. In this case, the ground state is stable, the ICR could not be determined experimentally. Hence, the ICR is calculated theoretically using both TALYS and EMPIRE predictions for (p,p), (p,pn) and (p,p2n) channels and are plotted in FIG.4.19. In this case, the ICR increases with energy up to around 15 MeV and attains a steady state (60% in the case of TALYS prediction and 35 % in the case of EMPIRE prediction). Since TALYS better represents the excitation function, the ICR value predicted by TALYS seems to be more acceptable as higher the incident energy larger the angular momentum transfer to the system.

4.2.6 $^{nat}Cd(p,x)^{112g,112m}$In reaction cross-section

The competing channels to produce ^{112}In nuclei are ^{112}Cd(p,n), ^{113}Cd(p,2n) and ^{114}Cd(p,3n) reaction channels with threshold energies, 3.397 MeV, 9.99 MeV and 19.117 MeV respectively. Theoretical calculation with TALYS indicates that in both the ^{112g}In and ^{112m}In cases the measured cross-section at 8.96 MeV

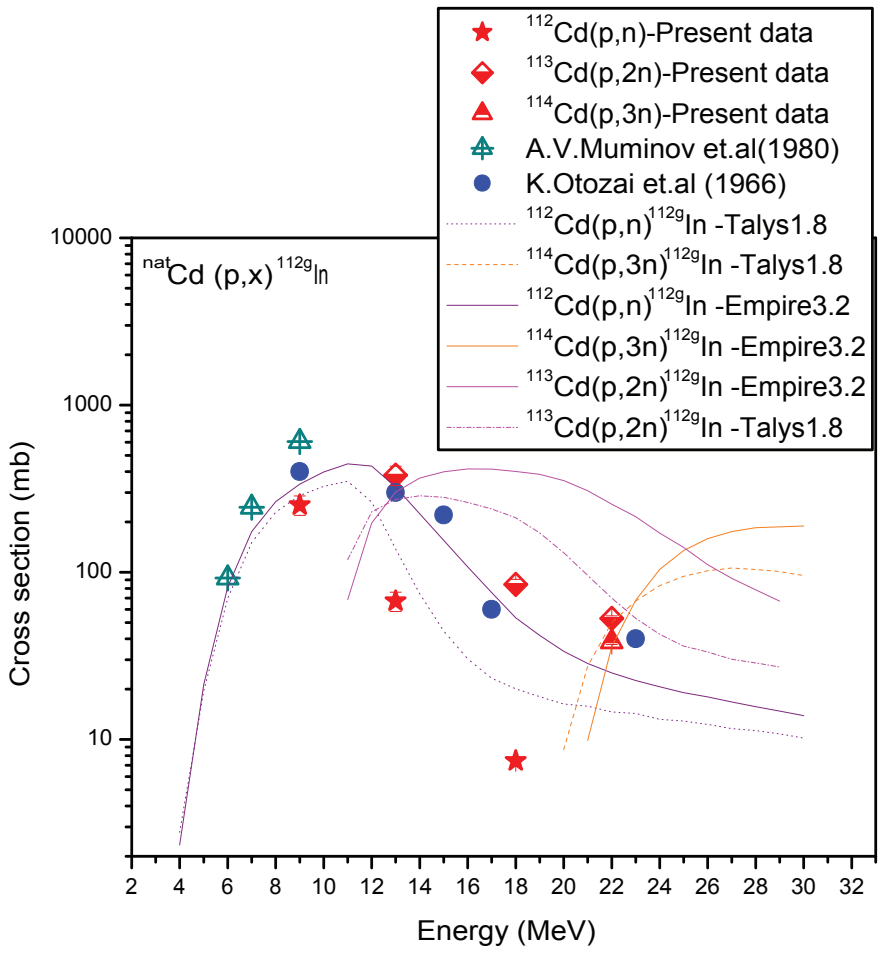

Figure 4.20: Experimentally measured and theoretically predicted excitation function for the ^{112g}In isotope.

may have the contribution from the (p,n) channel alone. In the case of ^{112g}In, on comparison with TALYS calculation, the observed contribution has ≈ 85% contribution from (p,2n) channel and ≈ 15% from (p,n) channel at 12.95 MeV. Whereas it is ≈ 66% contribution from (p,2n) channel and ≈ 34% from (p,n) channel in ^{112m}In case. At 17.89 MeV, the observed yield has ≈ 95% contribution from (p,2n) channel and ≈ 5% from (p,n) channel. Similarly, at 21.96 MeV the contribution from (p,n) channel is neglected and it has the only contribution from both the (p,2n) and (p,3n) channels. The production using TALYS shows

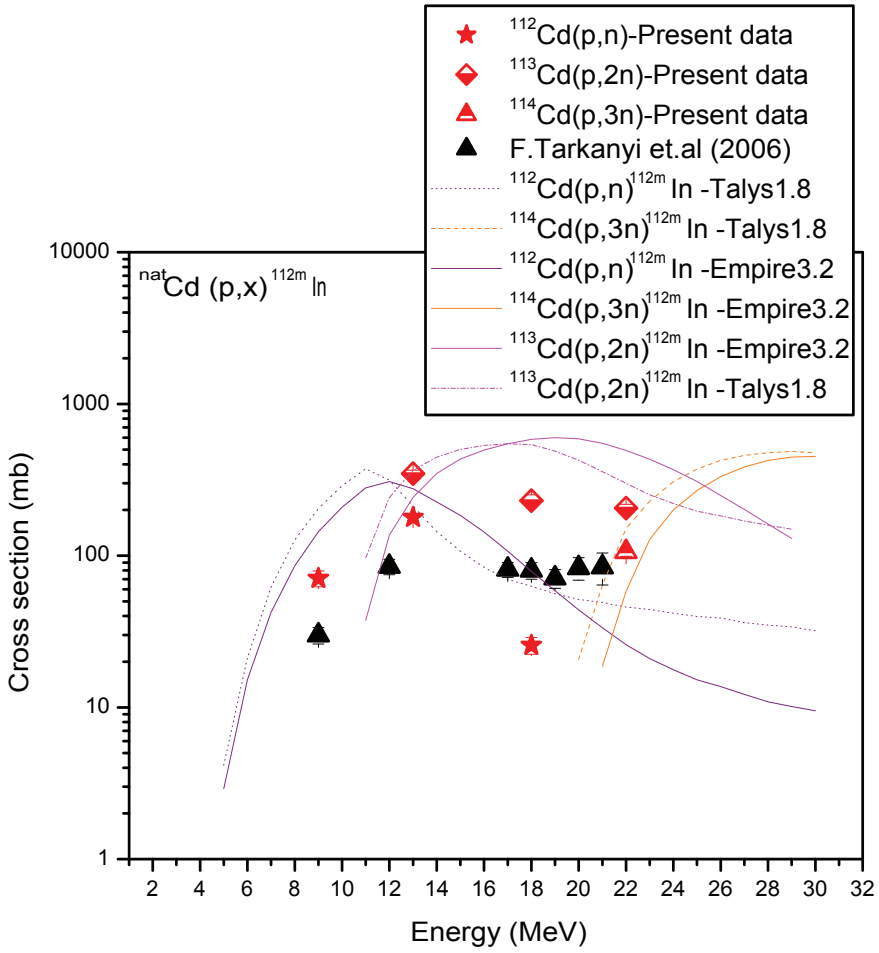

Figure 4.21: Experimentally measured and theoretically predicted excitation function for the ^{112m}In isotope.

that the observed yield has ≈ 58% contribution from (p,2n) channel and ≈ 42% from (p,3n) channel. For the ^{112m}In case, the observed contribution has ≈ 90% from (p,2n) channel and ≈ 10% from (p,n) channel at 17.89 MeV. At 21.96 MeV, the observed yield has ≈ 66% contribution from (p,2n) channel and ≈ 34% from (p,3n) channel. Hence, the contribution from these channels are seperated accordingly. The excitation function thus calculated for ^{112g}In and ^{112m}In isotopes, the available literature data[7, 18, 19] and the theoretical prediction are plotted in FIG.4.20 and FIG.4.21. In the case of ^{112g}In, the data

reported by A.V.Muminov et.al[19] and K.Otozai et.al [18] are in very good agreement with both the present experimental data and theoretically predicted data in the present interested energy region. It is to be noted that they have used the enriched cadmium as the target. But,in the case of ^{112m}In residual nucleus the data reported by F.Tarkanyi et.al[7], is slightly lower in the low energy region ((p,n) competing channel region) and is in good agreement in the higher energy region. This is so since the authors have measured the cumulative cross sections of the residual nuclei using cadmium isotopes having comparable abundances for the formation of the ^{112}In isotope.

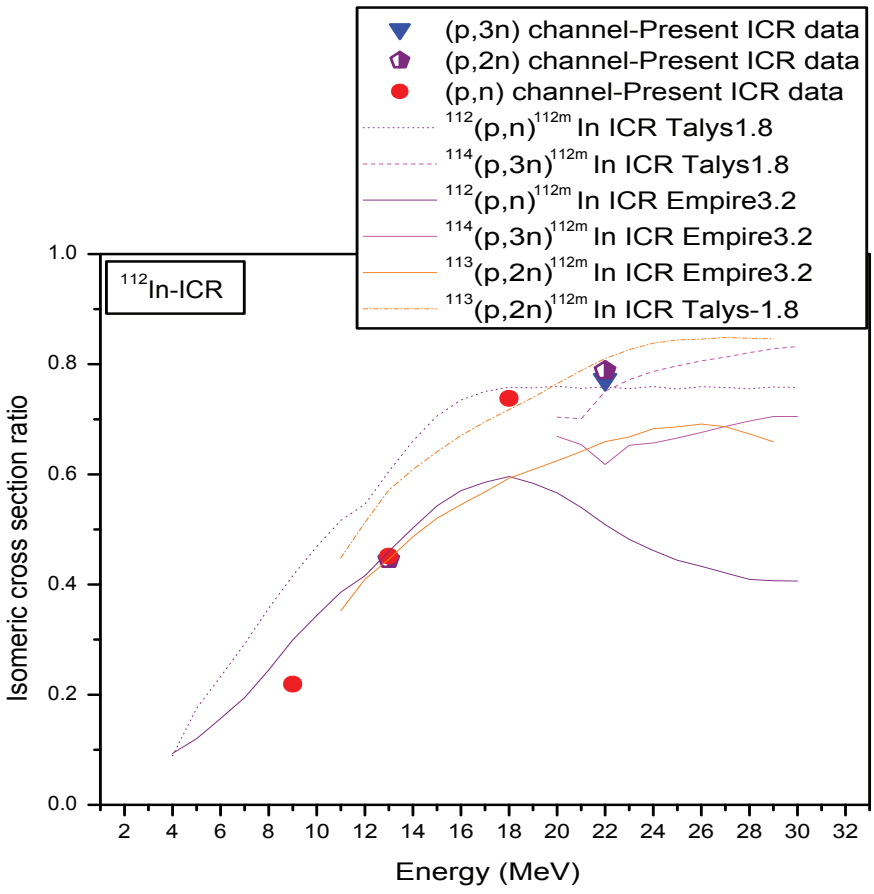

Figure 4.22: Experimentally measured and theoretically predicted isomeric cross-section ratio for the ^{112}In isotope.

The ^{112}In has three metastable states and a ground state. The long-lived

isomeric state decay to the ground state by 100% IT, and the other two isomeric state have half-life of the order of microsecond($t_{1/2}$=2.81μs and $t_{1/2}$=0.69μs). Since, the cross-section for both isomeric and ground state could be measured, the isomeric cross-section ratio for the production of ^{112}In is also calculated over the energy range and is plotted in FIG.4.22 along with the theoretical models EMPIRE and TALYS. The ICR shows a gradual increase in their value as incident energy increases, by favouring the population of high spin isomeric state (J_π=4+) of about ≈80% at energy 156 keV and low spin ground state (J_π=1+) of about ≈20%. This is to be expected since the higher states get more populated, irrespective of the reaction channels. In order to study the effect of reaction channels, the ICR is calculated for different reaction channels. Hence, energy increment has significant effect on ICR for single particle emission compared to multiparticle emission. This may be due to the distribution of spin over the multiparticle.

4.2.7 $^{nat}Cd(p,x)^{113m}$In reaction cross-section

The ^{113m}In can be produced through ^{112}Cd(p,γ), ^{113}Cd(p,n) and from ^{114}Cd(p,2n) reaction with threshold energies of 0 MeV, 0.462 MeV and 9.585 MeV respectively. The zero threshold ^{112}Cd(p,γ) reaction have much less than 0.01% cross-section and it gets diminished further as energy increases. Hence, the measured cross-section at 8.96 MeV is considered as the major contribution from (p,n) channel. Calculation by TALYS, at 12.95 MeV shows that the cross-section for (p,γ) channel is < 0.002%, very much less than the experimental error, and hence contribution to the yield is still less. The production cross-section at 12.95 MeV, 17.89 MeV and 21.96 MeV may be the contribution from both the ^{113}Cd(p,n) and ^{114}Cd(p,2n) reaction channels. In analysis with TALYS, the observed contribution has ≈ 80% contribution from (p,2n) channel and ≈ 20% from (p,n) channel at 12.95 MeV. At 17.89 MeV, the observed yield has ≈ 93% contribution from (p,2n) channel and ≈ 7 % from (p,n) channel. Similarly, at 21.96 MeV calculation using TALYS shows that the observed yield has ≈ 93.8% contribution from

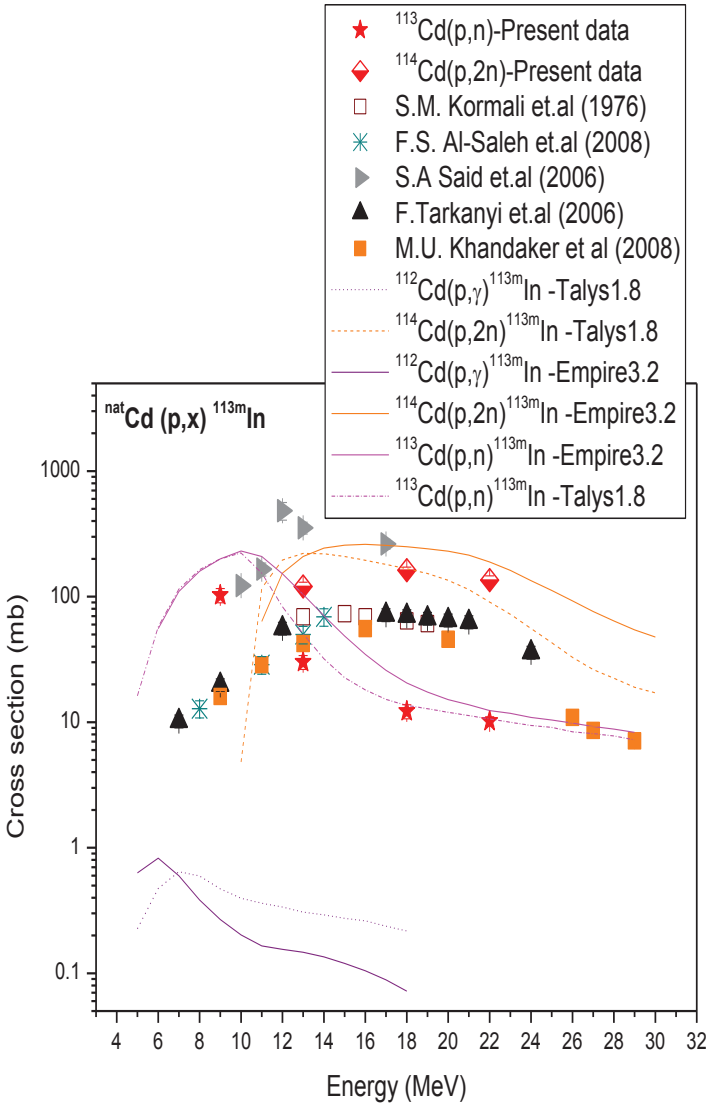

Figure 4.23: Experimentally measured and theoretically predicted excitation function for the ^{113m}In isotope.

(p,2n) channel and ≈ 6.2% from (p,n) channel. The observed cross-section have been deducted accordingly. The results of the above measurement are plotted in FIG.4.23 along with theoretical calculation and literature data [7, 10, 13, 20]. In this case the data of F.Tarkanyi et.al[7], M.U.Khandaker et.al[8], and F.S.Al-Saleh et.al[13] are in good agreement with the present measurement similar to the previous case. Similarly the data, using enriched isotope, by S.M.Kormali

et.al[10] is remarkably in good agreement with the present data, whereas the data, using enriched isotope, reported by S.A.Said et.al[20] is almost three times higher than the present data. However this may be from the unexploited tightly spaced and unresolved levels in the excitation energy range 1-4 MeV of ^{113}In nucleus[20] as mentioned in their paper.

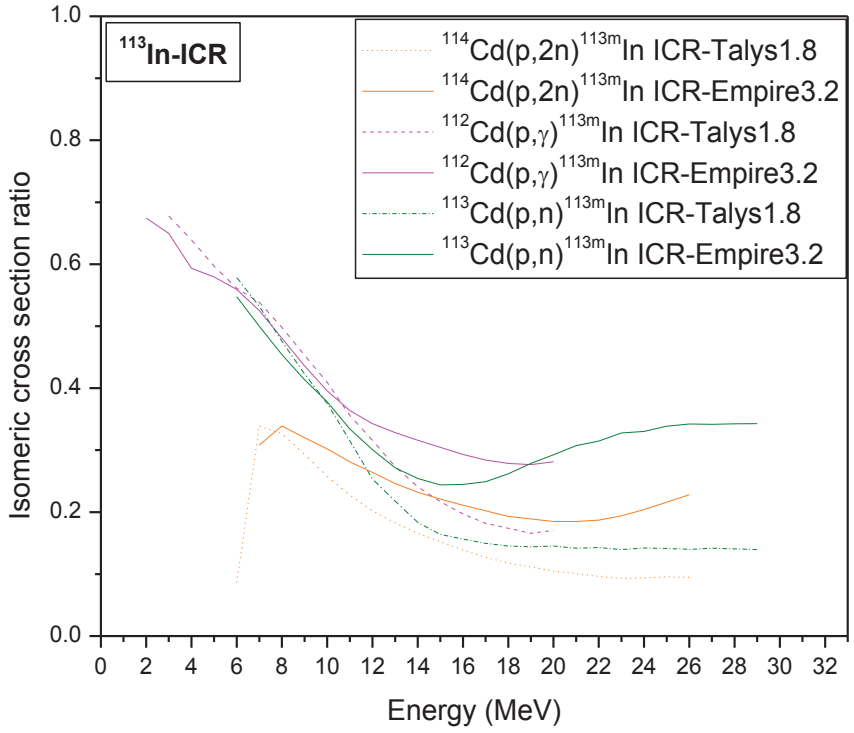

Figure 4.24: Theoretically predicted isomeric cross-section ratio for the ^{113}In isotope.

The ^{113}In has a stable ground state (Natural abundance of 4.29%) and a long lived ($t_{1/2}$=99.476 min) isomeric state. The isomeric state decays to the stable ground state by emitting a characteristic gamma-ray of 391.698 keV of 64.94% abundance, with 100% IT. In the present case, since the ground state is stable, the ICR calculated theoretically for (p,γ), (p,n) and (p,2n) channels, using TALYS and EMPIRE, and are plotted in FIG.4.24. The ICR shows the general decreasing trend with energy up to 18 MeV and a steady nature beyond that for

both (p,γ) and (p,n) channels. For (p,2n) channel it shows a decreasing trend up to around 25 MeV and steady state after that, $\approx$ 80% for (p,γ) channel, $\approx$ 85% for (p,n) channel and $\approx$ 90% for (p,2n) channel favouring high spin ground state. Here also the multiparticle emission is less affected by the incident energy.

4.2.8 $^{116}Cd(p,2n)^{115m}$In reaction cross-section

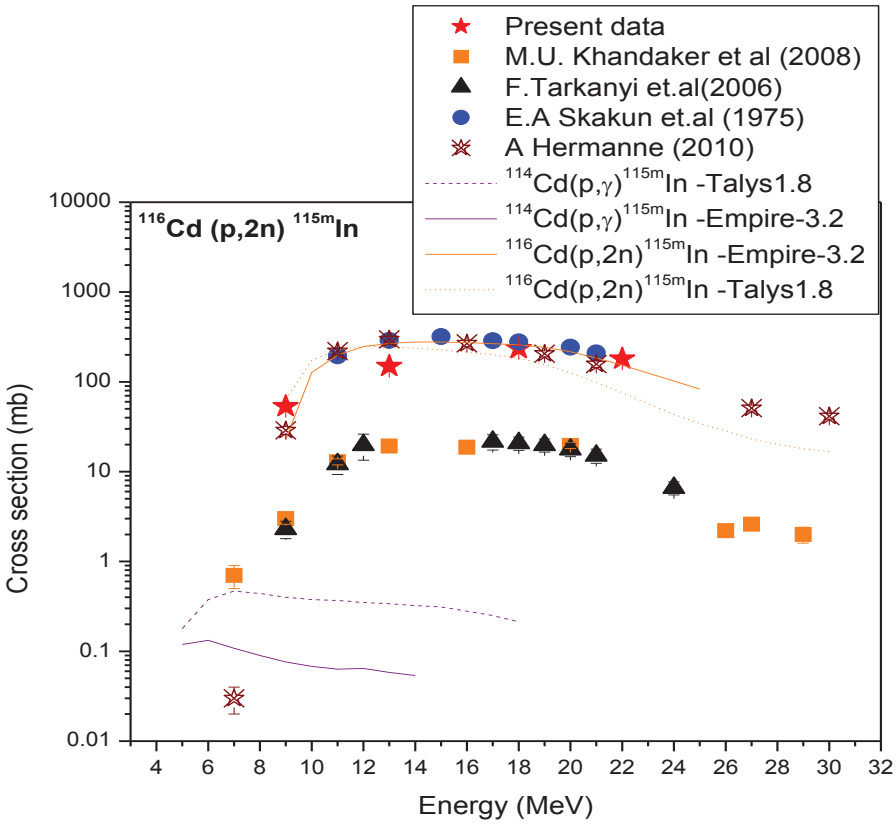

Figure 4.25: Experimentally measured and theoretically predicted excitation function for the ^{115m}In isotope.

In the present case ^{115m}In can be produced through the ^{114}Cd(p,γ), ^{116}Cd(p,2n) reaction with threshold energies 0 MeV and 8.09 MeV respectively. By the prediction of TALYS calculation, the activity induced through (p,γ) reac-

tion channel is less than $\approx 1\%$, and hence, the corresponding yield is much lesser at 8.96 MeV and even negligibly smaller, at higher energies the observed activity of ^{115}In is accounted purely for (p,2n) channel. The result has been plotted in FIG.4.25 along with theoretical calculation and literature data[7, 8, 17, 21, 22]. The measurements due to E.A.Skakun et.al[17, 21] and A.Hermanne et.al[22], using enriched isotopes, are in good agreement with the present data. As in the previous cases, the data due to F.Tarkanyi et.al[7] and M.U.Khandaker et.al[8] are comparable with the present data after renormalization with the isotopic abundance.

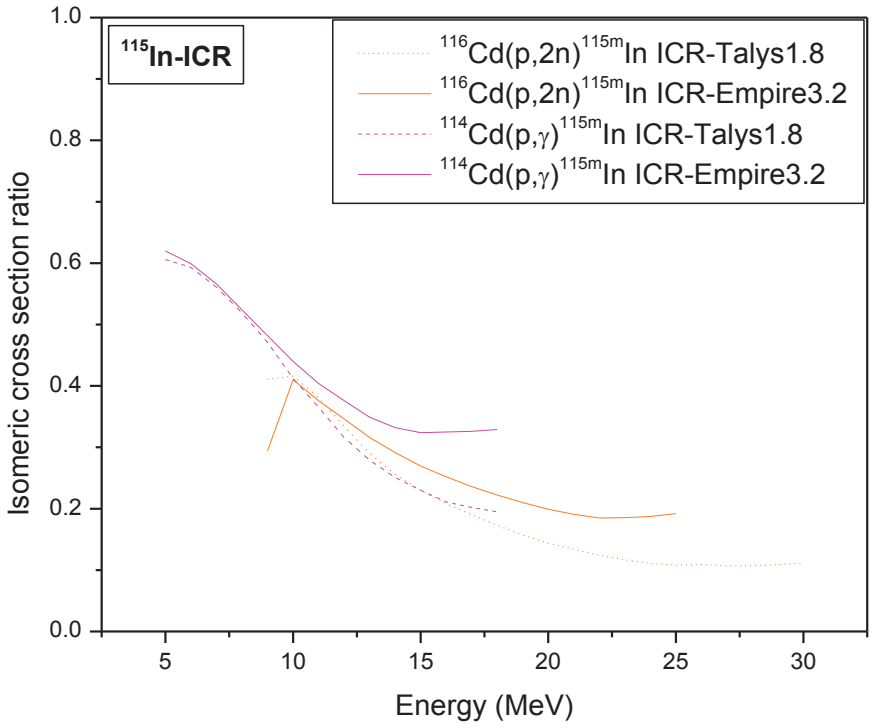

Figure 4.26: Theoretically predicted isomeric cross-section ratio for the ^{115}In isotope.

The nucleus ^{115}In has a long-lived ground state ($t_{1/2}$=4.41x10^{14} Year) and a 4.5 hours half-life isomeric state. The ^{115m}In isomer decay to its stable ground state by 95% IT, due to the longer half-life (more or less stable), the cross-section

for the ground state could not be measured in the present case. In this case also ICR calculated theoretically using TALYS and EMPIRE for both the (p,γ) and (p,2n) channels and are plotted in FIG 4.26. The ICR shows similar trends with other cases, favouring higher spin ground state (J_π=(9/2)+) over lower isomeric state (J_π=(1/2)-) at steady population region of energy.

4.2.9 $^{116}Cd(p,n)^{116m}$In reaction cross-section

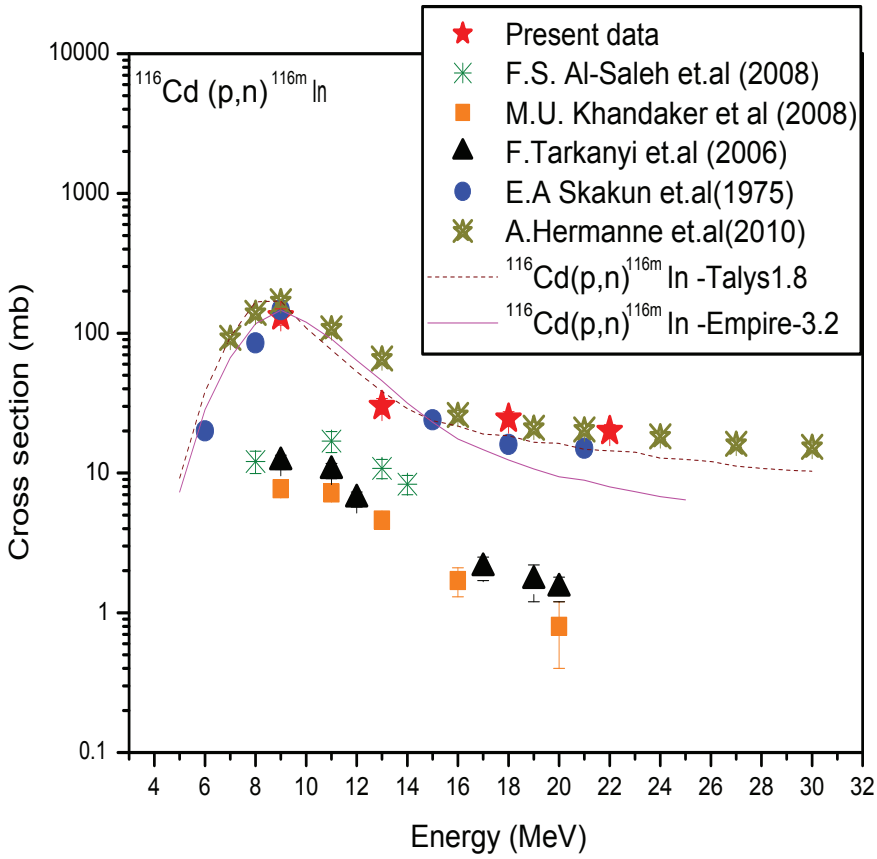

Figure 4.27: Experimentally measured and theoretically predicted excitation function for the ^{116m}In isotope.

The radioisotope ^{116m}In is produced through the reaction $^{116}Cd(p,n)^{116m}$In, and there is no mixing of data. The ^{116}In has a short-lived ground state ($t_{1/2}$=14.1 second) and two metastable states ^{116m_1}In ($t_{1/2}$=54.29 minute) and

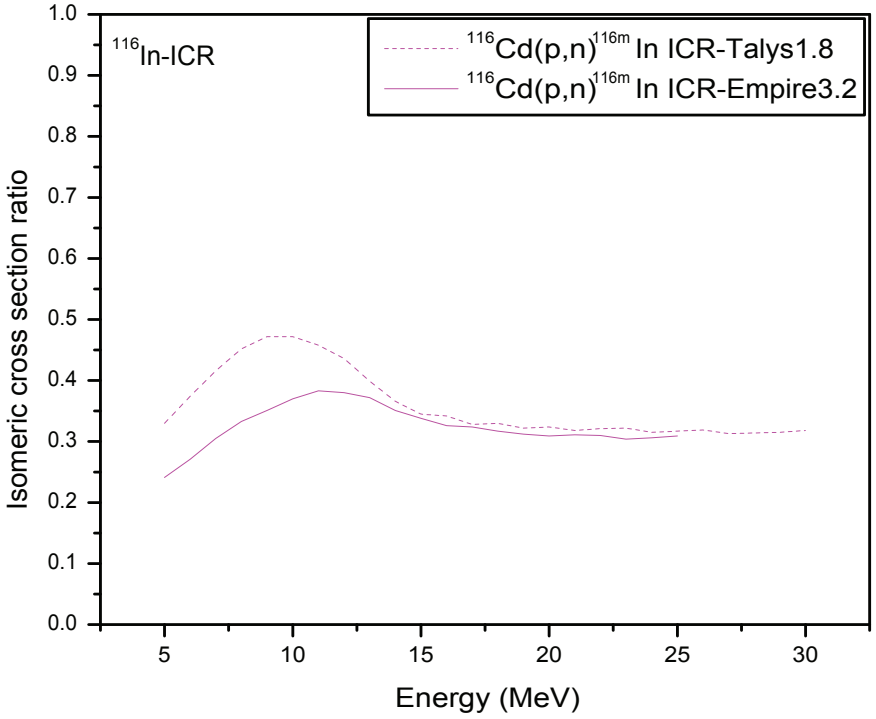

Figure 4.28: Theoretically predicted isomeric cross-section ratio for the ^{116}In isotope.

^{116m_2}In ($t_{1/2}$=2.18 second). The second isomeric state (^{116m_2}In) has a very short half-life and decays through 100% isomeric transition (IT) to the first isomeric state (^{116m_1}In). Hence, the isomeric cross-section for ^{116m_1}In will have a total contribution from both the isomeric states ^{116m_1}In and ^{116m_2}In. Excitation function thus calculated is plotted in FIG.4.27 along with the theoretical calculation and the available literature data[7, 8, 13, 17, 22]. Here also, the data due to F.Tarkanyi et.al[7], M.U.Khandaker et.al[8] by normalizing with the enriched isotopic abundances and the data due to A.Hermanne[22] and E.A.Skakun[17], using enriched isotope, are in good agreement with the present data where as, the data due to F.S.Salah et.al[13] using natural isotopes are considerably lower than the present measurement. Also, the theoretical representation (EMPIRE) and experimental data differ significantly in their report[13]

Since, the ground state of ^{116}In has the half-life of 14.1 second and the gamma counting was performed after about one hour, the ground state activity could not be measured. Hence, the ICR could be calculated theoretically using TALYS and EMPIRE and are plotted in FIG.4.28. The ICR shows an increasing trend up to about $\approx$ 45% at 10 MeV and decreases to about $\approx$ 30% up to 15 MeV and steady state after that. In this case, the preference of higher spin state at high energies, which is a general trend all other cases, is not seen. This case is particularly an odd one in the present work as well as in our earlier analysis [15]. No straight forward explanation could be assigned to this case. Further, this is to be verified experimentally.

4.2.10 YIELD

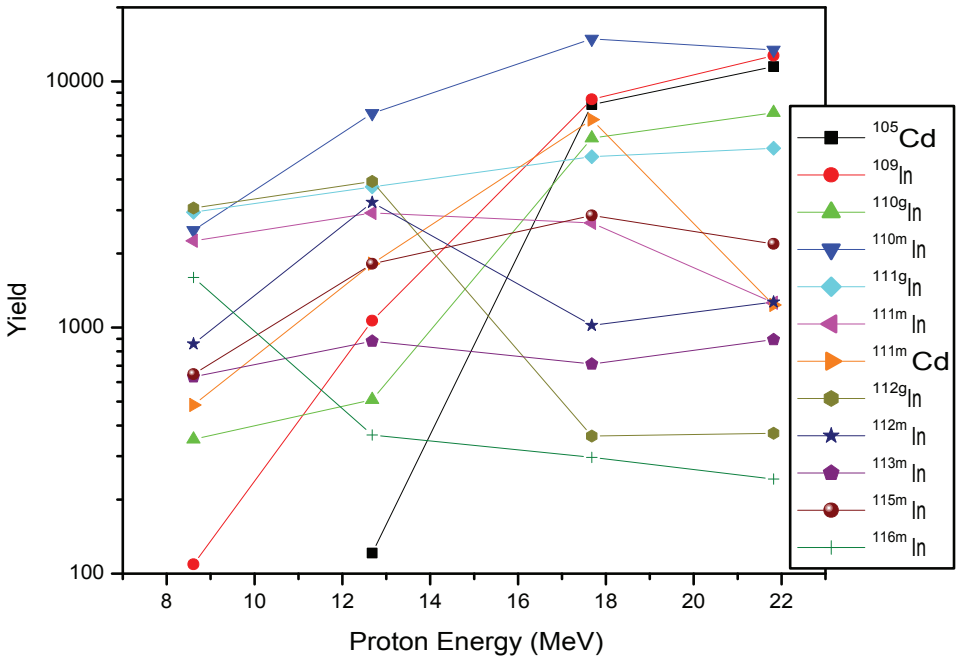

Figure 4.29: Yield of the ^{116m,115m,113m,112g,112m,111g,111m,110g,110m,109g}In and ^{105,111m}Cd residual nucleus.

For the sake of completeness, the integrated yield of each isotope is calculated as the production cross-section of particular isotope at given incident energy on

activation of the natural target sample of mixed isotope and is given by Y= $n_1\sigma_1\phi$+$n_2\sigma_2\phi$+$n_3\sigma_3\phi$ etc, where n_1, n_2 and n_3 are the number of nuclei present in the target ϕ is the flux of the incident beam and σ_1, σ_2, σ_3 etc. are their respective channel cross-sections. The yield thus calculated for isotopes of interest at various incident energies are plotted in FIG.4.29. In this case, ^{110m}In shows highest production rate over the energy range under study. Similar calculations help in identifying the optimum condition for production of particular radioactive isotopes for application purposes.

Bibliography

[1] M. Herman, R. Capote, M. Sin, A. Trkov, B.V. Carlson, P. Oblozinsk y, C.M. Mattoon, H. Wienke, S. Hoblit, Young-Sik Cho, G.P.A. Nobre, V.A. Plujko and V. Zerkin, EMPIRE-3.2 Malta- modular system for nuclear reaction calculations and nuclear data evaluation, INDC(NDS)-0603 BNL-101378-2013.

[2] A.J. Koning, S. Hilaire and S Goriely.,TALYS-1.8, Nuclear reaction program, Nuclear Data Section (IAEA, Vienna, December 26 2015) December 26, 2015.

[3] F.Tarkanyi, F. Ditroi, A.Hermanne, S.Takacs, M.Baba , Applied radiation and isotopes, Vol 107 10 (2016) 391.

[4] M Al-Abyad , H.M.EL-Showaimy , M.B.Challan, A.M.Khalaf and M.N.H.Comsan, in Arab J. of Nucl. Sci. and Application 44 (2011) 111-121.

[5] National Nuclear Data Center. National Nuclear Data Center, www.nndc.bnl.gov/.

[6] MM Musthafa, Manoj Kumar Sharma, BP Singh, R Prasad, Applied radiation and isotopes, Vol 62 3(2005) 419-428.

[7] F. Tarkanyi, B. Kiraly, F. Ditroi, S. Takacs, J. Csikai, A. Hermanne, M.S. Uddin, M.Hagiwara, M. Baba, T. Ido, Yu.N. Shubin, S.F. Kovalev, Nucl. Instrum.Meth. B 245 (2006) 379.

[8] M.U. Khandaker, K. Kim, M.W. Lee, K.S. Kim, G.N. Kim, Y.S. Cho, Y.O. Lee, Nucl.Instrum.Meth. B 266 (2008) 48774887.

[9] F.M. Nortier, S.J. Mills, G.F. Steyn, Appl. Radiat. Isot. 41 (1990) 1201.

[10] S.M. Kormali, D.L. Swindle, E.A. Schweikert, J. Radioanal. Chem.31(1976) 437.

[11] A.J. Koning and J.P. Delaroche, Nucl. Phys. A713, 231 (2003).

[12] C. Kalbach, Phys. Rev. C 37, 2350 (1988).

[13] F.S. Al-Saleh, Exfor data base:(¡http://www-nds.iaea.org/exfor/¿ Exfor D0467005) 2008.

[14] B. Satheesh, M.M Musthafa, B.P Singh, R.Prasad, Int.J.Mod.Phys. E, 21 (2012)1250059.

[15] Muhammed Shan P.T, M.M. Musthafa, Najmunnisa T, Mohamed Aslam P, Rajesh K.K, Hajara K, Surendran P, J.P. Nair, Anil Shanbagh, S. Ghugre, Nuclear Physics A 974 (2018) 921.

[16] N.G. Zaitseva, O. Knotek, A. Kowalew, P. Mikecz, E. Rurarz, V.A. Khalkin, V.A.Ageev, A.A. Klyuchnikov, L.A. Kuzina, A.F. Linev, Appl. Radiat. Isot. 41 (1990) 177.

[17] E.A. Skakun, A.P. Kljucharev, N. Rakivnenko, I.A. Romanij, Russ. Acad. Sci. Phys.39 (1) (1975) 18.

[18] K. Otozai, S. Kume, A. Mito, H. Okamura, R. Tsujino, Y. Kanchiku, H. Gotoh, Nucl. Phys.80 (1966) 335.

[19] A.V.Muminov, S.Mukhamdev, A.Vasidov, Atomnya Energiya 49(1980)101.

[20] S.A. Said, E.K. Elmaghraby, F.I. Asfour, Appl. Radiat. Isot.64 (2006) 1655.

[21] E.A. Skakun, V.G. Batiy, Y.N. Rakivnenko, O.A. Rastrepin, Yadernaya Fizika 45 (1987) 614.

[22] A.Hermanne, F.Tarkanyi, S.Takacs, P.Van den Winkel, R.Adam Rebeles, A.Ignatyuk and S.F. Kovalev, Applied Radiation and Isotopes 68 (2010) 14 -17

Chapter 5

Comprehensive Analysis

Excitation functions and isomeric cross-section ratio for 20 reactions induced by proton on natural isotopes of indium and cadmium have been studied in the present work. Many of the isotopes so produced are having interest in medical, industrial and astrophysical applications. The production cross-section and isomeric cross-section ratio of the indium and cadmium isotopes and the dependence of isomeric cross-section ratio on spin, parity and energy difference of the ground state and isomeric state, incident energy, exit channel, and the life time of the states have been investigated in this chapter. The different nuclear properties such as Ground and isomeric state spin, parity, lifetime, and energy gap between the states are tabulated in Table 5.1. The detailed discussion of the individual isotope has been done in the previous chapter 4. Isotopes under study like ^{115}In, ^{113}In and ^{111}Cd are produced in both the channels. Hence this chapter is devoted to a comprehensive analysis to derive general characteristic of nuclear reaction mechanism in the mass region of around A=110. In the present section, the theoretical analysis using the code Talys 1.8 has been used in the discussion and it shows better reproducibility for proton-induced reaction.

Figure 5.1 shows the analysis of excitation function for the production of ^{115m}In nucleus through the reaction channels ^{115}In (p,p), and ^{116}Cd (p,2n). Theoretical calculation for ^{114}Cd(p,γ) using Talys 1.8 is also shown in the figure. It is seen that, at moderate excitation energies, the reaction cross section for

Nuclide	Ground state Half-life	Isomeric state Half-life	Ground state Spin/Parity	Metastable state Spin/Parity	Energy gap (keV)
^{115}In	$4.41 * 10^{14}$Y	4.49 h	9/2+	1/2-	336.24
^{114}In	71.9 s	49.51 d	1+	5+	190.27
^{113}In	Stable	99.476 min	9/2+	1/2-	391.698
^{112}In	14.88 min	20.67	1+	4+	156.61
^{111}In	2.80 d	7.7 min	9/2+	1/2-	537.81
^{110}In	4.9 h	69.1 min	7+	2+	62
^{111}Cd	stable	48.50 min	1/2+	11/2-	396.22

Table 5.1: Decay characteristics of the ^{115}In, ^{114}In, ^{113}In, ^{112}In, ^{111}In, ^{110}In and ^{111}Cd residual nucleus.

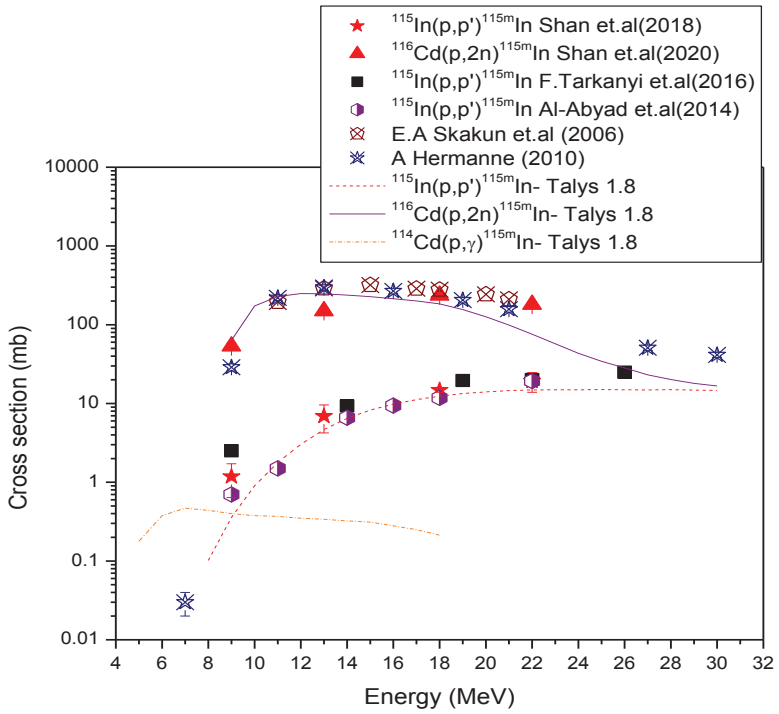

Figure 5.1: Experimentally measured and theoretically predicted excitation function for the ^{115m}In isotope produced through proton induced reaction on natural indium and cadmium.

^{116}Cd(p,2n) reaction is higher by an order compare with that produced through ^{115}In(p,p) reaction channel. Whereas, the isotope production through ^{114}Cd(p,γ) channel is still less by two order when it compare with (p,p) channel. Similarly,

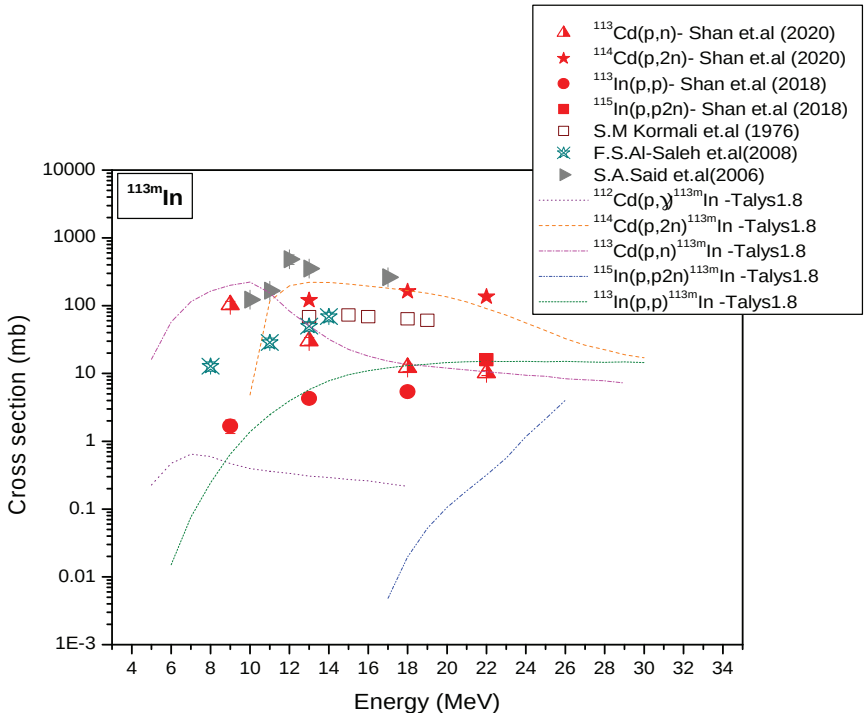

Figure 5.2: Experimentally measured and theoretically predicted excitation function for the ^{113m}In isotope produced through proton induced reaction on natural indium and cadmium.

the production cross-section for the ^{113m}In residual nucleus produced through the reaction channels ^{114}Cd (p,2n) and ^{115}In (p,p2n) is higher by more than an order of magnitude when it is produced through ^{113}In (p,p) reaction channels. Whereas, the cross-section for the ^{113}Cd (p,n) channel is comparable with the ^{115}In (p,p2n) channel up to 18 MeV. Here also, the (p,γ) channel contribution is less by almost two order. This may be attributed to the higher separation energy of proton compare to neutron. Similarly, the residual nucleus ^{111m}Cd is produced through the reaction channels ^{111}Cd (p,p), ^{112}Cd (p,pn), ^{113}Cd (p,p2n), and ^{115}In (p,nα) and are plotted in figure 5.3. The production cross-section for the ^{111m}Cd nucleus through the reaction channel ^{112}Cd (p,pn) is comparable with the ^{111}Cd (p,p) over the energy range 12-22 MeV. The multiparticle emission reaction is more populated than the single particle emission reaction.

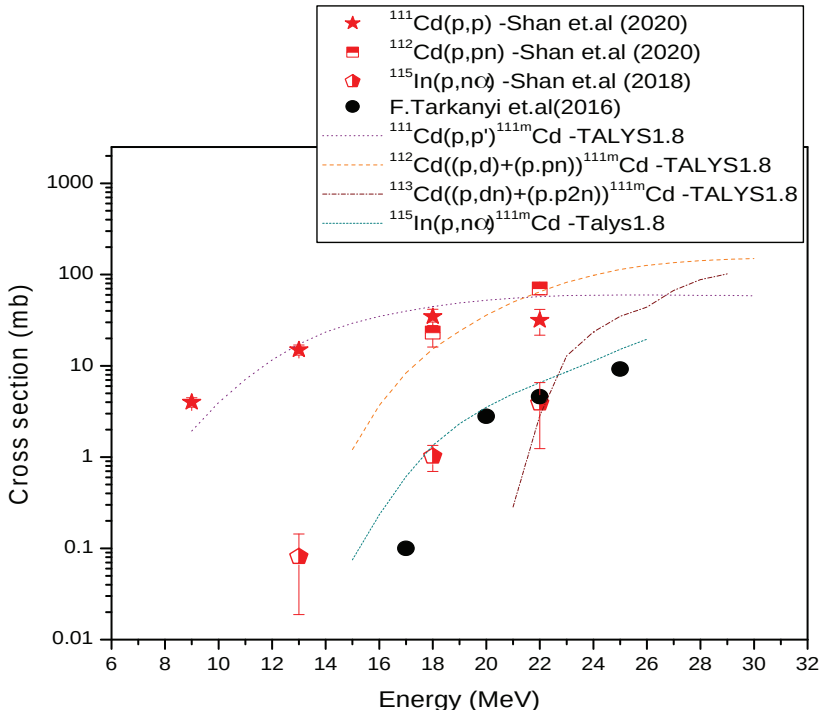

Figure 5.3: Experimentally measured and theoretically predicted excitation function for the ^{111m}Cd isotope produced through proton induced reaction on natural indium and cadmium.

In order to see the effect of angular momentum transfer in the emission channel and its dependence on parameters like spin, parity and lifetime of the isomeric pairs, the isomeric cross-section ratio (ICR) for the production of the isotopes ^{110}In, ^{111}In, ^{112}In, ^{113}In, ^{115}In, and ^{111}Cd are analysed in terms of the above parameters and are plotted through figures 5.4 to 5.9. Figures 5.4 and 5.5 show the isomeric cross-section ratio for the isotopes ^{110}In and ^{111}In produced through (p,n), (p,2n) and (p,3n) channels, as a function of excitation energy. From these figures it is observed that the ICR shows a similar trend, qualitatively and quantitatively. It depends more on excitation energy available than the type of channel producing the particular isomeric pair. The small observed variation in the case of (p,n) channel may be attributed to the onset of pre-equilibrium at energy around 18 MeV that carries away relatively larger energy limiting

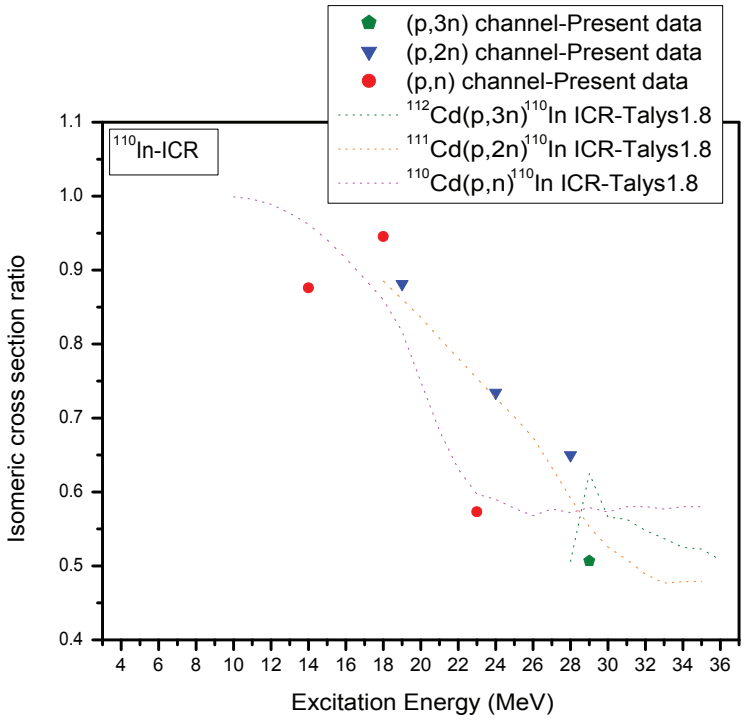

Figure 5.4: Experimentally measured and theoretically predicted ICR as a function of excitation energy for the ^{110}In isotope.

the excitation energy to the residual nucleus. Figure 5.6 shows the ICR for the production of ^{112}In isotope through ^{112}Cd(p,n), ^{113}Cd(p,2n) and ^{114}Cd(p,3n) channels as a function of excitation energy. Here also the ICR shows similar trend irrespective of the channel. However, in this case the isomeric state being higher spin state, ICR shows an increasing trend and gets saturated somewhere at an excitation energy of 28 MeV. The similar nature of ICR is seen in the case of the isomeric cross-section ratio of the ^{115}In and ^{113}In nucleus produced through ^{114}Cd(p,γ), ^{115}In(p,p), ^{116}Cd(p,2n), ^{112}Cd(p,γ), ^{113}Cd(p,n), ^{113}In(p,p), ^{114}Cd(p,2n) and ^{115}In(p,p2n) channels, and are shown in figures 5.7 and 5.8. However, in the case of nuclei production through (p,p) reaction channel the notable discrepancy seen at low energies may be attributed to the coulomb effect in the exit channel, which will be prominent at lower excitation energies. The coulomb interaction may lead to the population of a higher angular momentum

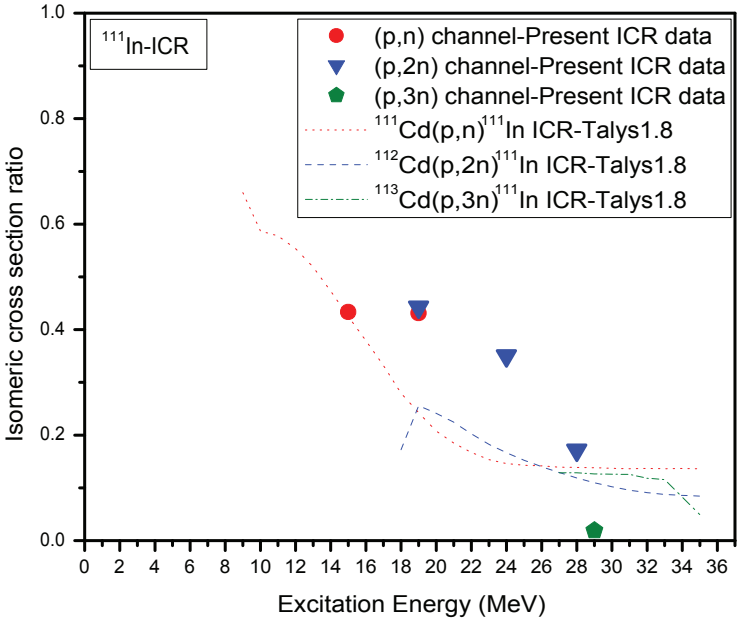

Figure 5.5: Experimentally measured and theoretically predicted ICR as a function of excitation energy for the ^{111}In isotope.

state. Hence, the ground state in the present cases. In the case of (p,p2n) channel the slight separation from the other channels may be due to the fact that the excitation energy under consideration may not be sufficient enough to reach the saturation point of the channel. Figure 5.9 shows the ICR for the production of ^{111}Cd through the channels ^{111}Cd(p,p), ^{112}Cd(p,np), ^{113}Cd(p,p2n) and ^{115}In(p,nα). Here also a slight deviation in the case of (p,pn) and (p,p2n) channels may be attributed to the fact that the excitation energies under discussion are not enough for ICR to be saturated.

Further in figures 5.10, 5.11, 5.12 and 5.13, the isomeric cross-section ratio has been plotted for the cases with a finite value of angular momentum difference in the case of single-particle emission and multiparticle emission. Figure 5.10 shows the ICR for the residual nucleus ^{110}In and ^{111}Cd produced through the single-particle emission channel and figure 5.11 shows the same residual nucleus produced through the multiparticle emission channel, where the angular

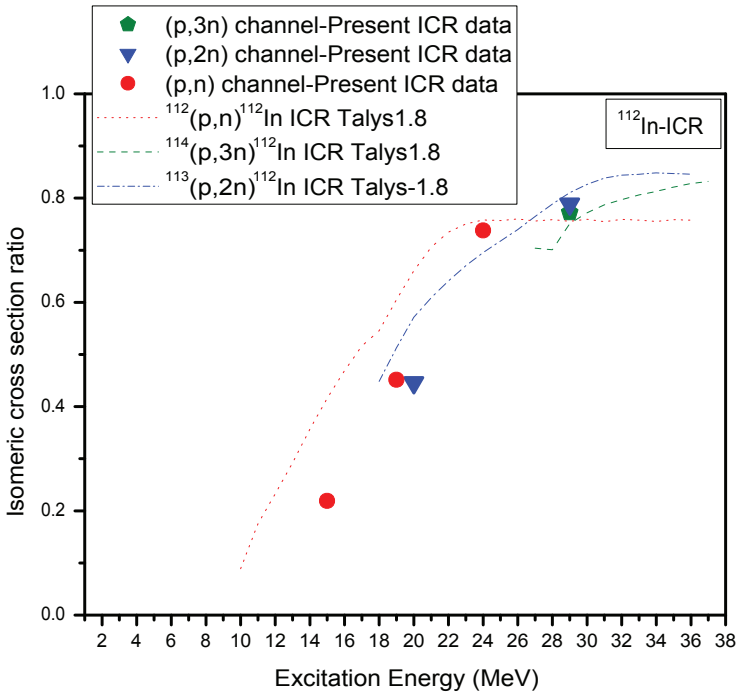

Figure 5.6: Experimentally measured and theoretically predicted ICR as a function of excitation energy for the ^{112}In isotope.

momentum difference of this case is 4. Figure 5.12 shows the ICR of the residual nucleus ^{115}In, ^{113}In and ^{111}In produced through the single particle emission channel and figure 5.13 shows the ICR of the same nucleus are produced through the multiparticle emission channel, with an angular momentum difference of 5. From figure 5.10 it is seen that the single particle emission through ^{111}Cd(p,p) and ^{110}Cd(p,n) reaction channel shows a steady increase/decrease in ICR up to 18 MeV and both get saturated. In the case ^{111}Cd isotopes the population of higher spin state gets saturated to a value of $\approx$ 62% and in the case of ^{110}In it is saturated to a value of around $\approx$ 45%. In the case of ^{112}Cd(p,pn) channel, in figure 5.11, the population of higher spin state gets saturated to a value of $\approx$ 65%, whereas in the case of ^{111}Cd(p,2n) reaction channel, it is saturated to a value of around $\approx$ 55%. This indicates that there is a slight favoring of higher spin state for multiparticle emission. The other channels are below the

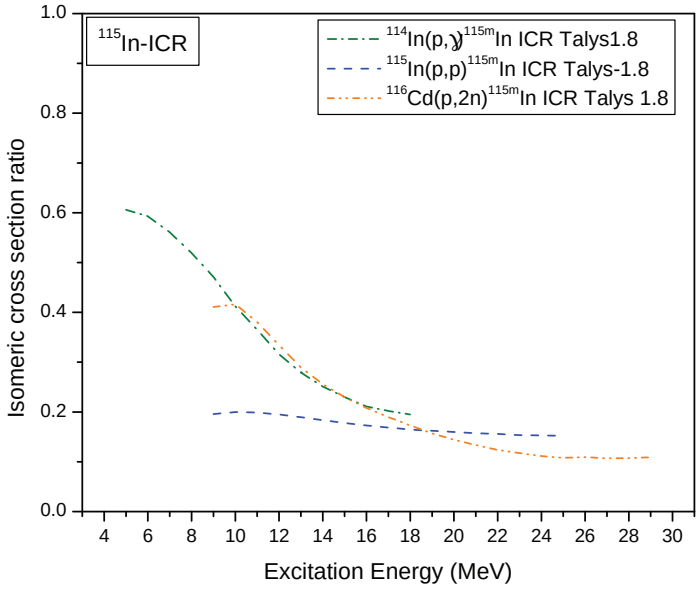

Figure 5.7: Theoretically predicted ICR verses excitation energy for the ^{115}In isotope.

saturation region at this energies. Similarly, in the case of nuclei ^{115}In, ^{113}In and ^{111}In produced through single particle emission, in figure 5.12, the ICR decreases steadily up to 22 MeV and get saturated thereafter. Here, in all the cases the population of high spin state is saturated to a value of about 85%. In the case of the same isotopes produced through multiparticle emission channels, the ICR shows saturation of higher spin state with a population of about 90%. A small enhancement of high spin state is noticed for multiparticle emission, in this case also.

To check whether the isomeric cross-section ratio depends on the life-time of the ground and isomeric state, the correlation between the isomeric population with the lifetime are analysed for the present system. The lifetime is related to the width of the excited states. Shorter the life time larger will be the width of the state. As the width of the state increases, there is more probability for the coupling of levels. This may increase the isomeric population to that state. Isotope produced with similar channel is plotted for this analysis so that

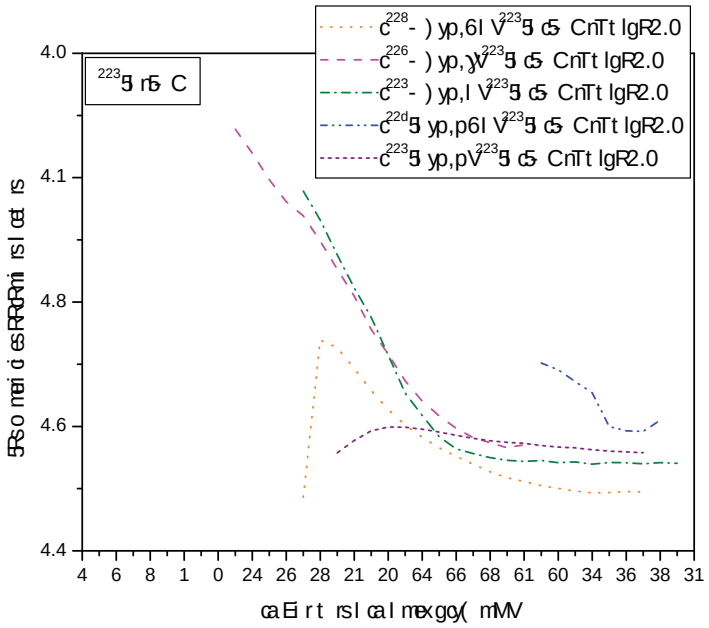

Figure 5.8: Theoretically predicted ICR verses excitation energy for the ^{113}In isotope.

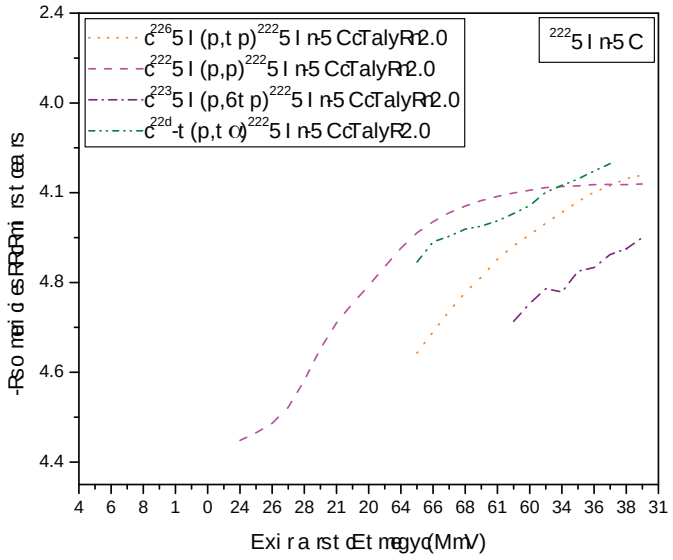

Figure 5.9: Theoretically predicted ICR verses excitation energy for the ^{111}Cd isotope.

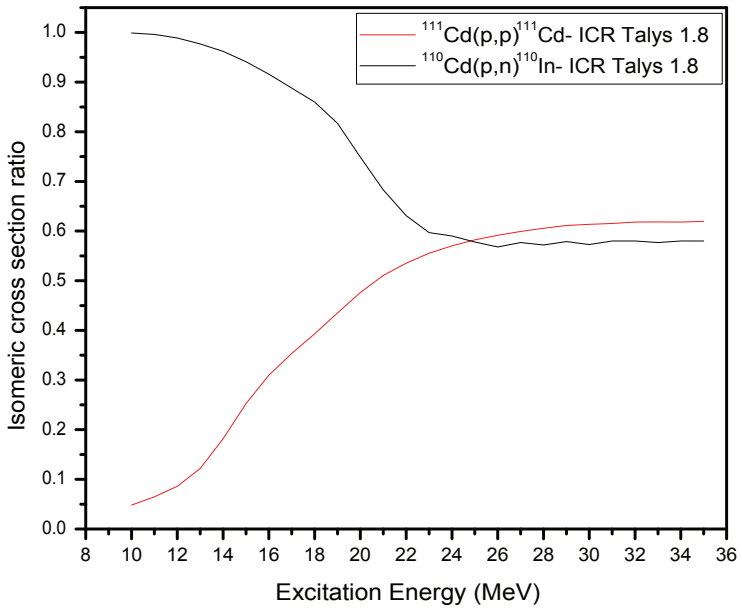

Figure 5.10: Talys.1.8 predicted ICR as a function of excitation energy for the ^{110}In and ^{111}Cd isotopes produced through single-particle emission channel.

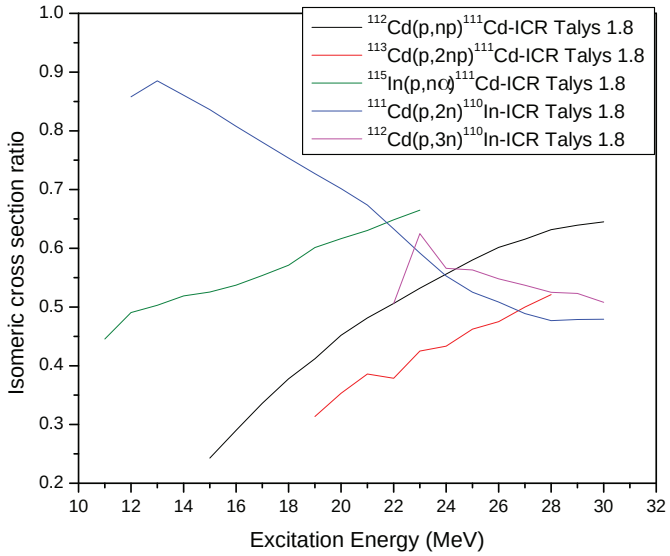

Figure 5.11: Talys.1.8 predicted ICR as a function of excitation energy for the ^{110}In and ^{111}Cd isotopes produced through multiparticle emission channel.

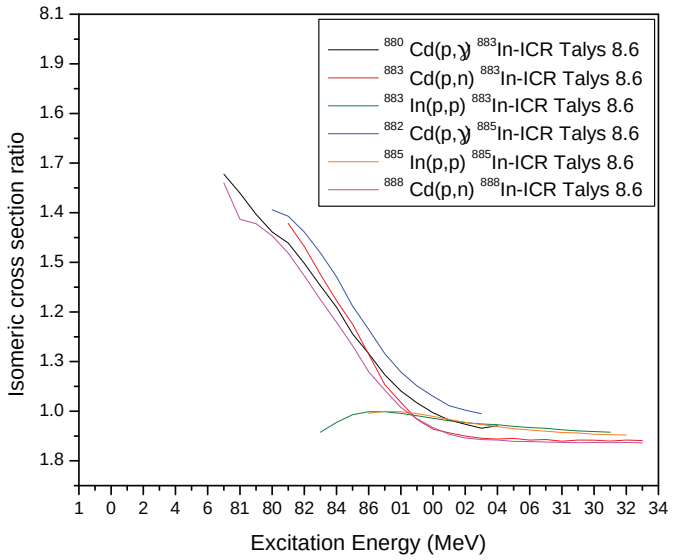

Figure 5.12: Talys.1.8 predicted ICR as a function of excitation energy for the ^{115}In, ^{113}In and ^{111}In isotopes produced through single-particle emission channel.

complex mixing can be avoided to the maximum. Accordingly cases with two-particle emission channels and are plotted in figure 5.14. Two-particle emission channels have considered as there are more number of data in the present case. However, on the analysis of all the available systems under the present study, no correlation is seen between the population of the isomeric state and the life-time of the state.

In order to check whether there is any effect of parity change on the relative population. Cases with parity change and cases with no change in parity are cross-checked. In the present case the nuclei ^{110}In, ^{112}In and ^{114}In are having the same parity for the ground state and isomeric state. For the nuclei ^{111}In, ^{113}In, ^{115}In and ^{111}Cd the parity for ground state is ^{+}ve and that for the isomeric state is ^{-}ve. On analysing the present data no commendable effect of parity is observed in the relative population of the isomeric state.

In order to see the effect of difference in energy between the ground state and isomeric states the data plotted in figure 5.14 is analysed in terms of the energy difference between the isomeric pairs. A notable correlation is observed. The

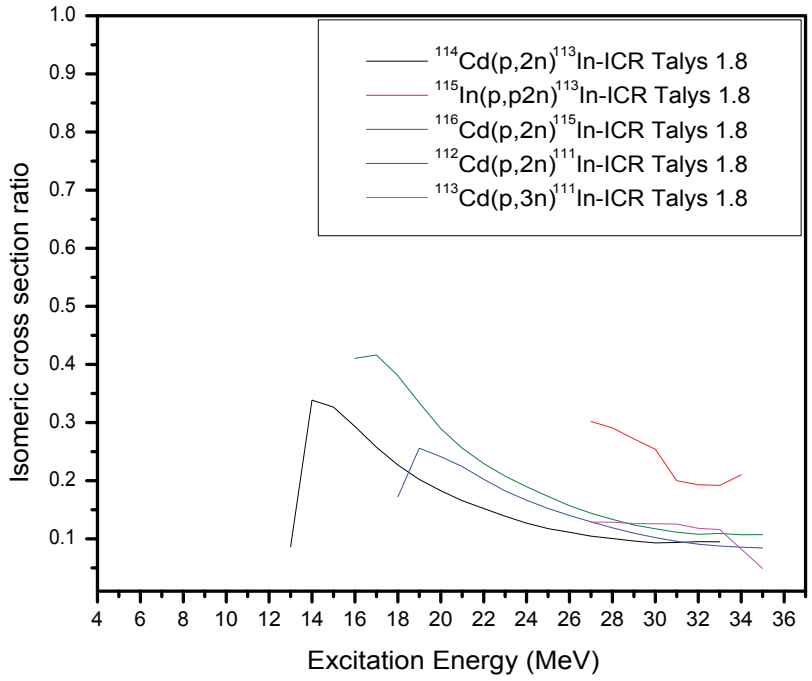

Figure 5.13: Talys.1.8 predicted ICR as a function of excitation energy for the ^{115}In, ^{113}In and ^{111}In isotopes produced through multiparticle emission channel.

result of this observation is shown in figure 5.15 as the plot of relative population of higher spin state, at an excitation energy of 32 MeV, against energy difference between the states. Most of the channels with single and two-particle emission get saturated at the excitation energy of 32 MeV. From this figure it is seen that the population of high spin state shows an increment with the energy difference. However, in the case of ^{111}Cd there is a notable deviation from the general behavior. This may be due to the fact that the proton in the emission channel. A similar trend is seen in the case of ^{114}In nucleus. However, a detailed analysis of large number of cases has to be done to make a conclusive statement. This detailed analysis is beyond the scope of this thesis and has to be considered for future studies.

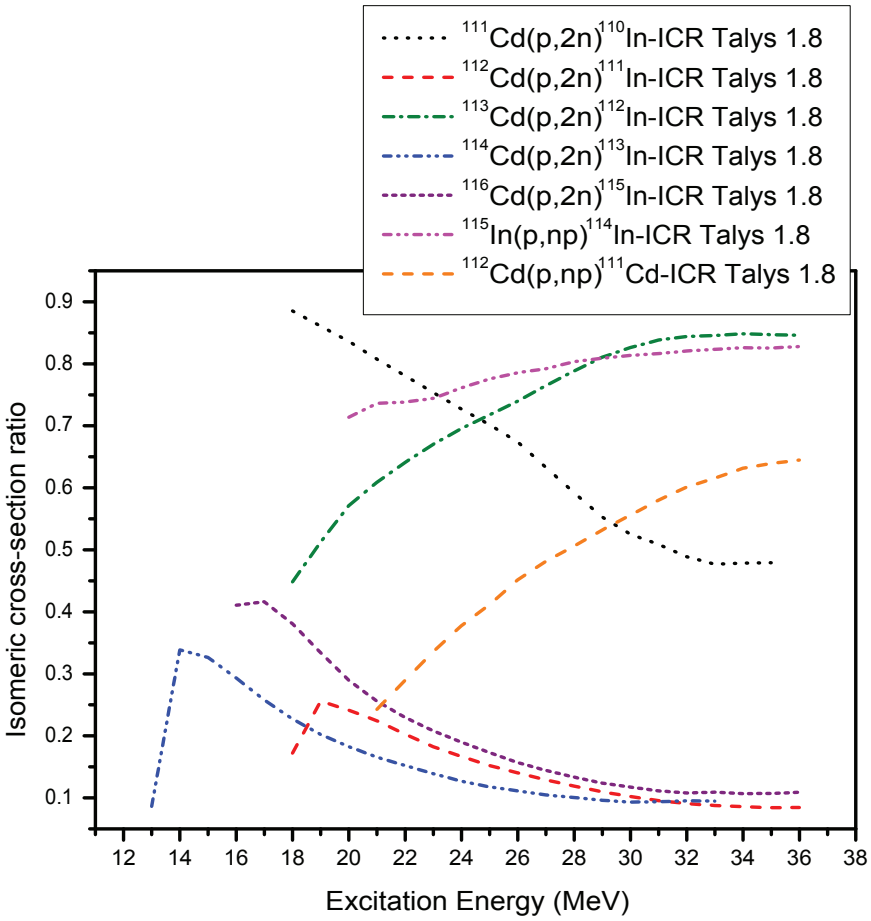

Figure 5.14: Theoretically predicted ICR for the residual nuclei ^{110}In, ^{111}In, ^{112}In, ^{113}In, ^{114}In, ^{115}In and ^{111}Cd produced through two particle emission channel.

5.1 Conclusion

In the present thesis, the effect of various nuclear level parameters on the relative population of various isomeric states are analysed based on the measurement and analysis of proton-induced reaction on natural indium and cadmium. It is established that the relative population depends significantly on the spin of the state and the excitation energy available for the system. In the region of saturation of population, it is noted that the population of the states does not have significant dependence on the emission channel viz. nature of the emission

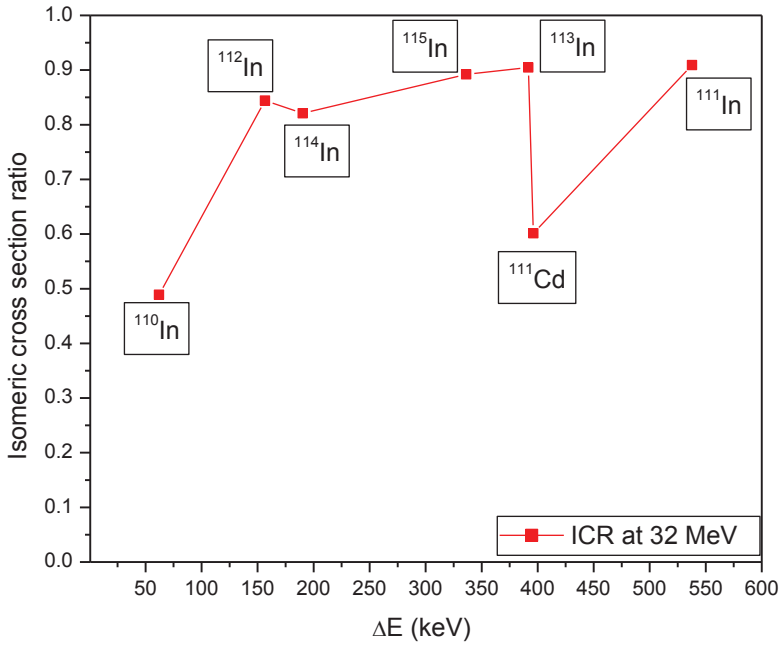

Figure 5.15: Relative population of higher spin state against energy difference between the states for the ^{110}In, ^{111}In, ^{112}In, ^{113}In, ^{114}In, ^{115}In and ^{111}Cd nucleus at an excitation energy of 32 MeV.

channel, number of emitted particles, and type of emitted particles. However, a slight favoring of a higher spin state for multiparticle emission is noted. Though an effect of line broadening is expected to reflect on the higher population of broader states, such a correlation between lifetime or level width with relative population could not be seen in the present case. However, a conclusive remark can be made only after studying a large number of similar cases with isomeric states of a wide range of life-time. This opens the scope for further investigation as a future study. On the other hand, the relative population is found to affect by the energy difference between the states. Larger the energy difference higher the relative population of high spin state. Whereas, when the energy gap is lesser the saturation is limited to around 50%. There is a notable deviation of one case in the present analysis. Hence, this case also needs a detailed study opening scope for future studies with a large number of cases.